UNIVERSITÄT ZU LÜBECK
INSTITUTE OF MATHEMATICS AND
IMAGE COMPUTING

Modular Multi-Shape Registration

Modulare Multiform-Registrierung

Masterarbeit

im Rahmen des Studiengangs
Mathematik in Medizin und Lebenswissenschaften
der Universität zu Lübeck

Vorgelegt von
Rosa Antonia Kowalewski

Ausgegeben und betreut von
Prof. Jan Lellmann
Institute of Mathematics and Image Computing

Mit Unterstützung von
Barbara Gris, PhD
Laboratoire Jacques-Louis Lions, Sorbonne Université

4. September 2019

MIC

IM FOCUS DAS LEBEN

Eidesstattliche Erklärung

Ich versichere an Eides statt, die vorliegende Arbeit selbstständig und nur unter Benutzung der angegebenen Quellen und Hilfsmittel angefertigt zu haben.

Lübeck,
September 10, 2019

Rosa Antonia Kowalewski

Abstract

The deformation module approach introduced by [Gri16] is a generic framework for integrating prior knowledge about desired deformation fields in shape and image registration. Deformation modules allow to build diffeomorphic deformations that satisfy a given structure, for example locally affine transformations, scalings and rotations, or a combination. The diffeomorphisms are built by integrating a flow of constrained velocity fields.

However, in applications such as modeling of respiratory motion in abdominal images for operation planning, one often encounters situations where a single deformation model is not adequate. While it makes sense to consider diffeomorphic deformations of the seperate organs, breathing motion results in a non-smooth and possibly discontinuous displacement field at organ boundaries. To be able to use different constrained deformations for different organs, we combine the model with a framework to introduce region boundary constraints for multiple interacting objects in a shape or image, as introduced in [Arg14]. Deformation fields are built for each object separately, while their interaction is incorporated by constraints on the deformation of the object boundaries.

We derive theoretical results on the existence of optimal trajectories for the constrained registration problem and provide numerical results to demonstrate the potential of our approach.

Kurzfassung

Der in [Gri16] eingeführte Deformationsmodul-Ansatz berücksichtigt Vorwissen über gewünschte Deformationsfelder in der Form- und Bildregistrierung. Deformationsmodule ermöglichen es, diffeomorphe Deformationen zu generieren, die einer bestimmten Struktur entsprechen: zum Beispiel lokal affine Transformationen, lokale Skalierungen und Rotationen oder deren Kombination. Die Diffeomorphismen ergeben sich als Lösung der Flussgleichung zeitabhängiger eingeschränkter Geschwindigkeitsfelder.

In einigen Anwendungen wie der Modellierung der Atembewegung in Bildern des Abdomens zur Operationsplanung reicht ein einziges Deformationsmodell jedoch nicht aus, um eine plausible Deformation zu erhalten. Während diffeomorphe Deformationen innerhalb einzelner Organe plausibel sind, führt die Atembewegung zu einem nichtglatten, möglicherweise diskontinuierlichen Verschiebungsfeld an den Organgrenzen. Um für verschiedene Organe verschiedene Vorgaben formulieren zu können, kombiniert die hier vorgestellte Methode das Modell mit dem Ansatz in [Arg14], der Deformationen an den Grenzen mehrerer interagierender Objekte einschränkt. Deformationsfelder werden für jedes Objekt separat bestimmt und anschließend unter Berücksichtigung der Einschränkungen an den Objektgrenzen zusammengefügt.

Inhalt dieser Arbeit sind theoretische Ergebnisse zur Existenz von Minimierern des aufgestellten Registrierungsproblems sowie numerische Ergebnisse, die das Potenzial des Ansatzes aufzeigen.

Acknowledgements

I have received a great amount of support and inspiration which led me to write these words today.

My huge acknowledgement and greatfulness are dedicated to Barbara Gris. I am very thankful that she made it possible for me to pursue my research studies at Laboratoire Jacques-Louis Lions in Paris. Not only did I learn a great amount of theoretical concepts and practical tools under her supervision. Her passion and endurance are a great source of inspiration for me. Her support helped me to succeed in a great project. Working with her taught me to not shy away from difficult questions, but take the chance to develop new ways of thinking. I also thank her for the opportunity to attend the SIAM conference during my stay, where I even learned mathematics in french in the end. It has been a pleasure to work together and I am very much looking forward to our future collaborations.

I would like to thank Jan Lellmann for being a great advisor and the initiator of my mathematical journey. He layed the foundations for my research stay at Carola Schönlieb's group in Cambridge and made it possible for me to proceed my studies in Paris. I feel enlightened after every of our meetings and highly value his advice.

Thanks to Carola Schönlieb who invited me to Cambridge for my research internship. I feel very honored to have had the opportunity of joining the Cambridge Image Analysis group at DAMTP. I am greatful to her for making it possible for me to attend conferences and meet reasearchers at the Isaac-Newton-Institute, and even supporting me in attending a workshop in Stockholm.

I was very happy to meet Ozan Öktem in Cambridge. He promoted the progress of my project, asking me questions and bringing me in touch with Barbara Gris. I am grateful for the invitation to Stockholm, where I had the chance to complete my first project in collaboration with Barbara, which laid the foundations for my master's thesis.

A very big *Thank you* to Thomas Vogt for always helping me out with mathematical questions and being a great partner for discussions of all kind. Thanks to Leander Lacroix, for being available to answer my coding questions, and exploring unconventional places in Paris with me.

Cheers to Caterina and Stephanie, with whom I shared some moments of frustration as well as many bright moments of insight during my studies.

And most important, thanks to my mother and my sister for their infinite love and support.

Contents

1 Introduction **3**
- 1.1 Image Registration . . . 3
  - 1.1.1 Large Diffeomorphic Deformations . . . 4
  - 1.1.2 Parametric Diffeomorphic Deformations . . . 5
  - 1.1.3 Constrained Diffeomorphic Deformations for Multiple Shapes . . . 6
- 1.2 Outline . . . 6

2 Mathematical Background **9**
- 2.1 Large Deformation Diffeomophic Metric Mapping . . . 9
  - 2.1.1 The Registration Problem . . . 9
  - 2.1.2 Shape Spaces . . . 10
  - 2.1.3 The Diffeomorphism Group . . . 11
  - 2.1.4 Reproducing Kernel Hilbert Spaces . . . 12
  - 2.1.5 The LDDMM Registration Problem for Shapes . . . 13
  - 2.1.6 Geodesic Shooting . . . 15
  - 2.1.7 Hamiltonian Geodesic Equations . . . 15
- 2.2 Constrained LDDMM for Multi-Shapes . . . 19
- 2.3 Deformation Modules . . . 22

3 Multi-Shape Deformation Modules **29**
- 3.1 Definition of the Framework . . . 29
- 3.2 Existence of Large Deformations for Multi-Shape Modules . . . 31
- 3.3 The Constrained Registration Problem . . . 33
- 3.4 Existence of Geodesic Flows . . . 34
- 3.5 The Hamiltonian Function and Shooting Equations . . . 39
- 3.6 Geodesic Variables for Landmarks . . . 42

4 Numerical Results **49**
- 4.1 Translation of Shapes in a Background . . . 49
- 4.2 Local Scalings and Translation . . . 55

5 Conclusion **65**

A Appendix **67**
- A.1 Explicit Formulation of Geodesic Variables for Landmarks with Identity Constraints . . . 67

Notation

Shapes and Deformations

$\mathcal{O}$	Shape space	(Def. 2.1)
$q\colon [0,1] \mapsto \mathcal{O}$	Time-evolving shape	
q_t	Shape at time t	
$\dot{q}_t$	Derivative with respect to time at t	
$\mathrm{T}_{q_t}\mathcal{O}$	Tangent space of $\mathcal{O}$ at q_t	
$\xi\colon \mathcal{O} \times C_0^l(\mathbb{R}^d, \mathbb{R}^d) \to \mathrm{T}\mathcal{O}$	Infinitesimal action	(Def. 2.1)
$V \subset C_0^l(\mathbb{R}^d, \mathbb{R}^d)$	Space of vector fields	
$v\colon [0,1] \mapsto V$	Time-dependent velocity field	
v_t	The velocity at time t	
$\dot{\phi}_t = v_t \circ \phi_t$	Flow equation of deformations	(Def. 2.4)
$\dot{q}_t = \xi_{q_t}(v_t)$	Evolution the shape defined by the flow equation	
ϕ^v	Diffeomorphism defined by the flow of v	
$\mathrm{Diff}_0^l(\mathbb{R}^d)$	Set of diffeomorphisms acting on $\mathbb{R}^d$ that are of class C^l with inverse of class C^l, converging to identity at infinity	(p. 9)
Diff_V	Group of diffeomorphisms associated with the admissible Banach space V	(Def. 2.7)

Image and Shape Registration

q_S	Source Shape (to be deformed)	
q_T	Target Shape (to be reached)	
$\mathcal{J}$	Energy functional of the registration problem	(p. 9)
$\mathcal{U}$	Data similarity term, depending on the deformed shape and the target	
$\mathcal{R}$	Regularization term depending on the deformation	
$\mathcal{H}$	Hamiltonian function used for geodesic shooting	(Def. 2.10)
H	Reduced Hamiltonian function	(Th. 3.13)

Deformation Modules **(Def. 2.18)**

$\mathcal{M}$	Deformation module
H	Space of controls
$\zeta\colon \mathcal{O} \times \mathrm{H} \to V$	Field generator
$c\colon \mathcal{O} \times \mathrm{H} \to \mathbb{R}^+$	Cost function
$\mathrm{Z}_q\colon \mathrm{H} \to \mathrm{H}^*$	Cost operator satisfying the property $(\mathrm{Z}_q h \vert h)_{\mathrm{H}^*,\mathrm{H}} = c_q(h)$

Multi-Shape and Constrained Registration

$\mathbf{M}^{multi}$	Multi-shape combination of deformation modules	(Def. 3.1)
$\mathrm{C}_q^{\mathrm{state}} \colon V \to \mathrm{Y}$	State constraints	(Def. 2.13)
$\mathrm{C}_q \coloneqq \mathrm{C}_q^{\mathrm{kin}} \colon V \to \mathrm{Y}$	Kinetic constraints values	(Def. 2.13)
Y	Space of constraints (Banach space)	

Reproducing Kernel Hilbert Spaces (RKHS) and Kernels **(Def. 2.6)**

K	Reproducing kernel
$\tilde{\mathrm{K}}(x,y)$	the $d \times d$ kernel matrix for $x, y \in \mathbb{R}^d$
$\mathrm{k}(x,y) = \exp\left(-\frac{\|x-y\|}{\sigma^2}\right)$	Gaussian distribution
$\tilde{\mathrm{K}}_{a,b} \coloneqq \tilde{\mathrm{K}}(a,b) \in \mathbb{R}^{d^{n_1} \times n_2}$	with $a = (a^1, ..., a^{n_1}) \in (\mathbb{R}^d)^{n_1}$, $b = (b^1, ..., b^{n_2}) \in (\mathbb{R}^d)^{n_2}$ the $dn_1 \times dn_2$ kernel matrix with values $\left(\tilde{\mathrm{K}}(a,b)\right)_{i,j} = \mathrm{k}(a^i, b^j)$
$\delta_x(v) \coloneqq v(x)$	the point evaluation functional

General Notation

C_0^l	Space of l-times continuously differentiable functions that converge to zero at infinity	
X^*	Dual space of a space X	
$\langle \cdot, \cdot \rangle_X$	Scalar product in the Hilbert space X	
$(\mu \| x)_{X^*,X} = \mu(x)$	Dual pairing of an element $\mu \in X^*$ in the dual space X^* of X, with $x \in X$	
∂_x	Derivative with respect to x	(p.9)

Chapter 1: Introduction

In this thesis we derive an approach for incorporating prior knowledge of deformation and object boundary motion in image and shape registration. The proposed framework is an extension of the deformation modules introduced in [Gri16] and makes use of the idea of multiple shape registration presented in [ATTY15a]. The goal is to provide a framework for medical image registration that makes it possible to incorporate prior knowledge about the structure of deformations of different organs and tissues in the human body.

1.1 Image Registration

In image analysis one is often not only interested in the analysis of a single image, but in comparing the information given in different images. For this reason, image registration is an important field in image analysis. The applications range from astro- and geophysics over computer vision to medicine and biology [Mod04]. In medical applications, imaging can help to monitor tumor growth, facilitate treatment verification, improve interventions, or compare patient's data to an anatomical atlas. The general image registration problem can be stated as follows.

Problem 1.1. **[Mod04] Image Registration**

Find a reasonable transformation such that a transformed version of a template image is similar to a reference image.

The essential question mathematical models adress in image registration is to provide a mathematical formulation for the terms *reasonable* and *similar* for a given application. Because of the varying nature of images and represented objects in a wide range of applications there is no common technique of registration applicable to all registration tasks. Registration methods are unique to each problem. For example in medical imaging a reasonable transformation of bones would be a rigid or affine one, while for soft tissues a non-rigid transformation is considered. The similarity measure of the images can depend on the represented objects as well as on the modality.

The choice of the mathematical model depends on the given information about the represented objects. When prior knowledge is given, the model can be adapted in the mathematical setting. This leads to precise but more complex models. Complex models will usually lead to a high computation time and memory requirements. Some applications require fast and cost efficient computations. For example shape changes that arise during a surgery due to intervention have to be corrected numerically in real-time.

Therefore, a compromise between accuracy and cost (in terms of time, storage, or other limited resources) has to be made. Research literature shows many different approaches to the problem 1.1, taking into account specific prior knowledge and requirements of limited resources for computation.

In general, one can distinguish between parametric and non-parametric image registration techniques. In parametric image registration, the transformation is composed

from a finite number of basic deformations. Thus the transformation can be described by a finite number of parameters, that are interpretable for the given setting. In non-parametric image registration, the deformation is given by a vector at each transformed point. This allows for a richer variety of deformations, as they are not restricted to certain basis functions.

1.1.1 Large Diffeomorphic Deformations

An example for non-parametric registration techniques is the Large Deformation Diffeomorphic Metric Mapping. Three advantages of this model are referenced in the name of this method:

- it can produce large deformations,
- deformations are continuously differentiable and have a continuously differentiable inverse (i.e., they are diffeomorphic),
- it provides a metric d_V on the space of deformations.

Elastic deformation models pioneered in [Bro81] generated a deformation $\phi(x)$ of $x \in \mathbb{R}^d$ by perturbations $v(x)$ from the identity,

$$\phi(x) = \mathrm{Id}(x) + v(x). \tag{1}$$

However, [CRM+96] pointed out that elastic deformation cannot guarantee diffeomorphisms for large vector fields $v(x)$. They proposed a transformation on the basis of a fluid flow of vector fields, described by the flow equation

$$\dot{\phi}_t = v_t(\phi_t(x)) \tag{2}$$

In general, the deformation $\phi(x)$ resulting from equation (1) is not invertible. Beg et. al [BMTY05] further developed this approach to a framework that provides a metric for the image orbit.

Since then, the underlying theory of Riemannian geometry has been extensively studied [MM07, Arg14, BBM14]. A further development resulting from the Riemanian geometric viewpoint is the shooting method. The metric d_V is a right-invariant Riemannian metric and therefore allows to formulate a principle of least action for the flow. By the principle of least action the possible flows of velocity fields are selected to be geodesic flows. They describe the shortest path from an initial deformation ϕ_0 to a deformation ϕ_1. [DGM98] and [MTY02] described a Euler-Lagrange formulation of the shooting equations. Equivalently a Hamiltonian reduction can be formulated, as in [MTY15], [MM07].

Furthermore, several extensions of the LDDMM model exist. For example, in the metamorphosis model, the points transformed by the deformations are allowed to vary in intensity values, allowing for a mass-preserving deformation. Moreover, S. Arguillère proposed a framework for multiple interacting objects in a common background

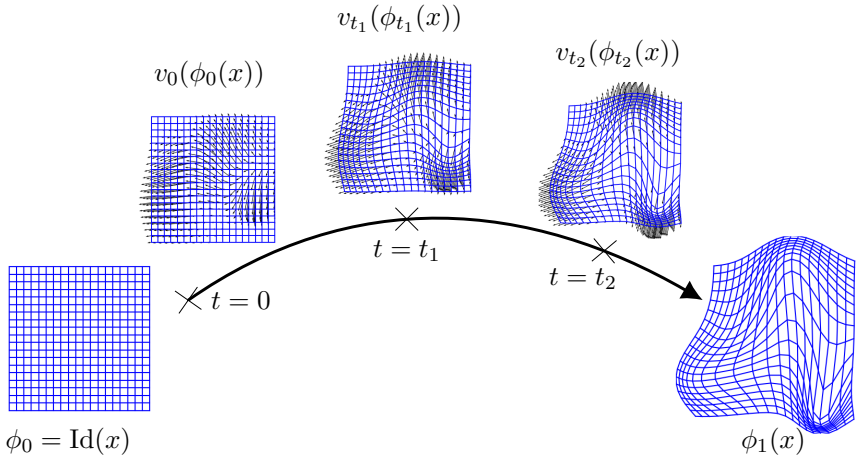

Figure 1: The deformation ϕ is evolving over time as the flow of the time-dependent vector field v. The flow equation (2) is a central tool for the construction of diffeomorphic deformations in LDDMM as well as in our proposed framework. The figure shows the deformation ϕ_0 equal to the identity at time $t = 0$, the vector fields v_t applied to the deformation ϕ_t at intermediate time points $t_1, t_2 \in [0, 1]$, and the resulting deformation ϕ_1. The gradient $\dot{\phi}$ of the deformation ϕ is equal to the vector field $v_t(\phi_t(x))$ at each time point t. The deformation ϕ is the solution of the flow equation which amounts to the integral of $\dot{\phi}$.

[ATTY15b]. This framework makes it possible to build a combination of deformations that are diffeomorphisms of different segmented regions in the ambient space that still leads to a coherent global deformation. The contribution of the thesis at hand is an extension of Arguillère's multi-shape registration framework. We will refer to this framework as multi-shape LDDMM, opposed to the multi-shape modular approach that we propose. The modular approach provides parametric deformations, as opposed to LDDMM as a non-parametric framework.

1.1.2 Parametric Diffeomorphic Deformations

For specific medical applications the non-parametric image registration approach can have two drawbacks. (1) The resulting deformation is not easily interpretable, and (2) the deformation can be implausible in the real world. Therefore approaches have been developed that rely on the theory of LDDMM, that provide the advantages pointed out in the previous section, and at the same time parameterize the deformations beforehand with meaningful variables.

The poly-affine and poly-rigid diffeomorphic deformations introduced in [ACAP09] and [APA03] provide locally rigid and affine deformations. The framework has been applied to registration of bones [SPR12] and cardiac motion [MSBP15], [RDSP15]. The GRID model (Growth by random iterated diffeomorphisms) [GSS06] aims to model biological growth as a parameterized diffeomorphic deformation. A diffeomorphism is generated by a sequence of local small deformations around seed points where the growth is located. Another approach for parametric diffeomorphic image registration is the Diffeons model [You12]. Here, the velocity field belongs to an object-dependent Hilbert subspace of

a Hilbert space of finite energy velocities. The Hilbert subspace is finitely generated by basis functions called diffeons. This setting allows to design a metric that induces different amounts of deformations inside and outside a shape.

These approaches only incorporate a certain type of prior knowledge, such as rigidity or growth. To combine different types of local deformations into a diffeomorphism, B. Gris introduced the *deformation modules* approach in [Gri16]. Deformation modules generalize the previous approaches, as modules for locally rigid deformations or a growing deformation can be defined. They require few conditions on the constraints (i.e., the prior knowledge one wants to incorporate). The modular approach allows very easy parametrization of certain deformations which can be combined to arbitrary complex deformations.

In a deformation module, a vector field is generated by a field generator depending on a low-dimensional parameter. As in LDDMM, the final deformation is built by the flow of a time-dependent vector field. In the GRID and Diffeons model, the same deformation can potentially arise from different parameters. Because the regularization cost is the norm of the vector field, generators that build the same deformation are associated with the same cost. This is not coherent in a setting where one generator is more plausible than another. Opposed to that, the cost for deformation modules is dependent on the object as well as the generator and therefore can be defined coherent with priors. Following some weak restrictions on the cost, it also defines a metric on the space of deformations, which allows to describe geodesics and apply the shooting method.

1.1.3 Constrained Diffeomorphic Deformations for Multiple Shapes

The frameworks of deformation modules and multi-shape LDDMM both provide important features for the application to medical image registration. Using deformation modules, prior knowledge of deformations can be modeled. However, the resulting deformation is always a diffeomorphism, which is not plausible when considering different organs in an image. The deformation of organs in the human body is supposed to be diffeomorphic inside the organs but can be discontinuous at organ boundaries. To model this setting, the framework is lacking a way to combine different modules in a way that the deformations inside and outside the organs are not influencing each other but are still coherent at their boundaries.

In the framework of multi-shape registration such a combination is given. However, the framework has been formulated only for unparameterized diffeomorphic deformations. To make use of the advantages of these two frameworks, we propose the combination of both kinds of constraints. This will allow to build constrained diffeomorphisms by deformation modules that are linked at object boundaries.

1.2 Outline

The thesis is organized as follows. In chapter 2 we lay out the mathematical foundations for the framework. We explain concepts of diffeomorphism groups, reproducing kernel Hilbert spaces and geodesic shooting for the LDDMM registration problem. Then

we introduce the constrained optimal control problem for multiple interacting shapes. Furthermore, we explain the idea and central theoretical results from the modular deformation approach.

Chapter 3 covers the newly developed framework where the ideas of constrained multi-shape matching and deformation modules are combined. We define the setting and give a motivational example. Then we provide a proof of existence of minimizers of the matching problem. Furthermore, we derive the Hamiltonian system of equations for geodesic shooting.

In chapter 4, we present numerical results on a synthetic data set and compare our model to the multi-shape LDDMM setting as well as to the standard LDDMM setting without any boundary constraints and a compound modular deformation.

Chapter 5 will summarize and evaluate our contributions and give an outlook to possible future work.

Chapter 2: Mathematical Background

We will use the following notation throughout the thesis.

For a mapping $f\colon \mathbb{R}^d \to X$ of class C^l with compact support, following [ATTY15b] we define the norm

$$\|f\|_l = \sup\Big\{\Big|\frac{\partial^{l_1+\cdots+l_d} f(x)}{\partial x_1^{l_1}\ldots\partial x_d^{l_d}}\Big|_X | x \in \mathbb{R}^d, (l_1,\ldots,l_d) \in \mathbb{N}^d, l_1+\cdots l_d \le l\Big\}. \tag{3}$$

Let $d \in \mathbb{N}$ be fixed. A mapping $\phi\colon \mathbb{R}^d \to \mathbb{R}^d$ is called a C^l-diffeomorphism if it is a bijective mapping of class C^l with an inverse of class C^l. We consider C^l-diffeomorphisms that converge to identity at infinity with respect to the norm $\|\cdot\|_l$. The space of such diffeomorphisms is denoted by $\mathrm{Diff}_0^l(\mathbb{R}^d)$. Analogously we define $C_0^l(\Omega,\mathbb{R}^d)$ the space of functions from Ω to $\mathbb{R}^d$ of class C^l that converge to zero at infinity.

We will denote $(\mu|\delta)_{V^*,V} \coloneqq \mu(\delta)$ the dual pairing for $\mu \in X^*, \delta \in X$. In order to compute optimality conditions for the energy functional (2.9), we need to compute its variations in the following sense. For a Banach space X, $a \in X$ and a functional $F : X \to \mathbb{R}$, we define $\partial_x F(a) \in X^*$ in the dual space of X by

$$(\partial_x F(a)|\delta) \coloneqq \frac{\mathrm{d}}{\mathrm{d}t} F(a+t\delta)\Big|_{t=0} \tag{4}$$

if it exists. For a function $g\colon [0,1]\times X \to Y$, we denote $\dot{g} \coloneqq \frac{\mathrm{d}}{\mathrm{d}t} g$ its derivative with respect to the first variable (time).

2.1 Large Deformation Diffeomophic Metric Mapping

2.1.1 The Registration Problem

Consider two images $q_S \in \mathcal{O}$ and $q_T \in \mathcal{O}$ in the space $\mathcal{O} \coloneqq C_0^l(\Omega,\mathbb{R})$, where $\Omega \subset \mathbb{R}^d$ is a domain of $\mathbb{R}^d$. We will refer to q_S as the reference image or *source* shape, and q_T as the template image or *target* shape. The image registration problem is to find a *plausible* deformation ϕ, that maps the reference image *as close as possible* to the target image. A common way to model this problem is to consider the minimization of an energy functional

$$\mathcal{J}(\phi; q_S, q_T) \coloneqq \mathcal{U}(\phi\cdot q_S, q_T) + \mathcal{R}(\phi) \tag{5}$$

over the deformation ϕ. Here, the functional $\mathcal{U}\colon \mathcal{O}\times\mathcal{O} \to \mathbb{R}$ is a distance in the space of images, that models the similarity between two images. The functional $\mathcal{R}\colon \mathrm{D} \to \mathbb{R}$ models the plausibility of the deformation ϕ in the considered space of deformation D.

Many approaches for choices of $\mathcal{U}$ and $\mathcal{R}$ are proposed in the literature. The choice depends on the setting of the problem, including for example modalities of the images and the nature of the represented objects. While we will not go into details of the distance measure $\mathcal{U}$, we will in this work focus on a way of regularizing the deformation of the images.

For many applications it is desirable to have a deformation ϕ that is invertible, and both ϕ and ϕ^{-1} should be sufficiently smooth. This prevents the deformation from creating holes or foldings when applied to an image and preserves the local topology. Under this assumption the deformation ϕ is a diffeomorphism. The set of diffeomorphisms forms a group with the identity mapping as neutral element. The group of diffeomorphisms is essential in the Large Deformation Diffeomorphic Metric Mapping (LDDMM) framework. Our proposed framework makes use of the basic ideas of LDDMM, which is why this chapter is dedicated to the introduction to diffeomorphism groups, LDDMM and geodesic shooting.

Although the motivation for the registration problem considered in this thesis is medical image registration, we will use the notion of shapes instead of images. Shapes provide a more general framework to the problem. The image registration problem can be seen as a special case of the shape registration problem, so all derived results can be applied to images. Since images are mathematically modeled as functions on $\mathbb{R}^d$, they are of infinite dimension. In order to provide example demonstrations we will later consider the special case of landmarks as elements of a finite-dimensional shape space. This will make the derivation of explicit formulations easier and should help to get a better intuition of the framework.

In the following section we introduce the notion of shapes as introduced in [Arg14].

2.1.2 Shape Spaces

Definition 2.1. **[ATTY15b, Def. 2] Shape Space**

Let $\mathcal{O}$ be an open subspace of a Banach space X, $d \in \mathbb{N}$ and $k \in \mathbb{N}$. Assume that the group of diffeomorphisms $\mathrm{Diff}_0^l(\mathbb{R}^d)$ acts continuously on $\mathcal{O}$, according to the action $\cdot$ denoted by

$$\begin{aligned} \mathrm{Diff}_0^l(\mathbb{R}^d) \times \mathcal{O} &\to \mathcal{O} \\ (\phi, q) &\to \phi \cdot q. \end{aligned} \tag{6}$$

Then $\mathcal{O}$ is a C^k-shape space of order l on $\mathbb{R}^d$ if the following conditions are satisfied:

1. For each $q \in \mathcal{O}, \phi \in \mathrm{Diff}_0^l(\mathbb{R}^d) \mapsto \phi \cdot q$ is Lipschitz continuous, i.e.

$$\forall q \in \mathbb{R}^d \; \exists \gamma_q > 0 \colon \|\phi_1 \cdot q - \phi_2 \cdot q\|_{\mathcal{O}} \leq \gamma_q \|\phi^1 - \phi^2\|_l. \tag{7}$$

2. For all $q \in \mathcal{O}$, $\phi \mapsto \phi \cdot q$ is differentiable at $\phi = \mathrm{Id}_{\mathbb{R}^d}$. This differential is denoted by ξ and is called the infinitesimal action of $C_0^l(\mathbb{R}^d)$.

3. The mapping $(q, v) \in \mathcal{O} \times C_0^l(\mathbb{R}^d) \mapsto v \cdot q$ is continuous and its restriction to $\mathcal{O} \times C_0^{l+k}(\mathbb{R}^d)$ is of class C^k.

An element q of $\mathcal{O}$ is called a *shape*, and $\mathbb{R}^d$ is referred to as the *ambient space*.

In particular, we will consider shapes as a functions $q\colon M \to \mathbb{R}^d$, where M is a compact manifold. Then $\mathcal{O}$ is equal to the Banach space $X = C^p(M, \mathbb{R}^d)$ and for any $q \in X$, $x \in M$, the diffeomorphism ϕ acts on q according to

$$(\phi \cdot q)(x) \coloneqq \phi(q(x)). \tag{8}$$

Example 2.2

1. Let $M = \{1, ..., n\}$. Then q is the set of n points in $\mathbb{R}^d$ and $\mathcal{O}$ is the space of landmarks.
2. Let $M = [0, 1]$. Then q is a curve in $\mathbb{R}^d$.
3. Let $M = (\cos(t), \sin(t))$, $t \in [0, 1]$. Then q is a closed curve in $\mathbb{R}^d$.

For the shapes we will consider, $\phi \cdot q$ should only be supported on a compact subset K of $\mathbb{R}^d$. This property will be required for the existence of minimizers for the registration problem. The shapes satisfy the following definition:

Definition 2.3. **[Arg14, Th. 10.1] Compactly Supported Shape**

A shape $q \in \mathcal{O}$ is of compact support, if there exists a compact subset K of $\mathbb{R}^d$, such that for some $\gamma_q > 0$ and for $\phi^1, \phi^2 \in \mathrm{Diff}^l_0$ we have

$$\|\phi^1 \cdot q - \phi^2 \cdot q\|_{\mathcal{O}} \leq \gamma_q \|\phi^1_{|K} - \phi^2_{|K}\|_l, \tag{9}$$

where $\phi_{|K}$ denotes the restricion of ϕ on K.

Note that the example shapes in 2.2 are all of compact support, as the manifold $M \subset \mathbb{R}^d$ is compact for each example.

2.1.3 The Diffeomorphism Group

As motivated in section 2.1.1, we will consider diffeomorphisms $\phi \in \mathrm{Diff}^l_0(\mathbb{R}^d)$ as deformations for the shape registration framework, i.e, continuously differentiable maps that have countinuously differentiable inverses. Motivated by the concept of fluid dynamics, diffeomorphisms are built by the evolution of time-dependent flow of vector fields, according to the following evolution equation.

Definition 2.4. **[You10, 8.2.1] The Flow Equation**

Let $v : \Omega \times [0, 1] \to \Omega$, $v_t(x) \coloneqq v(x, t)$ be a time-dependent vector-field. The flow equation reads

$$\dot{\phi}_t = v_t \circ \phi_t,$$

and v is called the flow of ϕ.

To ensure that the evolved deformation ϕ_t^v is a diffeomorphism, it is necessary for v_t to satisfy strong enough smoothness constraints [You10].

Definition 2.5. [You10, Def. 8.12] Admissible Space

V is an *admissible space* if it is continuously embedded in $C_0^1(\Omega, \mathbb{R}^d)$, or equivalently if there exists a constant $c > 0$, such that $\|u\|_{1,\infty} \leq c\|u\|_V$ for all $v \in V$.

Note that the diffeomorphism generated by a given flow field is unique, while one diffeomorphism can generally evolve from more than one flow field.

As a sufficient condition for the well-posedness of the flow equation, one assumes v_t to be in an admissible space [You10]. Moreover, [You10, Theorem 8.7] states that the solution of the flow equation is a diffeomorphism. The concept of reproducing kernel Hilbert spaces (RKHS) yields a family of such spaces and will be introduced in the following section.

2.1.4 Reproducing Kernel Hilbert Spaces

In this section we will introduce reproducing kernel Hilbert spaces (RKHS). They fall into the class of admissible spaces and thus ensure the well-posedness of the flow equation for time-dependent vector fields in the space. The following definition summarizes the assumptions in [You10, chapter 9.1].

Definition 2.6. Reproducing Kernel Hilbert Space

Let $\Omega \subset \mathbb{R}^d$, and let $V \subset L^2(\Omega, \mathbb{R}^d) \cap C^0(\Omega, \mathbb{R}^d)$ be a Hilbert space with inner product $\langle \cdot, \cdot \rangle_V$. V is a *Reproducing Kernel Hilbert Space* (RKHS) if the point evaluation functional $\delta_x \colon V \to \mathbb{R}^d$, $\delta_x(v) \coloneqq v(x)$ is continuous on V for all $x \in \mathbb{R}^d$.

This property allows the definition of the reproducing kernel of V. The Riesz representation theorem [You10, Theorem A.10] states that, for every element μ in the dual space V^*, there exists a unique $h \in V$ with $\mu(v) = \langle h, v \rangle_V$, for all $v \in V$; moreover there exists a unique linear operator $\mathrm{K} \colon V^* \to V$ with $(\mu | v)_{V^*,V} = \langle \mathrm{K}\mu, v \rangle_V$. Defining $\delta_x^\alpha \in V^*, v \mapsto \langle \alpha, v(x) \rangle_{\mathbb{R}^d}$ for $x, \alpha \in \mathbb{R}^d$, it follows

$$\forall v \in V \colon \langle \mathrm{K}\delta_x^\alpha, v \rangle_V = \langle v(x), \alpha \rangle_{\mathbb{R}^d}. \tag{10}$$

The function $\alpha \mapsto \delta_x^\alpha$ is linear and the kernel K is unique. So $\mathrm{K}\delta_x^\alpha$ is linear in α. Let $x, y \in \mathbb{R}^d$ and consider the function $\alpha \mapsto (\mathrm{K}\delta_x^\alpha)(y)$. This is a linear function mapping from $\Omega \subset \mathbb{R}^d$ to $\mathbb{R}^d$, thus there exists a kernel matrix $\tilde{\mathrm{K}}(x, y) \in \mathbb{R}^d \times \mathbb{R}^d$:

$$\tilde{\mathrm{K}}(x, y)\alpha = (\mathrm{K}\delta_x^\alpha)(y). \tag{11}$$

The kernel K has the reproducing property in the following sense: For every function $v \in V$ the point evaluation at $x \in \mathbb{R}^d$ can be performed by taking an inner product with a function determined by the kernel. Moreover, one can show that every symmetric positive definite kernel K defines such a Hilbert space [Aro50, p.347].

Several choices of reproducing kernels haev been proposed. In this work we will use the Gaussian kernel. For the choice of a Gaussian kernel, the matrix $\tilde{\mathrm{K}}(x,y)$ can be written as $\tilde{\mathrm{K}}(x,y) = \mathrm{k}(x,y)\mathrm{Id}$, where $\mathrm{k}(x,y) = \exp\left(-\frac{\|x-y\|}{\sigma^2}\right)$ is the Gaussian distribution. The framework can be easily adapted to the choice of other kernels.

2.1.5 The LDDMM Registration Problem for Shapes

For the regularization term $\mathcal{R}(\phi)$ it is useful to have a metric on the space of deformations. Here we will conclude that for a subgroup of $\mathrm{Diff}_0^l(\Omega)$ that is defined by an admissible space V in the following definition, the norm on V determines a metric on the associated space of diffeomorphisms.

Definition 2.7

Let V be an admissible space of vector fields. We denote ϕ^v the solution of the flow equation, with

$$v \in X_V := \Big\{ v\colon [0,1] \times \Omega \to \mathbb{R}^d \Big| v_t \in V \quad \forall t \in [0,1], \\ \|v\|_{X_V} := \int_0^1 \|v_t\|_V \mathrm{d}t < \infty \Big\}. \tag{12}$$

Then we define $\mathrm{Diff}_V(\Omega) := \{\phi^v, v \in X_V(\Omega)\}$ the group of diffeomorphisms associated to V.

Then $\mathrm{Diff}_V(\Omega)$ is a subgroup of $\mathrm{Diff}_0^l(\Omega)$, as proven in [You10, Theorem 8.14] and [You10, Theorem 8.5]. The group Diff_V naturally comes with a metric as the next theorem taken from [You10] states.

Theorem 2.8. [You10, Th. 8.15] A Metric on Diff_V

Let V be an admissible Banach space. For $\psi, \bar{\psi} \in \mathrm{Diff}_V$ and $\phi^v \in \mathrm{Diff}_V$ the solution of the flow equation for a given time-dependent vector field v,

$$\mathrm{d}_V(\psi, \bar{\psi}) = \inf_{v_t \in V} \left\{ \int_0^1 \|v_t\|_V \mathrm{d}t, \quad \psi = \bar{\psi} \circ \phi_{t=1}^v \right\} \tag{13}$$

is a metric on Diff_V and $(\mathrm{Diff}_V, \mathrm{d}_V)$ is a complete metric space.

As the metric d_V provides a measure of distances in Diff_V, or equivalently a measure of lengths of paths in Diff_V, we can use it as a regularization term in the registration problem. In the following formulation of the registration problem we minimize not over the deformation ϕ itself, but over its flow v of velocity fields. By adding the flow equation as a constraint for the problem, this amounts to the same solution.

Problem 2.9

Let $q\colon [0,1] \to \mathcal{O}$, $v\colon [0,1] \to V$, and $q_S, q_T \in \mathcal{O}$. Consider the minimization of the

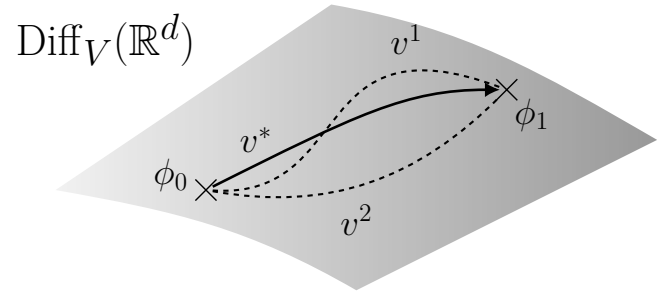

Figure 2: Different paths on the manifold $\mathrm{Diff}_V(\mathbb{R}^d)$ starting at ϕ_0 and ending at ϕ_1. The endpoint ϕ_1 can be reached from ϕ_0 by the flows of v^1, v^2 or v^*. In the shooting method only the shortest (i.e. geodesic) paths are considered, here indicated by v^*. The flows of v^1 and v^2 are longer in the sense that the energy $\int_0^1 \|v_t\|_V \mathrm{d}t$ is higher.

functional

$$\mathcal{J}(q,v) = \frac{1}{2}\int_0^1 \|v_t\|_V \mathrm{d}t + \mathcal{U}(q_1, q_T) \tag{14}$$

$$\begin{aligned} s.t. \qquad & \dot{q}_t = \xi_{q_t} v_t \\ & q_0 = q_S \end{aligned} \tag{15}$$

Here, q_S represents the source shape and q_T the target shape that is aimed to be reached. The time-dependent shape q is evolving from the source shape over time according to the flow equation of the velocity field v. Moreover, $\xi_{q_t}(v_t)$ is the infinitesimal action of v_t on q_t, giving the speed of the shape at time t, see definition 2.1.

First approaches attempted to solve this problem by optimizing over the time-dependent velocity fields, see for example the studies of [DGM98] and [MTY02]. However, this problem is very high-dimensional because (1) the velocity fields are continuous and (2) the flow of vector fields has to be computed over time. One diffeomorphism can be evolved from different time-dependent velocity fields, so there is more than one tuple (q, v) satisfying the flow equation with the same endpoint q_1 at time $t = 1$. The data term $\mathcal{U}(q_1, q_T)$ in the functional $\mathcal{J}$ has the same value for each of those tuples, while the values of the regularization term differ. If we fix the endpoint q_1, and therefore the data term $\mathcal{U}(q_1, q_T)$, the minimizer of $\mathcal{J}$ is also a minimizer of the regulization term. Since it defines a metric, the minimizer of the regularization term is unique.

Therefore, instead of optimizing over all possible flows, we can consider the subspace of optimal flows for a given diffeomorphism. This amounts to considering geodesics on the space of diffeomorphisms, or equivalently on the orbit of the reference shape q_S. The concept of geodesics on the $\mathrm{Diff}_V(\mathbb{R}^d)$ is visualized in figure 2. Indeed it can be shown that the optimal flow can be described only by the momentum at initial time. The idea of geodesic shooting takes advantage of this fact and will be introduced in the next section.

2.1.6 Geodesic Shooting

One can differentiate between two types of shooting equations, the Lagrangian and the Hamiltonian shooting equations. Originally the shortest geodesic paths on the diffeomorphisms were defined via a Lagrangian function given by the kinetic energy of the vector field v [BMTY05]. The geodesic controls are here the *momentum* $m_t \in V^*$ associated to v_t in the space V, given by $m_t = \mathrm{K}^{-1}v_t$. The shooting method is based on the fact that the geodesic controls satisfy a conservation law. This conservation law is a special case of the principle of least action [MTY15] which is a cornerstone in geometric and fluid mechanics [HSS09, MR13].

Seen as in the initial configuration, the momentum is a constant of motion [BH15, sec. 2.6, 2.11]. Through the conservation law, the momentum and therefore the velocity field over the whole time interval $[0, 1]$ is encoded. Adding this as a constraint to the problem 2.9 allows optimization over the initial momenta instead of time-dependent velocity field, which reduces the parameter space.

Opposed to the Lagrangian approach, one can consider the Hamiltonian reduction of the Lagrangian on $\mathbb{R}^d$. While the momentum $m_t \in V^*$ has the same dimension as the diffeomorphic flow ϕ^v, the momentum in the Hamiltonian reduction has the advantage of reduced dimensionality: the momentum m_t is replaced by the costate p_t which lies in the cotangent space $\mathrm{T}_{q_t}\mathcal{O}^*$ of the state $q_t \in \mathcal{O}$ [MTY15]. Considering shapes $q_t \in C^p(M, \mathbb{R}^d)$, the costate p_t has the same dimension as the manifold M. This is despite the fact that the diffeomorphism is extended to act on the entire space $\mathbb{R}^d$. For landmarks, curves or surfaces this significantly reduces the dimensionality.

Both approaches of geodesic shooting are widely used. In this thesis we will use the Hamiltonian reduction, as all problems are formulated in terms of shapes and can be applied to landmark, curve or image registration. In the next section, we will derive the shooting equations for the Hamiltonian framework.

2.1.7 Hamiltonian Geodesic Equations

In the following definition we introduce the Hamiltonian function for our particular setting. The definition is adapted from [MTY15, 3.4] to our framework. The costate $p_t \in \mathrm{T}^*_{q_t}\mathcal{O}$ is in the cotangent space of the shape space $\mathcal{O}$.

Definition 2.10. Hamiltonian Function

The Hamiltonian function $\mathcal{H}\colon \mathcal{O} \times \mathrm{T}^*_{q_t}\mathcal{O} \times V \to \mathbb{R}$ for the minimization problem 2.9 is defined as

$$\mathcal{H}(p_t, q_t, v_t) \coloneqq (p_t | \xi_{q_t} v_t)_{T^*_{q_t}\mathcal{O}, T_{q_t}\mathcal{O}} - \frac{1}{2}(K^{-1}v_t | v_t)_{V^*,V}. \tag{16}$$

The Pontryagin-Maximum-Principle (PMP) yields geodesic equations for the Hamiltonian system, that are equivalent to the conservation laws of the Lagrangian system described in the previous section [MTY15, 3.5]. For our setting, the PMP gives the

following system of equations. The theorem is adapted from [MTY15, theorem 1] to our notation.

Theorem 2.11. Hamiltonian Geodesic Equations

If v is an optimal solution for the minimization problem 2.9, there exists a time-dependent costate p_t such that the system

$$\dot{q}_t = \partial_p \mathcal{H}(p_t, q_t, v_t) \tag{17}$$
$$\dot{p}_t = -\partial_q \mathcal{H}(p_t, q_t, v_t) \tag{18}$$
$$v_t = \mathrm{K}\xi^*_{q_t} p_t \tag{19}$$

with the endpoint condition

$$p_1 = -\partial_q \mathcal{U}(q_1, q_T) \tag{20}$$

is satisfied.

As this is a well known result we don't provide a rigorous proof here, but show its general procedure in order to get an intuition of the meaning of equations (19). It follows the proof provided in [MTY15]. Adding a Lagrange multiplier for the condition $\dot{q}_t - \xi_{q_t} v_t = 0$ in the functional $\mathcal{J}(q, v)$ in problem 2.9 gives us the functional

$$\bar{\mathcal{J}}(q, p, v) = \mathcal{U}(q_1, q_T) + \frac{1}{2}\int_0^1 \|v_t\|^2 \mathrm{d}t + \int_0^1 (p_t | \dot{q}_t - \xi_{q_t} v_t)\mathrm{d}t. \tag{21}$$

Then

$$\bar{\mathcal{J}}(q, p, v) = \mathcal{U}(q_1, q_T) + \int_0^1 (p_t|\dot{q}_t) - \mathcal{H}(q_t, p_t, v_t)\mathrm{d}t, \tag{22}$$

the minimizer (q^*, p^*, v^*) of 2.9 is a stationary point of $\bar{\mathcal{J}}$ and must satisfy

$$\begin{aligned} \partial_q \bar{\mathcal{J}}(q^*, p^*, v^*) &= 0 \\ \partial_p \bar{\mathcal{J}}(q^*, p^*, v^*) &= 0 \\ \partial_v \bar{\mathcal{J}}(q^*, p^*, v^*) &= 0. \end{aligned} \tag{23}$$

In the following we will compute the expression for $\partial_q \bar{\mathcal{J}}(q^*, p^*, v^*)$, $\partial_p \bar{\mathcal{J}}(q^*, p^*, v^*)$ and $\partial_v \bar{\mathcal{J}}(q^*, p^*, v^*)$.

Variation of $\bar{\mathcal{J}}$ with respect to p. Let $\delta\colon [0,1] \to \mathrm{T}_{q_t}\mathcal{O}$, and $\delta_t \coloneqq \delta(t)$ be of compact support for all $t \in [0,1]$. Taking the variation of $\bar{\mathcal{J}}$ with respect to p yields

$$\begin{aligned} \left(\partial_p \bar{\mathcal{J}}(q, p, v)\middle|\delta\right) &= \frac{\mathrm{d}}{\mathrm{d}x}\Big|_{x=0} \bar{\mathcal{J}}(q, p + x\delta, v) \\ &= \frac{\mathrm{d}}{\mathrm{d}x}\Big|_{x=0} \left[\mathcal{U}(q_1, q_T) + \int_0^1 (p_t + x\delta_t | \dot{q}_t) - \mathcal{H}(q_t, p_t + x\delta_t, v_t)\right]\mathrm{d}t \end{aligned} \tag{24}$$

The dat term $\mathcal{U}(q_1, q_T)$ is independent of p and therefore the term $\frac{\mathrm{d}}{\mathrm{d}x}\mathcal{U}(q_1, q_T)$ is zero. Because $(p_t + x\delta_t|\dot{q}_t) - \mathcal{H}(q_t, p_t + x\delta_t, v_t)$ is continuously differentiable in t and in x we can apply the Leibniz integral rule. We have

$$\begin{aligned}\Big(\partial_p\bar{\mathcal{J}}(q,p,v)\Big|\delta\Big) &= \int_0^1 \frac{\mathrm{d}}{\mathrm{d}x}\Big|_{x=0} [(p_t + x\delta_t|\dot{q}_t) - \mathcal{H}(q_t, p_t + x\delta_t, v_t)]\mathrm{d}t \\ &= \int_0^1 (\delta_t|\dot{q}_t) - \frac{\mathrm{d}}{\mathrm{d}x}\Big|_{x=0} \mathcal{H}(q_t, p_t + x\delta_t, v_t)\mathrm{d}t \\ &= \int_0^1 (\delta_t|\dot{q}_t) - (\partial_p\mathcal{H}(q_t, p_t, v_t)|\delta_t)\mathrm{d}t \\ &= \int_0^1 (\delta_t|\dot{q}_t - \partial_p\mathcal{H}(q_t, p_t, v_t))\mathrm{d}t.\end{aligned} \tag{25}$$

This gives the expression

$$\partial_p\bar{\mathcal{J}}(q,p,v) = \int_0^1 \dot{q}_t - \partial_p\mathcal{H}(q_t, p_t + x\delta_t, v_t)\mathrm{d}t. \tag{26}$$

Because $\Big(\partial_p\bar{\mathcal{J}}(q,p,v)\Big|\delta\Big) = 0$ holds for every δ of compact support, we deduce

$$\dot{q}_t - \partial_p\mathcal{H}(q_t, p_t + x\delta_t, v_t) = 0 \tag{27}$$

for almost all $t \in [0,1]$.

Variation of $\bar{\mathcal{J}}$ with respect to v. Now let $\delta\colon [0,1] \to V$. Taking the variation of $\bar{\mathcal{J}}$ with respect to v yields

$$\begin{aligned}\Big(\frac{\partial}{\partial v}\bar{\mathcal{J}}(p,q,v)\Big|\delta\Big) &= \frac{\mathrm{d}}{\mathrm{d}x}\Big|_{x=0} \bar{\mathcal{J}}(q,p,v + x\delta) \\ &= \frac{\mathrm{d}}{\mathrm{d}x}\Big|_{x=0} \Big[\mathcal{U}(q_1,q_T) + \int_0^1 (p_t|\dot{q}_t) - \mathcal{H}(q_t,p_t,v_t + x\delta_t)\Big]\mathrm{d}t \\ &= \frac{\mathrm{d}}{\mathrm{d}x}\Big|_{x=0} \int_0^1 -\mathcal{H}(q_t,p_t,v_t + x\delta_t)\mathrm{d}t\end{aligned} \tag{28}$$

Again, since $\mathcal{U}(q_1, q_T)$ and $(p_t|\dot{q}_t)$ are independent of v the terms cancel. Now inserting the expression for $\mathcal{H}(q_t, p_t, v_t)$ leads to

$$\begin{aligned}\Big(\frac{\partial}{\partial v}\bar{\mathcal{J}}(p,q,v)\Big|\delta\Big) &= \int_0^1 \frac{\mathrm{d}}{\mathrm{d}x}\Big|_{x=0} \Big[(p_t|\xi_{q_t}(v_t + x\delta_t)) - \frac{1}{2}(\mathrm{K}^{-1}(v_t + x\delta_t)|v_t + x\delta_t)\Big]\mathrm{d}t \\ &= \int_0^1 (\xi^*_{q_t}p_t|\delta_t) - (\mathrm{K}^{-1}v_t|\delta_t)\mathrm{d}t.\end{aligned} \tag{29}$$

This yields the result

$$\xi^*_{q_t}p_t - \mathrm{K}^{-1}v_t = 0 \tag{30}$$

for almost all $t \in [0,1]$.

Variation of $\bar{\mathcal{J}}$ with respect to q. Let $\delta\colon [0,1] \to \mathcal{O}$ with $\delta_0 = 0$. This ensures that $q_t + x\delta_t$ satisfies the boundary condition $q_0 + x\delta_0 = q_S$, if q satisfies $q_0 = q_S$. Taking the variation of $\bar{\mathcal{J}}$ with respect to q yields

$$\begin{aligned}\left(\partial_q \bar{\mathcal{J}}(p,q,v)\middle|\delta\right) &= \frac{\mathrm{d}}{\mathrm{d}x}\Big|_{x=0} \bar{\mathcal{J}}(q + x\delta, p, v) \\ &= \frac{\mathrm{d}}{\mathrm{d}x}\Big|_{x=0} \Big[\mathcal{U}(q_1, q_T) + \int_0^1 (p_t|\dot{q}_t) - \mathcal{H}(q_t + x\delta_t, p_t, v_t)\Big]\mathrm{d}t\end{aligned} \tag{31}$$

Partial integration of the term $\int_0^1 (p_t|\dot{q}_t)$ yields

$$\int_0^1 (p_t|\dot{q}_t)\mathrm{d}t = \left[(p_t|q_t)\right]_{t=0}^1 - \int_0^1 (\dot{p}_t|q_t)\mathrm{d}t, \tag{32}$$

which yields, together with (31),

$$\begin{aligned}\left(\partial_q \bar{\mathcal{J}}(p,q,v)\middle|\delta\right) &= \frac{\mathrm{d}}{\mathrm{d}x}\Big|_{x=0} \Big[\mathcal{U}(q_1, q_T) + (p_1|q_1 + x\delta_1) - (p_0|q_0 + x\delta_0) \\ &\qquad + \int_0^1 -(\dot{p}_t|q_t + x\delta_t) - \mathcal{H}(q_t + x\delta_t, p_t, v_t)\mathrm{d}t\Big] \\ &= \left(\partial_q \mathcal{U}(q_1, q_T)\middle|\delta_1\right) + (p_1, \delta_1) - (p_0|\delta_0) \\ &\qquad - \int_0^1 (\dot{p}_t|\delta_t) + \left(\partial_q \mathcal{H}(q_t, p_t, v_t)\middle|\delta_t\right)\mathrm{d}t.\end{aligned} \tag{33}$$

This gives

$$(\dot{p}_t|\delta_t) + \partial_q \mathcal{H}(q_t, p_t, v_t) = 0 \tag{34}$$

for all $t \in [0,1]$, and the boundary condition

$$p_1 = -\partial_q \mathcal{U}(q_1, q_T). \tag{35}$$

Let us take a closer look at what the geodesic equations (19) mean. Computing $\partial_p \mathcal{H}(q_t, p_t, v_t)$ yields

$$\begin{aligned}\left(\partial_p \mathcal{H}(q_t, p_t, v_t)\middle|\delta_t\right) &= \frac{\mathrm{d}}{\mathrm{d}x}\Big|_{x=0} \Big[(p_t + x\delta_t|\xi_{q_t} v_t) - \frac{1}{2}(\mathrm{K}^{-1} v_t|v_t)\Big] \\ &= (\delta_t|\xi_{q_t} v_t).\end{aligned} \tag{36}$$

We see that the condition $\dot{q}_t = \partial_p \mathcal{H}(p_t, q_t, v_t)$ corresponds to the flow equation $\dot{q}_t = \xi_{q_t} v_t$.

The equation

$$v_t = \mathrm{K}\xi_{q_t}^* p_t \tag{37}$$

gives the relation between the costate p_t and the velocity field v_t. The terms $\mathrm{K}^{-1} v_t$ and $\xi_{q_t}^* p_t$ are both elements of V^*. While $m_t \coloneqq \mathrm{K}^{-1} v_t$ is of same dimension as the velocity field v_t, we see from

$$\mathrm{K}^{-1} v_t = \xi_{q_t}^* p_t \tag{38}$$

that it is supported only on $q_t(x) \subset \mathbb{R}^d$. This is why it is possible to reduce dimensionality by minimizing over the costate p instead of the momentum $m = \xi^*_{q_t} p$. This will also be of importance when we consider the LDDMM framework as a special case of deformation modules in chapter 2.3. The condition $\dot{p_t} = \partial_q \mathcal{H}(q_t, p_t, v_t)$ gives the conservation law for the costate p.

2.2 Constrained LDDMM for Multi-Shapes

In the LDDMM setting described in chapter 2.1, a global diffeomorphism of the whole ambient space is considered. This corresponds to assuming the ambient space to represent one homogeneous medium, with the same regularity assumptions over the whole space. In some applications this assumption may not be appropriate. In medical applications the shapes often correspond to different organs in the human body. The organs lie very close to each other in the human body. At the same time the organs might have different physical properties. This amounts to diffeomorphisms of different regularities acting on the shapes. Associating independent diffeomorphisms for each of the shapes will in general lead to inconsistencies of the overall deformation: Without taking the deformations of all shapes into account, overlapping of the shapes will be possible.

In [ATTY15a], this is solved by embedding the shapes into a background, that corresponds to the complement of the shapes. The background is deformed by a new deformation that is linked to the deformations of the shapes by linear boundary constraints. Through the boundary constraints the background boundaries can be forced to move with the shapes. This setting is modeled as the following constrained optimal control problem, that we adapted to our setting from [ATTY15a].

Problem 2.12. Constrained Registration Problem for Multi-Shapes

Let $\mathcal{O}^1, ..., \mathcal{O}^n$ be shape spaces, where $\mathrm{Diff}_0^{l_i}(\mathbb{R}^d)$ act smoothly with order l_i on $\mathcal{O}^i$ for $i = 1, ..., n$. Let $q_S, q_T \in \mathcal{O}$. Let $V^1, ..., V^k$ be reproducing kernel Hilbert spaces of vector fields on $\mathbb{R}^d$ of class $C_0^{l_i+k_i}$ with kernels K_i. Let $\xi \colon \mathcal{O} \times V \to \mathrm{T}_{q_t}\mathcal{O}$ be the infinitesimal action on $\mathcal{O}$ as in definition 2.1. Let Y be a Banach space and $C \colon \mathcal{O} \to L(V, \mathrm{Y})$ a bounded linear operator from V to Y. The multi-shape $q = (q^1, ..., q^n)$ is an element of the shape space $\mathcal{O} = \mathcal{O}^1 \times ... \times \mathcal{O}^n$.

Consider the minimization of the energy functional

$$\mathcal{J}(q, v) = \sum_{i=1}^{n} \int_0^1 \|v_i(t)\|^2_{V^i} \mathrm{d}t + \sum_{i=1}^{n} \mathcal{U}^i(q_1^i, q_T) \tag{39}$$

over the time-dependent vector fields $v^i, i = 1, ..., n$ such that

$$\begin{aligned} \dot{q^i}_t &= \xi^i_{q_t^i} v_t \\ q_0 &= q_S \\ \mathrm{C}_{q_t} v_t &= 0 \end{aligned} \tag{40}$$

for all $i = 1, ..., n$ for almost all $t \in [0, 1]$.

Compared to problem 2.9, the constraints are extended by the linear constraints $\mathrm{C}_{q_t} v_t = 0$, which links the velocities and therefore the deformations of different shapes. The interaction of the shapes is modeled by the continuous operator $C\colon \mathcal{O} \to L(V, Y)$ that takes values in the space of bounded linear operators from $V := \prod_{i=1}^{k} V^k$ to Y. Two special cases of constraints are introduced in the following definition. The state constraints depend only on the state of the shape $q \in \mathcal{O}$ while the kinetic constraints depend on the associated vector field $v \in V$.

Definition 2.13. State Constraints and Kinetic Constraints

Let Y be a Banach space. Let

$$\mathrm{C}^{\mathrm{state}}\colon \mathcal{O} \to \mathrm{Y} \tag{41}$$

be a continuous linear and differentiable function. We say the state constraints are satisfied for $q \in \mathcal{O}$, if $\mathrm{C}^{state}(q) = 0$.

Moreover, let $C\colon \mathcal{O} \times V \to \mathrm{Y}$ be a continuous function that is linear in v for every $q \in \mathcal{O}$, and

$$\mathrm{C}_q^{\mathrm{kin}}\colon V \to \mathrm{Y},\ v \mapsto \mathrm{C}_q^{\mathrm{kin}}(v) = C(q, v) \tag{42}$$

The kinetic constraints are satisfied for $v \in V$, if $\mathrm{C}_q^{\mathrm{kin}}(v) = 0$.

Remark 2.14

For state constraints, there exists an equivalent formulation of kinetic constraints, which was pointed out in [Arg14]. The state constraints $\mathrm{C}^{\mathrm{state}}$ are equivalent to the kinetic constraints $\mathrm{C}_q^{\mathrm{kin}}\colon V \to \mathrm{Y}, v \mapsto \mathrm{C}(q, v)$ with $C\colon \mathcal{O} \times V \to \mathrm{Y}, (q, v) \mapsto \partial_q \mathrm{C}^{\mathrm{state}} \xi_q(v)$ [Arg14, p. 157].

This can be shown as follows: We recall that the vector field v satisfies the flow equation

$$\dot{q} = \xi_q v. \tag{43}$$

Taking the derivative of $\mathrm{C}^{\mathrm{state}}(q_t)$ with respect to time gives

$$\frac{\mathrm{d}}{\mathrm{d}t}\mathrm{C}^{\mathrm{state}}(q) = \partial_q \mathrm{C}^{\mathrm{state}}(\dot{q}) = \partial_q \mathrm{C}^{\mathrm{state}} \xi_q(v) = \mathrm{C}_q^{\mathrm{kin}}(v). \tag{44}$$

So given $\mathrm{C}^{\mathrm{state}}(q_0) = 0$, the state constraints $\mathrm{C}^{\mathrm{state}}(q) = 0$ are equivalent to the kinetic constraints $\mathrm{C}_q^{\mathrm{kin}}(v) = 0$.

For the examples we will examine, it is intuitive to express the constraints as state constraints. However, for the implementation it is more convenient to have constraints on the velocity fields, which is the reason why we cover both in this thesis. In the following, two examples of constraints will be discussed.

Example 2.15. Identity Constraints

The identity constraints model the case that certain points of different shapes are

forced to coincide.

Assume that we want to study a cat's shape. The cat's body and the tail have very different properties, so it is sensible to assign them with different spaces of vector fields. In the model they are considered two distinct shapes $q^1 \in \mathcal{O}^1$ and $q^2 \in \mathcal{O}^2$. In order to attach the cat's tail to the body, the contact points of both shapes must be equal. Let $\bar{q}^1 \subset q^1, \bar{q}^2 \subset q^2$ be the subsets of the shapes q^1, q^2 that correspond to these contact points. Let v^i be the velocity field acting on q^i for $i = 1, 2$.

The corresponding state constraints function $\mathrm{C}^{\mathrm{state}}$ is

$$\mathrm{C}^{\mathrm{state}}(q) = \bar{q}^1 - \bar{q}^2. \tag{45}$$

The kinetic constraints are given by

$$\begin{aligned} \mathrm{C}_q^{\mathrm{kin}}(v) &= \xi^1_{\bar{q}^1}(v^1) - \xi^2_{\bar{q}^2}(v^2) \\ &= v^1(\bar{q}^1) - v^2(\bar{q}^2) \end{aligned} \tag{46}$$

This enforces that the tail and body of the cat are deformed in the same way at the contact points.

Example 2.16. Sliding Constraints

Another possible kind of constraints are sliding constraints. Especially for the application of modeling breathing motion in abdominal images these are of interest. In the setting of abdominal organs modeling, the organs are not stitched to each other at their boundaries. Instead, the organs can slide along the surrounding tissue. In [ATTY15a] sliding constraints that allow this kind of motion are introduced. The idea behind the sliding constraints is that the normals of the boundaries sliding along each other have the same direction. So the constraints are implemented forcing the normals of the deformed shapes to have the same direction. The sliding constraints are not yet implemented in our new proposed framework, but would be of high interest for future work. We refer to [Arg14] and [ATTY15a] for further details.

The latter example motivates the definition of the setting where shapes are embedded in a background. This was proposed in [Arg14], defining the background space as the product space of all shape spaces. Then the boundaries of the shapes are forced to coincide with the corresponding boundaries in the background. We will use this setting later in our examples.

The next theorem regarding existence of minimizers for problem 2.12 is taken from [Arg14] and adapted to our notation. We assume that $q \in \mathcal{O}$ is differentiable and $\dot{q}_t = \xi_{q_t} v_t$ has a unique solution.

Theorem 2.17. Existence of Minimizers for Multi-Shape Registration

Assume that V is a RKHS of vector fields of class C^{l+1} on $\mathbb{R}^d$, $q \mapsto \mathrm{C}_q$ is continuous and that $\mathcal{U}$ is bounded below and lower semi-continuous. If q_0 has compact support, then problem 2.12 has at least one solution.

Proof: The theorem is a direct consequence of [Arg14, Theorem 10.1]. ■

2.3 Deformation Modules

In this section we will define the notion of deformation modules as introduced in [Gri16]. We will explain the intuition behind the framework and then formally define it. Moreover, we cover some assumptions that have to be made in order to ensure the existence of optimal deformations.

Deformation modules allow to build vector fields satisfying certain constraints, for example allowing only local translations or local scalings. These vector fields are built by a generator function ζ, that depends on a geometrical descriptor and a control variable. The geometrical descriptor gives information about the geometry of the vector field. For the example of local translations, the geometrical descriptor corresponds to the points where the local translations are based. The control variables are coefficients defining the vectorfield. For the example of local translations, they correspond to translation vectors for each point of the geometrical descriptor. For the case of a rotation the control variable would correspond to a scalar defining the rotation angle.

The control variables are optimized so that the shape deformed by the resulting diffeomorphism fits the target. For each geometrical descriptor q, a cost function depending on the control variable h corresponds to the cost it takes to deform the geometrical descriptor by the resulting vector field $\zeta_q(h)$. The cost function will serve as a regularisation term in the registration problem. Since the geometrical descriptors move with the application of the vector field, a mechanism to update their positioning will be defined.

The following definition formalises this intuition.

Definition 2.18. [Gri16, Def. 18] Deformation Module

Let $k, l \in \mathbb{N}$. $\mathcal{M} \coloneqq (\mathcal{O}, \mathrm{H}, \zeta, \xi, c)$ is a C^k-deformation module of order l with geometrical descriptors in $\mathcal{O}$, controls in H, field generator ζ, infinitesimal action ξ and cost c, if

- $\mathcal{O} \subset \mathbb{R}^m$ is a C^k-shape space on $\mathbb{R}^d$ of order l with infinitesimal action $\xi \colon \mathcal{O} \times C_0^l(\mathbb{R}^d) \to \mathrm{T}\mathcal{O}$,
- H is a finite-dimensional Euclidean space,
- $\zeta \colon (q, h) \in \mathcal{O} \times \mathrm{H} \to \zeta_q(h) \in C_0^l(\Omega, \mathbb{R}^d)$ is continuous, with $h \mapsto \zeta_q(h)$ linear and $q \mapsto \zeta_q$ of class C^l,
- $c \colon (q, h) \in \mathcal{O} \times \mathrm{H} \to c_q(h) \in \mathbb{R}^+$ is a continuous mapping such that $q \mapsto c_q$ is smooth and for all $q \in \mathcal{O}, h \mapsto c_q(h)$ is a positive quadratic form on H, thus defining a smooth metric on $\mathcal{O} \times \mathrm{H}$.

Figure 3 visualizes how the deformed shape is obtained by the given initial shape and

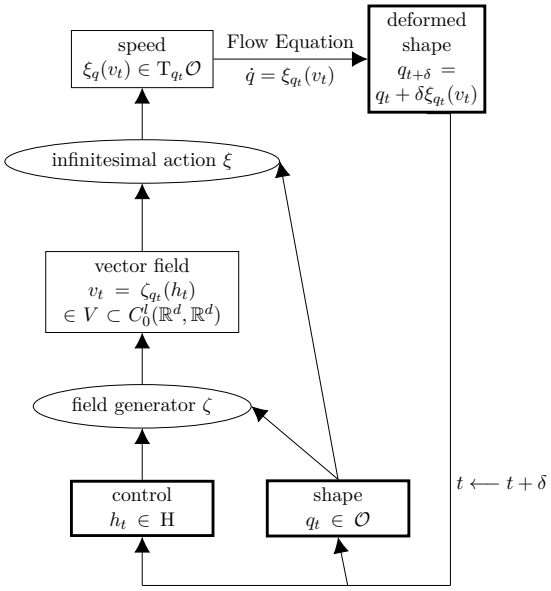

Figure 3: Evolution of the shape during time by a deformation module. Given a shape and control at time t, the field generator builds a velocity field $v = \zeta_{q_t}(h_t)$. Then the infinitesimal action gives the speed $\xi_{q_t}(v_t)$, which is an element of the tangent shape space, specifying how the velocity field acts on the shape q_t. The speed of q_t at time t is used in the shooting method to obtain the deformed shape at the next time step in the iteration. The control at time $t + \delta$ is updated depending on the shape $q_t + \delta$.

deformation module. For a given time point $t \in [0, 1]$, the control h_t and shape q_t are passed to the field generator to obtain the velocity field v_t. Then the vector field is lifted to the tangent space $\mathrm{T}_{q_t}\mathcal{O}$ by the infinitesimal action, which is also dependent on the shape. This gives the speed of the shape time point t. The deformation ϕ_t is obtained by integration of the flow equation and applied to the shape.

Notice that the shape and control are different for each time point. The shape evolves with the deformation in time. We will refer to a deformation ϕ that can be obtained by the flow created by a deformation module, as a modular deformation.

Example Collection of Deformation Modules

In the following we will present some examples of deformation modules. All examples are considered in two dimensions. For a broader overview we refer to [Gri16].

Example 2.19. Sum of Local Translations

A simple example is the sum of local translations, shown in figure 4. We consider a finite number of translation vectors attached to points. The points are called geometrical descriptors. If we consider a shape that is a set of landmarks, the geometrical descriptors can be the same as the points of the shape. A different possibility is where the geometrical descriptors are a certain subset of the ambient space, for example the mean point.

The velocity field results from the control vectors by convolution with the kernel K. If the geometrical descriptors are close to each other compared to the scale of

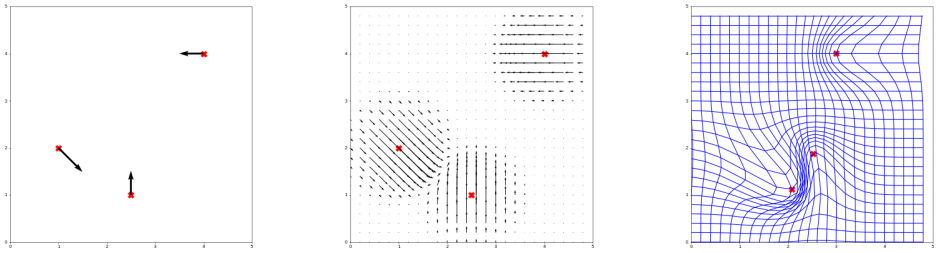

(a) Geometrical descriptors q_t (red crosses) and controls h_t (vectors) for a local translation deformation module

(b) The resulting vector field v_t at time $t = 0$.

(c) The deformed grid at time $t = 1$. The red crosses indicate the location of the transported geometrical descriptors.

Figure 4: Example of a local translation deformation module. The geometrical descriptors consist of three landmarks. The control variables are three translation vectors.

the reproducing kernel, the velocities generated by them will influence each other. If they are distant from each other the velocities still sum up, but the influence is very small.

Example 2.20. Local Scaling

A more structured deformation module is a local scaling, shown in figure 5. For a local scaling the geometrical descriptor q_t is one point that gives the scaling center. Then on a circle of radius $\sigma/3$ we set three equally distributed points $z^1(q_t), z^2(q_t)$ and $z^3(q_t)$ that build the support for the translation vectors of direction $z^i(q_t) - q_t$. By convolution with the kernel K, a velocity field results where velocities pointing away from the geometrical descriptor are getting smaller with increased distance from the scaling center. The control variable h_t is a scalar that determines the amount of scaling. By setting a negative value for the control variable, reduction can also be generated.

Example 2.21. LDDMM as a special case of Deformation Modules

In the case of LDDMM, the considered vector fields lie in a RKHS V_σ. Consider the space of controls

$$\mathrm{H} := V_\sigma \tag{47}$$

with the field generator

$$\zeta \colon \mathcal{O} \times \mathrm{H} \to V_\sigma, (q, h) \mapsto \zeta_q(h) = h. \tag{48}$$

Then for $v = \zeta_q(h)$, the cost function $c \colon \mathcal{O} \times \mathrm{H} \to \mathbb{R}^+$ can be defined by

$$c_q(h) = \|\zeta_q(h)\|^2_{V_\sigma} = \|h\|^2_{V_\sigma}. \tag{49}$$

This definition is equivalent to the LDDMM setting. Considering $\mathrm{H} = V_\sigma$ does not satisfy the definition of a deformation module in the sense of definition 2.18, where

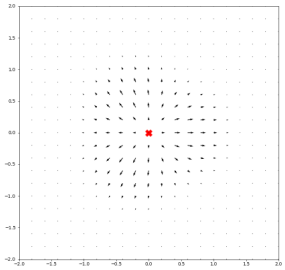

(a) The resulting vector field at time $t = 0$ for a positive control variable $h = 1$.

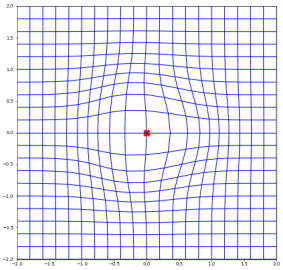

(b) The deformed grid for the positive control at time $t = 1$. The red crosses indicate the location of the transported geometrical descriptors.

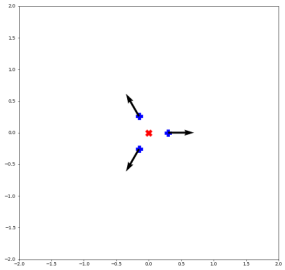

(c) The geometrical descriptor (red cross) defines the support and direction of three translation vectors used as intermediate tools to model a local scaling.

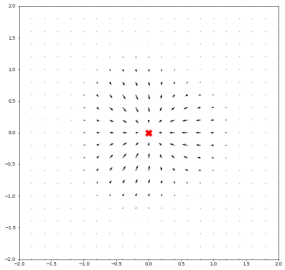

(d) The resulting vector field for a negative control $h = -1$ at time $t = 0$.

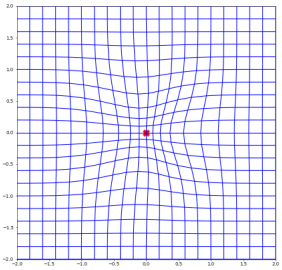

(e) The deformed grid at time $t = 1$ for a negative control. The red crosses indicate the location of the transported geometrical descriptors.

Figure 5: Example of a local scaling deformation module. The geometrical descriptors consist of one landmark. The control variables are three translation vectors located around the geometrical descriptor. The scale of the Gaussian reproducing kernel is set to 1. By chosing a positive or a negative control either a growing or a shrinking of the region around the geometrical descriptor can be modeled.

the space of controls is restricted to be finite-dimensional. However it is legitimate to consider this module because existence of optimal trajectories and minimizers has been shown and widely studied. With an abuse of notation we will write $\mathcal{M} = (\mathcal{O}, V_\sigma, \mathrm{Id}_\mathrm{H}, \xi, \|\cdot\|_{V_\sigma})$ and consider it as the LDDMM deformation module.

Following the idea of dimensionality reduction of the momentum in the Hamiltonian framework, we can define another deformation module that does satisfy the conditions of definition 2.18 for a finite-dimensional shape space. From the geodesic equations (19), we know that the geodesic velocity fields v lie in the subspace $\overline{\mathrm{H}}_{q_t} \coloneqq \{\mathrm{K}\xi^*_{q_t} p_t, p_t \in \mathrm{T}_{q_t}\mathcal{O}\}$. The momentum $\mathrm{K}^{-1}v_t$ is supported only on q_t, . The elements of $\overline{\mathrm{H}}_{q_t}$ can be seen as sums of local translations carried by the points $q_t(x), q_t \in \mathcal{O}$. In section 3.6 this is proved when we consider the background module for the multi-shape setting. This definition is not equivalent to the LDDMM setting,

as not the whole space V_σ of vector fields is considered. But since we know that the optimal velocity field lies in the subspace $\overline{\mathrm{H}}_{q_t}$, the solution of the minimization problem is the same for both settings.

In order to find optimal deformations for the registration problem, it has to be verified that optimal deformations between shapes that minimize the cost $c_{q_t}(h_t)$ exist. The following definition gives constraints on the choice of the cost. It gives a relation of the cost with the generated vector field. This will be the constraint ensuring existence of optimal deformations.

Definition 2.22. **[Gri16, Def. 19] Uniform Embedding Condition**

Let $\mathcal{M} = (\mathcal{O}, \mathrm{H}, \zeta, \xi, c)$ be a C^k-deformation module of order l. $\mathcal{M}$ satisfies the Uniform Embedding Condition (UEC) if there exists a Hilbert space of vector fields V continuously embedded in $C_0^{l+k}(\mathbb{R}^d)$, and a constant $\gamma > 0$, such that, for all $q \in \mathcal{O}$ and for all $h \in \mathrm{H}, \zeta_q(h) \in V$,

$$|\zeta_q(h)|_V^2 \leq \gamma c_q(h). \tag{50}$$

Now large deformations ϕ^v can be built by integrating a trajectory of vector fields $v : t \in [0,1] \mapsto v_t \in V$. Here, V is the same Hilbert space as in the definition of the UEC. The considered vector fields are assumed to be modular, so they can be built by $v_t = \zeta_{q_t}(h_t)$, where $(q_t, h_t) \in \mathcal{O} \times \mathrm{H}$. As the geometrical descriptor is transported by the flow, we assume for each $t \in [0,1]$ that $v_t \in \zeta_{q_t}(\mathrm{H})$, where $q_t = \phi_t^v(q_0)$ is the transported geometrical descriptor. The following definition gives the set of trajectories that will be considered for the registration problem.

Definition 2.23. **[Gri16, Def. 21] Controlled Path of Finite Energy**

Let $\mathcal{M} = (\mathcal{O}, \mathrm{H}, \zeta, \xi, c)$ be a deformation module. Let $a, b \in \mathcal{O}$. We denote $\Omega_{a,b}$ the set of measurable curves $t \mapsto (q_t, h_t) \in \mathcal{O} \times \mathrm{H}$, where q_t is absolutely continuous starting at a and ending at b, such that for almost every $t \in [0,1]$, $\dot{q}_t = \xi_{q_t}(\zeta_{q_t}(h_t))$ and

$$E(q,h) \coloneqq \int_0^1 c_{q_t}(h_t)\mathrm{d}t \leq \infty. \tag{51}$$

$\Omega_{a,b}$ is called a *controlled path of finite energy* starting at a and ending at b.

An essential question is the existence of optimal paths in $\Omega_{a,b}$. The following proposition states existence of geodesics for the deformation module framework. A proof can be found in [Gri16], chapter 4 proposition 20.

Proposition 2.24. **[Gri16, Prop. 20] Existence of Large Deformations**

Let $\mathcal{M}$ be a deformation module satisfying the UEC, with V being the corresponding

Hilbert space of vector fields. Let $(q, h) \in \Omega_{a,b}$ and $v_t = \zeta_{q_t}(h_t)$ for each $t \in [0, 1]$. Then $v \in L^2([0, 1], V)$, the flow ϕ^v exists, $h \in L^2([0, 1], \mathrm{H})$ and $q_t = \phi_t^v \cdot q_0$ for all $t \in [0, 1]$.

We will use this proposition later to prove the existence of large deformations for the multi shape framework. Moreover we will examine the existence of minimizers, where we will make use of the following theorem. The theorem states the existence of minimizing flows of the energy E, which is necessary for existence of minimizers of the registration problem.

Theorem 2.25. [Gri16, Th. 5] Existence of Geodesics

Let $\mathcal{M}$ be a deformation module that satisfies the UEC. If $\Omega_{a,b}$ is non-empty, the energy $E(q, h)$ reaches its minimum on $\Omega_{a,b}$.

The registration problem for the deformation modules framework can be stated as follows:

Problem 2.26. Registration Problem for Deformation Modules

Let $\mathcal{M} = (\mathcal{O}, \mathrm{H}, \zeta, \xi, c)$ be a C^k deformation module of order l. Let $q_S, q_T \in \mathcal{O}$. Consider the minimization of the functional

$$\mathcal{J}(q, h) = \int_0^1 c_{q_t}(h_t)\mathrm{d}t + \mathcal{U}(q_1, q_T) \tag{52}$$

over the $(q, h) \in \Omega \coloneqq \cup_{a,b \in \mathcal{O}} \Omega_{a,b}$, such that

$$\begin{aligned} q_0 &= q_S \\ \dot{q}_t &= \xi_{q_t}\zeta_{q_t}(h_t). \end{aligned} \tag{53}$$

The regularity term is now the integral over the cost, replacing the norm of the velocity fields in the LDDMM framework. As previously, the problem is constrained with the initial value $q_0 = q_S$ and the shape evolution induced by the flow equation. In the shape evolution the velocity field v_t in the LDDMM setting is replaced by the generated velocity field $\zeta_{q_t}(h_t)$ defined by the field generator ζ_{q_t} and the control h_t. The geodesics for problem 2.26 are usually described using a Hamiltonian system of geodesic equations, corresponding to the equations 19 for LDDMM.

Chapter 3: Multi-Shape Deformation Modules

3.1 Definition of the Framework

The idea of the multi-shape framework is to be able to incorporate different kinds of priors for the motion in different parts of the image, for example given by a segmentation. In this case, the shape space $\mathcal{O}$ is the product space of the spaces $\mathcal{O}^i = C^p(\Omega, \mathbb{R}^d)$ for $i = 1, ..., m$. We consider a multi-shape $q = (q^1, ..., q^m)$ of shapes $q^i \in \mathcal{O}^i$.

For segmented images we can construct the multi-shape in the following way. Let $\mathrm{I}\colon \mathbb{R}^d \to \mathbb{R}$ be an image suppported on $\Omega \subset \mathbb{R}^d$ and let $U = (U^1, ..., U^m)$ with $U^i \subset \Omega$, $U^i \cap U^j = \emptyset$ and $\bigcup_{i=1}^m U^i = \Omega$ for all $i, j \in \{1, ..., m\}, i \neq j$ be a segmentation of the image I. Then we define

$$q^i(x) \coloneqq \begin{cases} \mathrm{I}(x) & \text{, if } x \in U^i \\ 0 & \text{, else.} \end{cases} \tag{54}$$

The tuple $q = (q^1, ..., q^m)$ is the multi-shape that represents the image I that is the sum of images q^i supported on each part of the segmentation U^i of the segmentation.

In order to combine the framework of deformation modules with multi-shape registration, we define a new way of combining them. We will introduce a combination where for each shape q^i we consider a separate deformation module. The new multi-shape combination can be seen as an external combination, opposed to the compound module as an internal combination. It does fall into the class of a deformation modules, as the generated deformation does not act continuously on $\mathcal{O}$.

Definition 3.1. Multi-Shape Combination of Deformation Modules

Let $\mathcal{M}^i = (\mathcal{O}^i, \mathrm{H}^i, \zeta^i, \xi^i, c^i)$, $i = 1, ..., n$ be C^k-deformation modules on $\mathbb{R}^d$ of order l. Then $\mathbf{M}^{multi} = (\mathcal{O}, \mathrm{H}, \zeta, \xi, c)$ is the associated *multi-shape combination* of deformation modules $(\mathcal{M}^i)_i$, with

- shapes $q = (q^1, ..., q^n)$ in the shape space $\mathcal{O} = \mathcal{O}_1 \times ... \times \mathcal{O}_n$,
- controls $h = (h^1, ..., h^n)$ in $\mathrm{H} = \mathrm{H}_i \times ... \times \mathrm{H}_n$,
- $\zeta \coloneqq (\zeta^1, ..., \zeta^n)\colon (q, h) \in \mathcal{O} \times \mathrm{H} \mapsto (\zeta^1(q^1, h^1), ..., \zeta^n(q^n, h^n))$ $\in \prod_{i=1}^n C_0^{l^i}(\mathbb{R}^{d_i}, \mathbb{R}^{d_i})$,
- $\xi \coloneqq (\xi^1, ..., \xi^n)\colon C_0^{l^1} \times ... \times C_0^{l^n} \times \mathcal{O} \to \prod_{i=1}^n T\mathcal{O}^i \subset T\mathcal{O}$ and
- cost $c_q(h) = \sum_{i=1}^n c_{q^i}(h^i)^i\colon \mathcal{O} \times \mathrm{H} \to c_q(h) \in \mathbb{R}+$.

The following example is motivated by the problem of image registration, where different parts of the image given by a segmentation are desired to be deformed by different kinds of deformations. For the application in medical image registration, we assume to have segmentations of the different organs to register. Define the regions $U^1, ..., U^m$ of

the image domain Ω, that correspond to the segmented parts, and $U^{m+1} \coloneqq \Omega \setminus (\bigcup_{i=1}^{m} U^i)$ as the background region.

The goal is to find diffeomorphic constrained deformations for each region, where points on the boundaries $\partial U^1, ..., \partial U^m$ of $U^1, ..., U^m$ and corresponding points on the background boundary ∂U^{m+1} are transported by the same velocity field. The images are mathematically given as functions on Ω and have infinite dimension, and their boundaries are represented by curves. In order to simplify the example we will consider landmarks instead of curves. The landmarks lie on the boundaries of the segmented organs and can be viewed as a discretization of the infinite-dimensional setting. The purpose of this example is to derive the explicit geodesic equations in a case as simple as possible, in order to get an intuition of their meaning.

Throughout this chapter we will come back to this example and derive the explicit formulations of the geodesic equations.

Example 3.2. Translation of Landmarks in a Background

As a first example, we will study the case of landmarks. Let $\mathcal{O}^1 = (\mathbb{R}^2)^{N_1}$ and $\mathcal{O}^2 = (\mathbb{R}^2)^{N_2}$ be the shape spaces, N_1 and N_2 being the number of landmarks. Assume that q^1 and q^2 are sets of landmarks that represent a discretization of two curves in $\mathbb{R}^2$. Let $U^i \coloneqq U(q^i) \subset \mathbb{R}^2$ be an open set where the points $q^i_j, j = 1, ..., N_i$ lie on the boundary of $U(q^i)$ for $i = 1, 2$. For this example we will omit the time-dependency index t for the shape q_t and control h_t where it is clear, in order to reduce the amount of indices.

The background space is defined as $\mathcal{O}^3 = \mathcal{O}^1 \times \mathcal{O}^2$, following the work of [Arg14]. The elements $q^{3,i}_j \in q^{3,i} \in (q^{3,1}, q^{3,2}) =: q^3$ are landmarks on the boundary of U^3. If $q^i_j = q^{3,i}_j$, for $i = 1, 2$ and $j = 1, ..., N_i$ i.e., the boundary points of the background and the corresponding shape coindice, then $U^3 = \mathbb{R}^2 \setminus (U^1 \cup U^2)$.

For the modules $\mathcal{M}^1$ and $\mathcal{M}^2$, we choose a local translation of the shape $q^i = (q^i_1, ..., q^i_{N_i}) \in \mathcal{O}^i$. A local translation is defined by a point $z(q^i)$ and a translation vector h^i. We set $z(q^i) \coloneqq \frac{1}{N_i} \sum_{j=1}^{N_i} q^i_j$ as the mean of the landmarks in q^i. The control variable h^i is an element of $H^i = \mathbb{R}^2$. The field generator builds a vector field $v^i = \zeta^i_{q^i}(h^i) = \mathrm{K}_{\sigma_i}(z(q^i), \cdot)h^i$. The scale σ_i of the reproducing kernel K_{σ_i} describes the size of the region that is translated. For a translation of the whole shape q^i, the scale of σ_i is chosen to have a high value compared to the scale of the shape.

For the background we assume to have no prior knowledge or no restriction on the vector fields, except for the regularity of the field. This corresponds to a vector field as in classical LDDMM. Therefore the control variable is a vector field $h \in \mathrm{H}^3 \coloneqq V_{\sigma_3}$, where V_{σ_3} is the RKHS defined by the Gaussian Kernel with scale σ_3. The space H^3 is not finite-dimensional as required in the definition 2.18 of a deformation module, so M^3 is not a deformation module as introduced in [Gri16]. However, existence of optimal trajectories and minimizers have been shown for the LDDMM setting, so it is legitimate to consider H^3 as a space of controls.

In order to allow more irregular deformations in the background, the kernel size

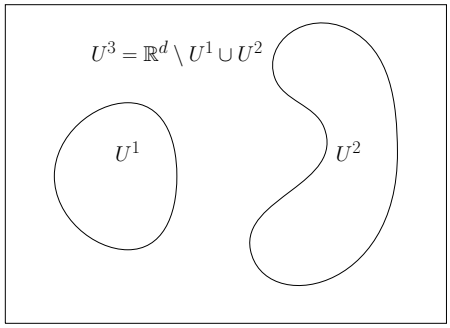

Figure 6: Shapes defined by the regions U^1 and U^2 in a background

σ_3 is chosen to be of much smaller scale than σ_1 and σ_2. The field generator $\zeta^3_{q^3}(h^3) = h^3$ maps the vectorfield h^3 to itself. The infinitesimal action $\xi^3_{q^3}(v^3) = (v^3(q_1^{3,1}), ..., v^3(q_{N_1}^{3,1}), v^3(q_1^{3,2}), ..., v^3(q_{N_2}^{3,2}))$ applies the generated vector field $v^3 = \zeta^3_{q^3}(h^3)$ to the points $q_i^{3,1}$ and $q_j^{3,2}$ for $i = 1, ..., N_1$, $j = 1, ..., N_2$.

For $i = 1, 2$, consider the cost function $c^i_{q^i}(h^i) = |h^i|^2_{H^i}$. The cost function describes the length of the translation vector. High translations are penalized more than small translations. For the background, let $c^3_{q^3}(h^3) = \|h\|_{V_{\sigma_3}}$ be the cost function defined as the norm in V_{σ_3}, as in the LDDMM setting.

For the multi-shape combination $\mathbf{M}^{multi}$, the vectorfield $\zeta_q(h) = (\zeta^1_{q^1}(h^1), \zeta^2_{q^2}(h^2), h^3)$ consists of three vector fields that are all defined on $\mathbb{R}^2$. In the next section we define a single large deformation on $\mathbb{R}^2$ from these three vector fields.

3.2 Existence of Large Deformations for Multi-Shape Modules

Until now $\mathbf{M}^{multi}$ was used to generate velocity fields on the shape space. The next step is to build large deformations from a trajectory of vector fields. This is done by integrating the time-dependent vector field $v^i_t = \zeta^i_{q^i_t}(h^i_t)$ over time according to the flow equation

$$\begin{aligned} \dot{\varphi^i}_t &= v^i_t \circ \varphi^i_t \\ \varphi^i_0 &= \mathrm{Id}_{\mathbb{R}^d}, \end{aligned} \tag{55}$$

for each $i \in \{1, ..., n\}$. If the UEC is satisfied for each module $\mathcal{M}^i$, then the deformations φ^i can be built for each v^i, as proved in [Gri16], see proposition 2.24. We will consider trajectories that satisfy the definition of *controlled paths of finite energy*. For the multi-shape framework we follow the definition 2.23.

Definition 3.3. Controlled Path of Finite Energy

Let $\mathbf{M}^{multi} = (\mathcal{O}, \mathrm{H}, \zeta, \xi, c)$ be a multi-shape combination of deformation modules with the modules $\mathcal{M}^i, i = 1, ..., n$, and let $a = (a_1, ..., a_n)$, $b = (b_1, ..., b_n) \in$

$\mathcal{O}= \mathcal{O}^1 \times ... \times \mathcal{O}^n$. Denote by $\Omega_{a,b}$ the set of measurable curves $t \mapsto (q_t, h_t) \in \mathcal{O} \times \mathrm{H}$, where for every i, q_t^i is absolutely continuous starting from a_i and ending at b_i, such that for almost every $t \in [0,1]$, $\dot{q^i}_t = \xi^i{}_{q_t^i}(v_t^i)$ with $v_t^i = \zeta^i_{q_t^i}(h_t^i)$, and

$$E^i(q^i, h^i) = \int_0^1 c^i_{q_t^i}(h_t^i)\mathrm{d}t < \infty. \tag{56}$$

The set $\Omega_{a,b}$ defined in this way is called the set of *controlled paths of finite energy* starting at a and ending at b. Then $\Omega \coloneqq \cup_{a,b\in\mathcal{O}}\Omega_{a,b}$ is the set of possible controlled paths of finite energy in $\mathcal{O}$.

Remark 3.4

The energy

$$E(q,h) = \int_0^1 c_{q_t}(h_t)\mathrm{d}t = \int_0^1 \sum_{i=1}^n c^i_{q_t^i}(h_t^i)\mathrm{d}t \tag{57}$$

of (q,h) is finite, as well for all curves in $\Omega_{a,b}$ due to 56.

Example 3.5. Large Deformation of Landmarks in a Background

For the framework in example 3.2, it is desired to have the diffeomorphisms φ_t^i only acting on points in the set U^i. To achieve this, the final deformation φ_1 for the multi-shape combination $\mathbf{M}^{multi}$ is built from the deformations of the modules according to

$$\psi_t(x) = \begin{cases} \varphi_t^1(x) & \text{, if } x \in \overline{U^1} \\ \varphi_t^2(x) & \text{, if } x \in \overline{U^2} \\ \varphi_t^3(x) & \text{, if } x \in U^3. \end{cases} \tag{58}$$

Here, $\overline{U^i}$ denotes the closure of U^i. Notice that the deformation ψ is in general not a diffeomorphism anymore, which is intentional and the goal of its construction. Instead it consists of diffeomorphisms on each subset U^i, that do not influence each other.

So far, the framework of a multi-shape deformation can be seen as multiple deformations that are studied separately on their shape spaces. In most applications certain interaction of the shapes between each other are desired. For example it could be plausible that the deformed shapes do not overlap. This is equivalent to the deformation ψ_t being injective, which is not true in general without further restrictions on φ_t. This can be incorporated in the model by additional constraints on the deformed shapes (or equivalently on the velocity field, see remark 2.14) in the optimization problem, as has been done in [Arg14].

3.3 The Constrained Registration Problem

In the following, the minimization problem for constrained image registration will be defined. The aim is to find the deformation that maps a given shape $q_S \in \mathcal{O}$ onto a target shape q_T. The similarity of the deformed shape to the source is measured by a function $\mathcal{U}\colon \mathcal{O} \times \mathcal{O} \to \mathbb{R}$.

Problem 3.6. Constrained Modular Registration Problem for Multi-Shapes

Let $q_t \coloneqq q(t)\colon [0,1] \to \mathcal{O}$ and $h_t \coloneqq h(t)\colon [0,1] \to \mathrm{H}$. Let Y be a Banach space. Let $C\colon \mathcal{O} \times V \mapsto Y$ be continuous in both variables and $C_q(v) \coloneqq C(q,v)$ linear in v. Consider the minimization of the functional

$$J(q,h) \coloneqq \sum_{i=1}^{m} \mathcal{U}^m(q_1^m, q_T) + \frac{1}{2}\int_0^1 c_{q_t}(h_t)\mathrm{d}t \tag{59}$$

over $(q,h) \in \Omega \coloneqq \cup_{a,b\in\mathcal{O}}\Omega_{a,b}$, such that

$$\begin{aligned} q_0 &= q_S \\ \dot{q}_t &= \xi_{q_t} \circ \zeta_{q_t}(h_t) \\ C_{q_t}(\zeta_{q_t}(h_t)) &= 0 \end{aligned} \tag{60}$$

for almost every $t \in [0,1]$.

The constraints $\mathrm{C}(v)$ are continuous and linear constraints on the vector field $v = \zeta_{q_t}(h_t)$. They can be of different kinds, as discussed in chapter 2.2. In the following the example of identity constraints for the multi-shape combination of translations of landmarks will be given.

Example 3.7. Identity Constraints for Landmarks in a Background

A possible choice of constraints for the previously discussed example is to ensure that the corresponding landmarks q_j^i and $q_j^{3,i}$ in the shape space $\mathcal{O}^1 \times \mathcal{O}^2$ and the background space $\mathcal{O}^3$ are transformed by the same vector field. This is the case of identity constraints as introduced in chapter 2.2. To incorporate the constraints into the minimization problem, they are formulated as the linear equation $\mathrm{C}_q v = 0$ with

$$\begin{aligned} \mathrm{C}_q(v) &\coloneqq \mathrm{C}_q(v^1, v^2, v^3) \\ &\coloneqq \begin{pmatrix} v^1(q^1) - v^3(q^{3,1}) \\ v^2(q^2) - v^3(q^{3,2}) \end{pmatrix} \overset{!}{=} \begin{pmatrix} 0 \\ 0 \end{pmatrix}. \end{aligned} \tag{61}$$

The constraints C_q here are kinetic constraints. The space of the constraints is in this case $\mathrm{Y} \coloneqq (\mathbb{R}^2)^{N_1} \times (\mathbb{R}^2)^{N_2}$ with e.g., the Euclidean norm.

3.4 Existence of Geodesic Flows

In this section we will analyse the possible paths resulting from the framework. Previously we discussed that for the LDDMM setting,

$$\mathrm{d}_V(\psi, \bar{\psi}) = \inf_{v_t \in V} \left\{ \int_0^1 \|v_t\|_V \mathrm{d}t, \psi = \bar{\psi} \circ \phi_{t=1}^v \right\} \tag{62}$$

defines a metric on the considered subgroup Diff_V of $\mathrm{Diff}_0^l(\mathbb{R}^d, \mathbb{R}^d)$. For the deformation modules framework a distance Dist_H can be defined using the cost function [Gri16, Def. 25].

Definition 3.8. [Gri16, Def. 25]

Let $a, b \in \mathcal{O}$ and $(q, h) \in \Omega_{a,b}$. The length of (q, h) is defined by

$$l(q, h) \coloneqq \int_0^1 \sqrt{c_{q_t}(h_t)} \mathrm{d}t = \int_0^1 \sqrt{\sum_{i=1}^n c^i_{q_t^i}(h_t^i)} \mathrm{d}t \tag{63}$$

and the distance between a and b is defined by

$$\mathrm{Dist}_\mathrm{H}(a, b) \coloneqq \inf\{l(q, h) | (q, h) \in \Omega_{a,b}\} \tag{64}$$

The following proposition extends [Gri16, Prop. 22] to our multi-shape framework.

Proposition 3.9

$\mathrm{Dist}_\mathrm{H}(a, b)$ is a metric on $\mathcal{O}$.

Proof: The argumentation follows the structure of the proof in [Gri16]. We will show non-negativity, symmetry and subadditivity for $\mathrm{Dist}_\mathrm{H}(a, b)$.

Nonnegativity. Let $(q, h) \in \mathcal{O} \times \mathrm{H}$. Because the cost $c_q(h)$ takes non-negative values, it follows that

$$l(q, h) = \int_0^1 \sqrt{c_q(h)} \mathrm{d}t \geq 0 \tag{65}$$

for all $q, h \in \mathcal{O} \times \mathrm{H}$, and

$$\mathrm{Dist}_\mathrm{H}(a, b) = \inf\{l(q, h) | (q, h) \in \Omega_{a,b}\} \geq 0 \tag{66}$$

for all $a, b \in \mathcal{O}$.

Symmetry We use the fact that for every element $(q, h) \in \Omega_{a,b}$ there exists an element $(\bar{q}, \bar{h}) \in \Omega_{b,a}$ with the same length. From linearity of ζ_{q_t} it follows that for $\bar{h}_t \coloneqq -h_t$, the generated vectorfield satisfies $\zeta_{q_t}(\bar{h}_t) = -\zeta_{q_t}(h_t)$. Moreover, the cost is a metric on H and therefore $c_{q_t}(h_t) = c_{q_t}(\bar{h}_t)$.

We define

$$\bar{q}_t \coloneqq q_{1-t} \quad \text{and} \quad \bar{h}_t \coloneqq -h_{1-t}. \tag{67}$$

Then $(\bar{q}, \bar{h}) \in \Omega_{b,a}$ because $\bar{q}_0 = q_1 = b$ and $\bar{q}_1 = q_0 = a$. We define the mapping $f\colon \Omega_{a,b} \to \Omega_{b,a}, f((q,h)) \coloneqq (\bar{q}, \bar{h})$ with The mapping f is one-to-one and

$$c_{\bar{q}_t}(\bar{h}_t) = c_{q_{1-t}}(-h_{1-t}) = c_{q_1-t}(h_{1-t}). \tag{68}$$

For the length of the paths (q,h) and $(\bar{q}, \bar{h})$ it follows

$$\int_0^1 \sqrt{c_{\bar{q}_t}(\bar{h}_t)}\mathrm{d}t = \int_0^1 \sqrt{c_{q_{1-t}}(h_{1-t})}\mathrm{d}t = -\int_1^0 \sqrt{c_{q_s}(h_s)}\mathrm{d}s = \int_0^1 \sqrt{c_{q_s}(h_s)}\mathrm{d}s, \tag{69}$$

and thus $l(q,h) = l(\bar{q}, \bar{h})$.

So we deduce

$$\begin{aligned} \mathrm{Dist}_\mathrm{H}(a,b) &= \inf\{l(q,h) | (q,h) \in \Omega_{a,b}\} \\ &= \inf\{l(q,h) | (q,h) \in \Omega_{b,a}\} = \mathrm{Dist}_\mathrm{H}(b,a) \end{aligned} \tag{70}$$

and Dist_H is symmetric.

Subadditivity. Furthermore, Dist_H is subadditive because for every $a, b, c \in \mathcal{O}$,

$$\begin{aligned} \mathrm{Dist}_\mathrm{H}(a,c) &= \inf\{l(q,h) | (q,h) \in \Omega_{a,c}\} \\ &\overset{(*)}{\leq} \inf\{l(\bar{q}, \bar{h}) + l(\tilde{q}, \tilde{h}) | (\bar{q}, \bar{h}) \in \Omega_{a,b}, (\tilde{q}, \tilde{h}) \in \Omega_{b,c}\} \\ &= \inf\{l(\bar{q}, \bar{h}) | (\bar{q}, \bar{h}) \in \Omega_{a,b}\} + \inf\{l(\tilde{q}, \tilde{h}) | (\tilde{q}, \tilde{h}) \in \Omega_{b,c}\} \\ &= \mathrm{Dist}_\mathrm{H}(a,b) + \mathrm{Dist}_\mathrm{H}(b,c) \end{aligned} \tag{71}$$

for all $a, b, c \in \mathcal{O}$.

For the inequality $(*)$ we use that the length of the path (q,h) from a to c can be expressed as the sum of the lengths of path segments $(\bar{q}, \bar{h}) \in \Omega_{a,z}$ and $(\tilde{q}, \tilde{h}) \in \Omega_{z,c}$, where z lies on the path (q,h). We define $(\bar{q}_t, \bar{h}_t) \coloneqq (q_{t/2}, \frac{1}{2}h_{t/2})$. Then $(\bar{q}_t, \bar{h}_t)$ still satisfies the flow equation

$$\dot{\bar{q}}_t = \frac{1}{2}\dot{q}_{t/2} = \frac{1}{2}\xi_{q_{t/2}}\zeta_{q_{t/2}}(h_{t/2}) = \frac{1}{2}\xi_{\bar{q}_t}\zeta_{\bar{q}_t}((2\bar{h}_t)) = \xi_{\bar{q}_t}\zeta_{\bar{q}_t}(\bar{h}_t), \tag{72}$$

and the length of $(\bar{q}_t, \bar{h}_t)$ is given by

$$l(\bar{q}, \bar{h}) = \int_0^1 \sqrt{c_{\bar{q}_t}(\bar{h}_t)}\mathrm{d}t = \int_0^1 \sqrt{c_{q_{t/2}}(\frac{1}{2}h_{t/2})}\mathrm{d}t = \int_0^{1/2} \sqrt{c_{q_s}(\frac{1}{2}h_s)}2\mathrm{d}t, \tag{73}$$

where we substituted $s = t/2$ and $\mathrm{d}t = 2\mathrm{d}s$. Because the cost is quadratic,

$$l(\bar{q}, \bar{h}) = \int_0^{1/2} \sqrt{\frac{1}{4}c_{q_s}(h_s)}2\mathrm{d}s = \int_0^{1/2} \sqrt{c_{q_s}(h_s)}\mathrm{d}s. \tag{74}$$

Analogously, we find that $(\tilde{q}, \tilde{h}) \coloneqq (q_{(1+t)/2}, h_{(1+t)/2})$ satisfies the flow equation and

$$l(\tilde{q}, \tilde{h}) = \int_{1/2}^1 \sqrt{c_{q_t}(h_t)}\mathrm{d}t. \tag{75}$$

Then we can build the concatenation $(\bar{q}.\tilde{q}, \bar{h}.\tilde{h})$ of paths $(\bar{q}, \bar{h})$ and $(\tilde{q}, \tilde{h})$ by

$$\bar{q}.\tilde{q} \coloneqq \begin{cases} \bar{q}_{2t}, & 0 \leq t < 1/2, \\ \tilde{q}_{2t}, & 1/2 \leq t \leq 1, \end{cases} \quad \text{and} \quad \bar{h}.\tilde{h} \coloneqq \begin{cases} \bar{h}_{2t}, & 0 \leq t < 1/2, \\ \tilde{h}_{2t}, & 1/2 \leq t \leq 1. \end{cases} \tag{76}$$

With (74) and (75), it follows that $l(\bar{q}.\tilde{q}, \bar{h}.\tilde{h}) = l(\bar{q}, \bar{h}) + l(\tilde{q}, \tilde{h})$.

Let $D \coloneqq \{l(\bar{q}, \bar{h}) + l(\tilde{q}, \tilde{h}) | (\bar{q}, \bar{h}) \in \Omega_{a,b}, (\tilde{q}, \tilde{h}) \in \Omega_{b,c}\}$. It follows that

$$D = \{l(\bar{q}.\tilde{q}, \bar{h}.\tilde{h}) | (\bar{q}, \bar{h}) \in \Omega_{a,b}, (\tilde{q}, \tilde{h}) \in \Omega_{b,c}\} \tag{77}$$

which is a subset of $\{l(q,h)|(q,h) \in \Omega_{a,c}\}$. This implies

$$\inf D \geq \inf\{l(q,h)|(q,h) \in \Omega_{a,c}\}. \tag{78}$$

Finally it needs to be shown that $\mathrm{Dist}_{\mathrm{H}}(a,b) = 0 \Leftrightarrow a = b$. Indeed it holds

$$\mathrm{Dist}_{\mathrm{H}}(a,b) = 0 \Rightarrow \inf\left\{ \int_0^1 \sqrt{c_{q_t}(h_t)}\mathrm{d}t \middle| (q_t, h_t) \in \Omega_{a,b} \right\} = 0 \tag{79}$$

and because the cost $c_{q_t}(h_t)$ is positive,

$$\Rightarrow \inf\left\{ \int_0^1 c_{q_t}(h_t)\mathrm{d}t \middle| (q_t, h_t) \in \Omega_{a,b} \right\} = 0. \tag{80}$$

Inserting the definition of the cost $c_{q_t}(h_t) = \sum_{i=1}^n c^i_{q^i_t}(h^i_t)$ yields

$$\begin{aligned} &\Rightarrow \inf\left\{ \int_0^1 \sum_{i=1}^n c^i_{q^i_t}(h^i_t)\mathrm{d}t \middle| (q,h) = ((q^1,h^1),...,(q^n,h^n)) \in \Omega_{a,b} \right\} = 0 \\ &\Rightarrow \inf\left\{ \sum_{i=1}^n \int_0^1 c^i_{q^i_t}(h^i_t)\mathrm{d}t \middle| (q,h) = ((q^1,h^1),...,(q^n,h^n)) \in \Omega_{a,b} \right\} = 0 \end{aligned} \tag{81}$$

The cost is nonnegative and therefore it follows

$$\Rightarrow \inf\left\{ \int_0^1 c^i_{q^i_t}(h^i_t)\mathrm{d}t \middle| (q^i_t, h^i_t) \in \Omega_{a^i,b^i} \right\} = 0 \tag{82}$$

for all $i = 1, ..., n$.

Consequently, as $\mathrm{Dist}_{\mathrm{H}^i}$ was previously shown to be a distance on $\mathcal{O}^i$ [Gri16, Prop. 22],

$$\begin{aligned} &\Rightarrow \mathrm{Dist}_{H^i}(a^i, b^i) = 0 \quad \forall i = 1, ..., n \\ &\Rightarrow a^i = b^i \quad \forall i = 1, ..., n \\ &\Rightarrow a = b. \end{aligned} \tag{83}$$

On the other hand, let $a = b$. Then (q_t, h_t) with $q_t \equiv a \ \forall t \in [0,1]$ and $h_t \equiv 0 \ \forall t \in [0,1]$ is an element of $\Omega_{a,b}$, with $c_{q_t}(h_t) = 0$. Therefore,

$$\mathrm{Dist}_{\mathrm{H}}(a,b) = \inf\{l(q,h)|(q,h) \in \Omega_{a,b}\} = l(q_t, h_t) = 0 \tag{84}$$

reaches the infimum 0. From non-negativity, symmetry, subadditivity and $\mathrm{Dist}_{\mathrm{H}}(a,b) = 0 \leftrightarrow a = b$ it follows that $\mathrm{Dist}_{\mathrm{H}}(a,b)$ is a distance on $\Omega_{a,b}$. ■

Now we will examine the important question of existence of minimizers for the energy $E = \int_0^1 c_{q_t}(h_t)\mathrm{d}t$. Minimizers of E correspond to geodesic flows considering the metric $\mathrm{Dist}_{\mathrm{H}}$. The next theorem adapted from 2.25 states the existence of minimizers:

Theorem 3.10. Existence of Geodesics

Let $\mathbf{M}^{multi}$ be a multi-shape combination of modules $\mathcal{M}^i = (O^i, H^i, \zeta^i, \xi^i, c^i)$, $i = 1, ..., n$, where each module $\mathcal{M}^i$ satisfies the UEC 2.22. Let $a, b \in \mathcal{O}$ be of compact support. Let $q \mapsto \mathrm{C}_q$ be continuous as a mapping from $\mathcal{O}$ to $L(V, Y)$ and $v \mapsto \mathrm{C}_q(v)$ linear and bounded. If $\Omega_{a,b}$ is non-empty, the minimum of the energy (57) on $\Omega_{a,b}$ exists and the minimizer satisfies the constraints $\mathrm{C}_{q_t}(v_t) = 0$ for almost every $t \in [0, 1]$.

Proof: We will show that from the existence of minimizers of $E^i(q^i, h^i)$ in Ω_{a^i,b^i}, shown in theorem 2.25, the existence of minimizers of $E(q, h)$ in $\Omega_{a,b}$ follows and that the minimizer still statisfies the constraints.

First we will verify that $\Omega_{a,b} = \prod_{i=1}^n \Omega^i_{a_i,b_i}$. For every $i \in \{1, ..., n\}$ the element $(q^i, h^i) \in \Omega^i_{a_i,b_i}$ satisfies the flow equation $\dot{q^i}_t = \xi^i_{q^i_t} \circ \zeta^i_{q^i_t}(h^i_t)$, so by definition $\dot{q} = \xi_{q_t} \circ \zeta_{q_t}(h_t)$. Since q is absolutely continuous for each component, it is absolutely continuous. Moreover, because $E^i(q^i, h^i) < \infty$ for all i, it follows $E(q, h) = \sum_{i=1}^n E^i(q^i, h^i) < \infty$. So $\Omega_{a,b} \supset \prod_{i=1}^n \Omega^i_{a_i,b_i}$.

On the other hand, if $\dot{q} = \xi_{q_t} \circ \zeta_{q_t}(h_t)$, then the flow equation is by definition satisfied componentwise and q^i is absolutely continuous for each component. From $E(q, h) < \infty$ and positivity of $E^i(q^i, h^i)$ for each i it follows that if $E(q, h) < \infty$, $E^i(q^i, h^i) < \infty$ for each i. So we have $\Omega_{a,b} \subset \prod_{i=1}^n \Omega^i_{a_i,b_i}$.

The energy $E(q, h)$ takes only non-negative values and thus is bounded from below. Moreover, as $\Omega_{a,b}$ is non-empty by assumption, it follows that the infimum is finite. Therefore we can find a minimizing sequence of E. Let (q^j, h^j)in $\Omega_{a,b}$ be a minimizing sequence that satisfies the constraints.

We will show that, up to extraction of a subsequence, $q^j \to q^\infty$ uniformly in $\mathcal{O}$, $h^j \to h^\infty$ weakly in $L^2([0, 1], H)$, so that and (q^∞, h^∞) satisfy the constraints for almost every t. Then optimality of (q^∞, h^∞) follows by a variant of lower-semicontinuity: From the proof of 2.25, we know that for each component $((q^i)^j, (h^i)^j)$ of (q^j, h^j), $(q^i)^j \to (q^i)^\infty$ uniformly and $(h^i)^j \to (h^i)^\infty$ weakly in $L^2([0, 1], H)$, and all E^i are lower semi-continuous with respect to this kind of convergence. Therefore their sum E is also lower semi-continuous, which together with the fact that (q^i, h^i) is a minimizing sequence implies that (q^i, h^i) is a minimizer.

In order to apply this argument, we first need to show that $q^j \to q^\infty$ uniformly and $h^j \to h^\infty$ weakly in $L^2([0, 1], H)$. We use the convergence of each component that has been shown in [Gri16]: For all $i = 1, ..., n$, h^i converges weakly to $(h^i)^\infty$ in $L^2([0, 1], H^i)$, so for all $f^i \in (\mathrm{H}^i)^*$: $(f^i|(h^i)^j - (h^i)^\infty)_{H^{i*},H^i} \to 0$. Let $(f^1, ..., f^n)$ be a basis in H^*. For $h^j \in \mathrm{H} = \prod_{i=1}^n H^i$ and $f \coloneqq (f^1, ..., f^n) \in \mathrm{H}^*$ it follows

$$(f|h^j - h^\infty)_{H^*,H} = \sum_{i=1}^n (f^i|(h^i)^j - (h^i)^\infty)_{H^{i*},H^i} \to 0, \tag{85}$$

so h^j converges weakly in $\prod_{i=1}^n L^2([0, 1], H^i) = L^2([0, 1], \prod_{i=1}^n H^i)$. Moreover, $(q^i)^j$ converges uniformly to $(q^i)^\infty$ in $C([0, 1], \mathcal{O}^i)$, so q^j converges to q^∞ in $\prod_{i=1}^n C([0, 1], \mathcal{O}^i)$.

Finally we need to prove that (q^∞, h^∞) still satisfies the constraints if they are satisfied for every (q^j, h^h). With the same argument as for h^∞, we get that $v^j \coloneqq \zeta_{q^j}(h^j)$ converges weakly to $v^\infty \coloneqq \zeta_{q^\infty}(h^\infty)$ in $L^2([0, 1], \prod_{i=1}^n V^i) = \prod_{i=1}^n L^2([0, 1], V^i)$, as weak convergence of all components was shown in the proof of [Gri16, Theorem 5]. In the same proof, it

was shown that there exists a compact set L of $\mathcal{O}$ such that for all $t \in [0,1]$, $q_t^\infty \in L$ and $q_t^j \in L \quad \forall j$.

We will show now that for almost all $t \in [0,1]$ the constraints $\mathrm{C}_{q_t^\infty}(v_t^\infty) = 0$ are satisfied. Define $\nu : t \mapsto \mathrm{C}_{q_t^\infty}(v_t^\infty)$. We show

(i) $\nu \in L^2([0,1], \mathrm{Y})$ and

(ii) $(\nu|w) = 0 \quad \forall w \in L^2([0,1], \mathrm{Y}^*) = (L^2([0,1], \mathrm{Y}))^*$

as this implies $\nu = 0$ for almost all t, which is what we want to show.

We first verify (i), i.e., $\nu \in L^2([0,1], \mathrm{Y})$. We have

$$\int_0^1 \|\mathrm{C}_{q_t^\infty}(v_t^\infty)\|_Y^2 \mathrm{d}t \leq \int_0^1 \|\mathrm{C}_{q_t^\infty}\|_{L(V,Y)}^2 \|(v_t^\infty)\|_V^2 \mathrm{d}t. \tag{86}$$

From the proof of [Gri16, Theorem 5], we know that $\{q_t^\infty, t \in [0,1]\}$ is contained in the compact set L. Since L is compact and $q_t^\infty \mapsto \mathrm{C}_{q_t^\infty}$ is continuous, $q_t^\infty \mapsto \mathrm{C}_{q_t^\infty}$ is uniformly continuous. This shows that $\mathrm{C}_{q_t^\infty}$ is uniformly bounded on $[0,1]$, i.e., there exists an $\alpha \in \mathbb{R}$ with $\|\mathrm{C}_{q_t^\infty}\|_{L(V,Y)}^2 \leq \alpha^2$. Then

$$\int_0^1 \|\mathrm{C}_{q_t^\infty}(v_t^\infty)\|_Y^2 \mathrm{d}t \leq \int_0^1 \|\mathrm{C}_{q_t^\infty}\|_{L^2}^2 \|(v_t^\infty)\|_{L(V,Y)}^2 \mathrm{d}t \leq \alpha^2 \|v^\infty\|_{L^2([0,1],V)} < \infty, \tag{87}$$

and thus $\nu \in L^2([0,1], \mathrm{Y})$.

Now we show (ii), i.e., $\langle \nu, w \rangle = 0$ for all $w \in L^2([0,1], \mathrm{Y})$. For every $w \in L^2([0,1], \mathrm{Y}^*)$ and every $j \in \mathbb{N}$, we have

$$\begin{aligned}
&|(\nu|w)_{L^2([0,1],Y),(L^2([0,1],Y^*)}| \\
=&\Big| \int_0^1 (\mathrm{C}_{q_t^\infty}(v_t^\infty)|w_t)_{\mathrm{Y},\mathrm{Y}^*} \mathrm{d}t \Big| \\
\overset{(*)}{=}&\Big| \int_0^1 (\mathrm{C}_{q_t^\infty}(v_t^\infty) - \mathrm{C}_{q_t^j}(v_t^j)|w_t)_{\mathrm{Y},\mathrm{Y}^*} \mathrm{d}t \Big| \\
=&\Big| \int_0^1 (\mathrm{C}_{q_t^\infty}(v_t^\infty) - \mathrm{C}_{q_t^\infty}(v_t^j) + \mathrm{C}_{q_t^\infty}(v_t^j) - \mathrm{C}_{q_t^j}(v_t^j)|w_t)_{\mathrm{Y},\mathrm{Y}^*} \mathrm{d}t \Big| \\
\overset{(**)}{\leq}&\Big| \int_0^1 (\mathrm{C}_{q_t^\infty}(v_t^\infty) - \mathrm{C}_{q_t^\infty}(v_t^j)|w_t)_{\mathrm{Y},\mathrm{Y}^*} \mathrm{d}t \Big| + \Big| \int_0^1 (\mathrm{C}_{q_t^\infty}(v_t^j) - \mathrm{C}_{q_t^j}(v_t^j)|w_t)_{\mathrm{Y},\mathrm{Y}^*} \mathrm{d}t \Big|,
\end{aligned} \tag{88}$$

where we used $(*)$ that the constraints are satisfied for (q^j, v^j) for all j for almost all t, and then $(**)$ the subadditivity.

For the first term in (88) it holds

$$\Big| \int_0^1 (\mathrm{C}_{q_t^\infty}(v_t^\infty - v_t^j)|w_t)_{\mathrm{Y},\mathrm{Y}^*} \mathrm{d}t \Big| \leq \int_0^1 \|\mathrm{C}_{q_t^\infty}\|_{L(V,\mathrm{Y})} \|v_t^\infty - v_t^j\|_V \|w_t\|_{\mathrm{Y}^*} dt, \tag{89}$$

and applying the Hölder inequality yields

$$\Big| \int_0^1 (\mathrm{C}_{q_t^\infty}(v_t^\infty - v_t^j)|w_t)_{\mathrm{Y},\mathrm{Y}^*} \mathrm{d}t \Big| \leq \Big(\int_0^1 \alpha^2 \|w_t\|_{\mathrm{Y}^*}^2 \Big)^{1/2} \Big(\int_0^1 \|v_t^\infty - v_t^j\|_V^2 \mathrm{d}t \Big)^{1/2}. \tag{90}$$

This expression is a linear and bounded functional in $(v^\infty - v^j)$. As $v^j \to v^\infty$ weakly, this implies that (90) converges to zero for $j \to \infty$.

For the second term in (88), we have

$$\Big| \int_0^1 (\mathrm{C}_{q_t^\infty}(v_t^j) - \mathrm{C}_{q_t^j}(v_t^j)|w_t)_{\mathrm{Y},\mathrm{Y}^*}\mathrm{d}t \Big| \leq \int_0^1 \|\mathrm{C}_{q_t^\infty} - \mathrm{C}_{q_t^j}\|_{L(V,\mathrm{Y})}\|w_t\|_{\mathrm{Y}^*}\|v_t^j\|_V \mathrm{d}t. \tag{91}$$

Again, as all q_t^j and q_t are contained in the compact set L, and the mapping $q_t \mapsto \mathrm{C}_{q_t}$ is continuous, the mapping is uniformly continuous in L. As $q^j \to q^\infty$ uniformly on $[0,1]$, this implies that $\|\mathrm{C}_{q_t^\infty} - \mathrm{C}_{q_t^j}\|_{L(V,\mathrm{Y})} \leq \alpha(j)$ for some $\alpha(j)$, not depending on t, with $\alpha(j) \overset{j\to\infty}{\longrightarrow} 0$. We pursue

$$\begin{aligned} \Big| \int_0^1 (\mathrm{C}_{q_t^\infty}(v_t^j) - \mathrm{C}_{q_t^j}(v_t^j)|w_t)_{\mathrm{Y},\mathrm{Y}^*}\mathrm{d}t \Big| &\leq \alpha(j) \int_0^1 \|w_t\|_{\mathrm{Y}^*}\|v_t^j\|_V \mathrm{d}t \\ &\overset{(***)}{\leq} \alpha(j)\|w\|_{L^2([0,1],Y^*)}\|v^j\|_{L^2([0,1],V)}, \end{aligned} \tag{92}$$

where for $(***)$ we applied the Hölder inequality. Furthermore, the UEC yields

$$\|v^j\|_{L^2}^2 \leq \int_0^1 \gamma c_{q_t}(h_t)\mathrm{d}t = \gamma E(q^j, h^j), \tag{93}$$

for some $\gamma < \infty$. Because (q^j, h^j) is a minimizing sequence, there is some $\beta < \infty$ with

$$E(q^j, h^j) \leq \beta \tag{94}$$

for all j. Then

$$\alpha(j)\|w\|_{L^2}\|v^j\|_{L^2} \leq \alpha(j)\gamma\beta\|w\|_{L^2}, \tag{95}$$

which converges to zero for $j \to \infty$ because $\alpha(j)$ converges to zero for $j \to \infty$.

All in all, we have shown that both terms in (88) converge to zero as $j \to \infty$. Therefore

$$|\langle \nu, w\rangle| \leq \epsilon \quad \forall w \in L^2([0,1],\mathrm{Y})^* \quad \forall \epsilon > 0, \tag{96}$$

which implies

$$|\langle \nu, w\rangle| = 0 \quad \forall w \in L^2([0,1],\mathrm{Y})^*. \tag{97}$$

Therefore $\nu = 0$ in $L^2([0,1], Y)$. This finally yields

$$\mathrm{C}_{q_t^\infty}(v_t^\infty) = 0 \quad \text{for a.e. } t \in [0,1], \tag{98}$$

which concludes the proof. ■

Having ensured the existence of geodesics, we can now examine the principle of least action for the energy E. We will state the Hamiltonian system for our setting and derive the geodesic equations analoguously to (19) that describe the nature of the geodesics.

3.5 The Hamiltonian Function and Shooting Equations

In this section we derive the geodesic equations for the Hamiltonian system of the constrained registration problem. The system of equations corresponds to the system (100) for LDDMM. It describes how the deformed shape and the time-dependent velocity field

can be obtained from the initial shape q_0 and initial momentum p_0 (see section 2.1.7).

Compared to the Hamiltonian system for deformation modules, the system for the constrained multi-shape framework is extended by a term corresponding to the constraints. In the Hamiltonian function, a Lagrange multiplier $\lambda \in \mathrm{Y}^*$ for the constraints is introduced. Analoguous to [Arg14], we define the Hamiltonian function $\mathcal{H}\colon \mathcal{O} \times \mathrm{T}^*_{q_t}\mathcal{O} \times \mathrm{H} \times \mathrm{Y}$,

$$\mathcal{H}(q,p,h,\lambda) \coloneqq (p|\xi_q \circ \zeta_q(h))_{\mathrm{T}^*_q\mathcal{O},\mathrm{T}_q\mathcal{O}} - \frac{1}{2}c_q(h) - (\lambda|\mathrm{C}_q\zeta_q(h))_{\mathrm{Y}^*,\mathrm{Y}}\,. \tag{99}$$

The geodesic equations read

$$\begin{aligned} \dot{q} &= \frac{\partial}{\partial p}\mathcal{H}(qp,h,\lambda) \\ \dot{p} &= -\frac{\partial}{\partial q}\mathcal{H}(qp,h,\lambda) \\ \frac{\partial}{\partial h}\mathcal{H}(qp,h,\lambda) &= 0 \\ \frac{\partial}{\partial \lambda}\mathcal{H}(qp,h,\lambda) &= 0. \end{aligned} \tag{100}$$

To compute the so called *reduced Hamiltonian* H, h and λ are chosen depending on q and p so that the last two constraints are satisfied.

As the cost function is quadratic and positive definite (see definition 3.1) and H is finite-dimensional, there exists an invertible symmetric operator $\mathrm{Z}_q\colon \mathrm{H} \to \mathrm{H}^*$ such that $c_q(h) = (\mathrm{Z}_q h|h)_{\mathrm{H}^*,\mathrm{H}}$. First, the constraint $\frac{\partial}{\partial h}\mathcal{H} = 0$ leads to the equation

$$\frac{\partial}{\partial h}\mathcal{H}(qp,h,\lambda) = \zeta_q^*\xi_q^* p - \mathrm{Z}_q h - \zeta_q^*\mathrm{C}_q^*\lambda = 0. \tag{101}$$

Solving (101) for h gives

$$h_{qp} = \mathrm{Z}_q^{-1}\zeta_q^*(\xi_q^* p - \mathrm{C}_q^*\lambda). \tag{102}$$

The constraint $\frac{\partial}{\partial \lambda}\mathcal{H} = 0$ leads to

$$\partial_\lambda \mathcal{H} = \mathrm{C}_q\zeta_q(h) = 0. \tag{103}$$

By inserting (102) it follows

$$\partial_\lambda \mathcal{H} = \mathrm{C}_q\zeta_q\mathrm{Z}_q^{-1}\zeta_q^*(\xi_q^* p - \mathrm{C}_q^*\lambda) = 0. \tag{104}$$

Now solving for λ gives first

$$\mathrm{C}_q\zeta_q\mathrm{Z}_q^{-1}\zeta_q^*\xi_q^* p = \mathrm{C}_q\zeta_q\mathrm{Z}_q^{-1}\zeta_q^*\mathrm{C}_q^*\lambda_{qp} \tag{105}$$

and then, assuming $\mathrm{C}_q\zeta_q\mathrm{Z}_q^{-1}\zeta_q^*\mathrm{C}_q^*$ is invertible,

$$\lambda_{qp} = (\mathrm{C}_q\zeta_q\mathrm{Z}_q^{-1}\zeta_q^*\mathrm{C}_q^*)^{-1}\mathrm{C}_q\zeta_q\mathrm{Z}_q^{-1}\zeta_q^*\xi_q^* p. \tag{106}$$

In [Arg14] it is stated that if C_q is surjective, the invertibility of the corresponding term $\mathrm{C}_q\mathrm{K}\mathrm{C}_q$ (where K is the reproducing kernel) in the multi-shape LDDMM setting follows. In the following proposition we provide a proof for the modular multi-shape setting.

Proposition 3.11

Let $\mathrm{C}_q\zeta_q \colon \mathrm{H} \to Y$ be surjective. Then the matrix $\mathrm{C}_q\zeta_q\mathrm{Z}_q^{-1}\zeta_q^*\mathrm{C}_q^*$ is invertible.

Proof: Define $f \colon \mathrm{H} \to \mathrm{Y}, f \coloneqq \mathrm{C}_q\zeta_q$. H is of finite dimension and $f \colon \mathrm{H} \to \mathrm{Y}$ is surjective by assumption, so Y must be of finite dimension. Because Y is of finite dimension, $f\mathrm{Z}_q^{-1}f^* \colon \mathrm{Y}^* \to \mathrm{Y}$ is invertible if and only if it is injective.

We first show that f^* is injective. For $\alpha \in \ker f^*$, by definition $f^*(\alpha) = 0$ and for all $h \in \mathrm{H}$: $\big(f^*(\alpha)\big|h\big)_{\mathrm{H}^*,\mathrm{H}} = 0$. f is surjective, so for all $y \in \mathrm{Y}$ there exists $h \in \mathrm{H}$ with $y = f(h)$. Then for all $y \in \mathrm{Y}$ it follows

$$\big(\alpha\big|y\big)_{\mathrm{Y}^*,\mathrm{Y}} = \big(\alpha\big|f(h)\big)_{\mathrm{Y}^*,\mathrm{Y}} = \big(f^*(\alpha)\big|h\big)_{\mathrm{H}^*,\mathrm{H}} = 0 \tag{107}$$

and therefore $\alpha = 0$. Therefore, $\mathrm{Z}_q^{-1}f^*$ is injective as both f^* and Z_q^{-1} are injective.

It remains to be shown that $f\big|_{\mathrm{Im}(\mathrm{Z}_q^{-1}f^*)}$ is injective. Let $\alpha \in \ker(f), h \in \mathrm{Im}(\mathrm{Z}_q^{-1}f^*)$ and $\lambda \in \mathrm{Y}^*$ such that $h = \mathrm{Z}_q^{-1}f^*(\lambda)$. Then

$$\big(\mathrm{Z}_q h|\alpha\big)_{\mathrm{H}^*,\mathrm{H}} = \big(f^*\lambda|\alpha\big)_{\mathrm{H}^*,\mathrm{H}} = \big(f^*\lambda\big|\alpha\big)_{\mathrm{H}^*,\mathrm{H}} = \big(\lambda\big|f\alpha\big)_{\mathrm{Y}^*,\mathrm{Y}} = 0 \tag{108}$$

for all $\alpha \in \ker(f)$.

It follows $h = 0$ or $h \notin \ker(f)$ as otherwise setting $\alpha = h$ would contradict the positive definiteness of Z_q.

So we obtain $\mathrm{Im}(\mathrm{Z}_q^{-1}f^*) \cap \ker(f) = \{0\}$. As the kernel $\ker(f_{\big|_{\mathrm{Im}(\mathrm{Z}_q^{-1}f^*)}})$ of f restricted on $\mathrm{Im}(\mathrm{Z}_q^{-1}f^*)$ is trivial and $C_q\zeta_q$ is linear, $f\big|_{\mathrm{Im}(\mathrm{Z}_q^{-1}f^*)}$ is injective.

All in all, $\mathrm{C}_q\zeta_q\mathrm{Z}_q^{-1}\zeta_q^*\mathrm{C}_q^* = f\mathrm{Z}_q^{-1}f^*$ is injective and therefore invertible. ■

Remark 3.12. Surjectivity of $\mathrm{C}_q\zeta_q$

Surjectivity of $\mathrm{C}_q\zeta_q$ is an important assumption in proposition 3.11. For the LDDMM multi shape setting, surjectivity becomes almost straightforward when the constraints are discretized to a finite number [ATTY15a]. Then they are true as soon as the points on which the constraints are defined are all distinct.
For our framework using deformation modules, we need to choose the space of controls H to be of the same or higher dimension as the space of constraints Y. If this is not given in the first place, the controls can be extended by adding for example local translations of the boundary points with a high penalty. For our examples of shapes in a background, C_q is always surjective as the dimension of the background space is at least the same as the number of constraints.

Having expressions of h_{qp} and λ_{qp}, the Hamiltonian function can be expressed depending only on the state q and the momentum p. This new function is referred to as the *reduced Hamiltonian* and we will denote it by $H(q,p)$.

Theorem 3.13. Reduced Hamiltonian for the Constrained Registration Problem

Defining the reduced Hamiltonian $H \colon \mathcal{O} \times \mathrm{T}_q^*\mathcal{O} \mapsto \mathbb{R}$,

$$H(q,p) \coloneqq \mathcal{H}(q,p,h_{qp},\lambda_{qp}), \tag{109}$$

the system of equations (100) for the Hamiltonian (99) is equivalent to

$$\begin{aligned} \dot{q} &= \frac{\partial}{\partial p}\mathcal{H}(q,p,h_{qp},\lambda_{qp}) \\ \dot{p} &= -\frac{\partial}{\partial q}\mathcal{H}(q,p,h_{qp},\lambda_{qp}) \end{aligned} \tag{110}$$

with

$$\begin{aligned} h_{qp} &= \mathrm{Z}_q^{-1}\zeta_q^*(\xi_q^* p - \mathrm{C}_q^*\lambda_{qp}) \\ \textit{and } \lambda_{qp} &= (\mathrm{C}_q\zeta_q\mathrm{Z}_q^{-1}\zeta_q^*\mathrm{C}_q^*)^{-1}\mathrm{C}_q\zeta_q\mathrm{Z}_q^{-1}\zeta_q^*\xi_q^* p \end{aligned} \tag{111}$$

In practice during the integration of $\dot{p}$ and $\dot{q}$, the geodesic variables h_{qp} and λ_{qp} are computed at every time step.

3.6 Geodesic Variables for Landmarks

Let us go back to the example 3.2 where we considered multiple shapes embedded in a background. In general, we want to define the background module in such a way that the deformation is not restricted to a particular type of modular deformation. It should correspond to the LDDMM framework, where the only restriction on the velocity field v is that it is an element of a RKHS V_σ. As mentioned earlier this setting does not satisfy the definition of a deformation module, where the space of controls is assumed to be finite. However we can define a finite-dimensional representation for $\mathrm{H} = V_\sigma$.

In this section we will prove that if finite-dimensional shape spaces are considered, we can define a finite-dimensional space $\overline{\mathrm{H}}_q$ and of the space H exists such that the solution of the problem 3.6 lies in $\overline{\mathrm{H}}_q$.

Consider the modules $\mathcal{M}^i = (\mathcal{O}^i, \mathrm{H}^i, \zeta^i, \xi^i, c^i)$ for $i = 1, ..., m$. Each of the modules $\mathcal{M}^i$ is assumed to model the deformation of N_i points, the shape spaces are given by $\mathcal{O}^i \coloneqq (\mathbb{R}^d)^{N_i}$. The spaces of controls H^i are restricted to be finite-dimensional. The background module $\mathcal{M}^{m+1} = (\mathcal{O}^{m+1}, \mathrm{H}^{m+1}, \zeta^{m+1}, \xi^{m+1}, c^{m+1})$ is given by

- the background shape space $\mathcal{O}^{m+1} \coloneqq \prod_{i=1}^m \mathcal{O}^i$ being the product space of all other shape spaces,
- the space of controls $\mathrm{H}^{m+1} \coloneqq V_{\sigma_{m+1}}$ being a RKHS defined by the Gaussian kernel $\mathrm{K}_{\sigma_{m+1}}$,
- the field generator $\zeta^{m+1}\colon \mathcal{O}^{m+1} \times \mathrm{H}^{m+1}; (q_t, h_t) \mapsto h_t$ as the identity mapping of controls,
- and the cost function $c_{q_t}^{m+1}(h_t) \coloneqq \int_0^1 \|h_t\|_{V_{\sigma_{m+1}}} \mathrm{d}t$.

In the following section, we will consider $q \in \mathcal{O}$ and $h \in \mathrm{H}$ for a specific time point and omit the index for the time-dependency, in order to reduce the number of indices. For q_j^i and h_j^i the index i refers to the module index and the index j to its component.

The point $q_j^{m+1,i}$ is the point on the background boundary, corresponding to the point q_j^i on the boundary of shape q^i.

We make the following assumption on the boundary constraints.

Assumption 3.14

There exists a linear function $g_q \colon \mathrm{T}_q\mathcal{O} \to \mathrm{Y}$ such that the constraints function $\mathrm{C} \colon \prod_{i=1}^{m+1} \mathcal{O}^i \times C^l(\mathbb{R}^d, \mathbb{R}^d) \to \mathrm{Y}$ can be written as

$$\mathrm{C}(q, v) = \mathrm{C}_q(v) = g_q(\xi_q(v)). \tag{112}$$

This assumption implies that the boundary constraints only take velocities of points into account that belong to the shape q. As the goal of using constraints in our example is to link the deformations of points in the shapes q^i and $q^{m+1,i}$, this assumption holds. The following example shows how the function g_q can be written as a matrix for the case of identity constraints of landmarks.

Example 3.15. Identity Constraints for Points

For the special case of identity constraints, the space of constraints Y is given by $Y = (Y^1, ..., Y^m) = (\mathrm{T}^*_{q^1}\mathcal{O}^1, ..., \mathrm{T}^*_{q^m}\mathcal{O}^m)$ and the constraints function C_q is given by $C_q(v) = \big(v^1(q^1) - v^{m+1}(q^{m+1,1}), ..., v^m(q^m) - v^{m+1}(q^{m+1,m})\big)$. Therefore it can be written componentwise as $\mathrm{C}_q(v) = \big(\mathrm{C}_q^1(v), ..., \mathrm{C}_q^m(v)\big)$ with $C_q^i(v) = v^i(q^i) - v^{m+1}(q^{m+1,i})$. In this case we have

$$C_q(v) = g_q\xi_q(v) = g_q(v^1(q^1), ..., v^{m+1}(q^{m+1})) = \sum_{i=1}^{m} g_q^i(v^i(q^i)) \tag{113}$$

Let $N = \sum N_i$. The function g_q is given by $g_q = (g_q^1, ..., g_q^{m+1})$ with

$$\begin{aligned} g_q^i &= (0, ..., 0, \mathrm{Id}_{N_i}, 0, ..., 0), \ i = 1, ..., m \\ \text{and} \quad g_q^{m+1} &= -\mathrm{Id}_N, \end{aligned} \tag{114}$$

Id_{N_i} being at the ith position in g_q^i.

Now recall the expression for the geodesic control

$$h_{qp} = {\mathrm{Z}_q}^{-1}\zeta_q^*(\xi_q^* p - \mathrm{C}_q^*\lambda_{qp}), \tag{115}$$

which, using the assumption 3.14, we will now write

$$h_{qp} = {\mathrm{Z}_q}^{-1}\zeta_q^*\xi_q^*(p - g_q^*\lambda_{qp}). \tag{116}$$

The idea behind the representation of the geodesic controls is to make use of the fact that they are only supported on points that belong to the shape q. This was pointed

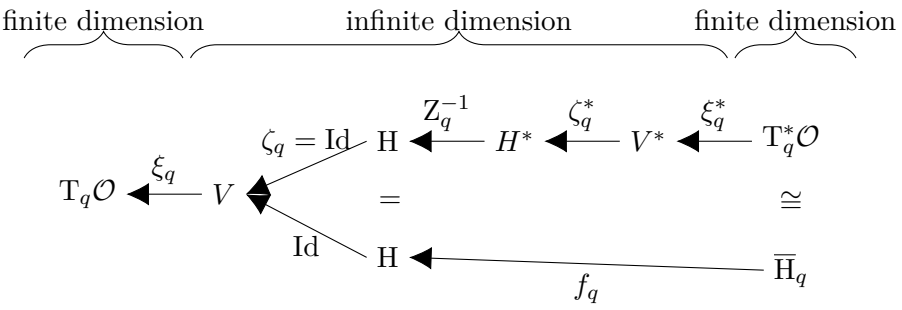

Figure 7: The diagram motivates the definition of a function f_q that corresponds to the functions $\mathrm{Z}_q^{-1}\zeta_q^*\xi_q^*$. This helps to avoid the expression of the geodesic controls in the infinite-dimensional space H. The function $\xi_q \mathrm{Id} f_q$ maps from the finite-dimensional space $\overline{\mathrm{H}}_q$ to the finite-dimensional space $\mathrm{T}_q\mathcal{O}$. Using this function does not need the expression of controls in infinite-dimensions. The space $\overline{\mathrm{H}}_q$ can be identified with $\mathrm{T}_q\mathcal{O} \cong \mathbb{R}^{dN}$, where $N = \sum_i^m N_i$ is the dimension of the product of shape spaces $\mathcal{O}^i$. What has to be verified is, that all controls that we want to consider, i.e., the geodesic controls, can be reached from f_q.

out in the previous chapter in section 2.1.7, where we studied the geodesic equations of the Hamiltonian system for LDDMM [1].

For our setting, a natural finite-dimensional representation for the background controls appears in equation (116): The geodesic controls depend on the term $(p - g_q^* \lambda_{qp})$ which is an element of the cotangent space $\mathrm{T}_q^*\mathcal{O}$ of the shape q. It has the same dimension as the shape. The idea now is to define the finite-dimensional space $\overline{\mathrm{H}}_q$ isomorphic to $\mathrm{T}_q^*\mathcal{O}$ and a function f_q that maps an element $\bar{h}_q \in \overline{\mathrm{H}}_q$ to an element h in the infinite-dimensional space H. The diagram in figure 7 visualizes this intuition.

As the space $\overline{\mathrm{H}}_q$ is of lower dimension than the original space of controls H, not all controls $h \in \mathrm{H}$ can be reached by f_q from $\bar{h}_q \in \overline{\mathrm{H}}_q$. In the following we will verify that all geodesic controls can be reached from $\overline{\mathrm{H}}_q$ by the mapping f_q.

First, to define the background control independently of the controls $h^i, i = 1, ..., m$, we need some preliminaries: We can compute the geodesic control h_{qp} and the function C_q componentwise, as we will show.

Because of linearity of C_q, g_q can be written as the sum $g_q(x) = \sum_{i=1}^{m+1} g_q^i(x^i)$ for $x = (x^1, ..., x^{m+1})$ and $g_q^i \colon \mathrm{T}_{q^i}\mathcal{O}^i \mapsto \mathrm{Y}$. Then writing

$$\begin{aligned}
(g_q^* \lambda | x)_{\mathrm{T}_q^*\mathcal{O}, \mathrm{T}_q\mathcal{O}} &= (\lambda | g_q x)_{\mathrm{Y}^*, \mathrm{Y}} = (\lambda | \sum_{i=1}^{m+1} g_q^i x^i)_{\mathrm{Y}^*, \mathrm{Y}} \\
&= \sum_{i=1}^{m+1} (\lambda | g_q^i x^i)_{\mathrm{Y}^*, \mathrm{Y}} = \sum_{i=1}^{m+1} ({g_{q^i}^i}^* \lambda | x^i)_{\mathrm{T}_{q^i}^*\mathcal{O}^i, \mathrm{T}_{q^i}\mathcal{O}^i} \\
&= ((g_q^{1*} \lambda, ..., g_q^{m+1*} \lambda) | (x^1, ..., x^{m+1}))_{\mathrm{T}_q^*\mathcal{O}, \mathrm{T}_q\mathcal{O}},
\end{aligned} \tag{117}$$

we find that $g_q^* = (g_q^{1*}, ..., g_q^{m+1*})$. Therefore, the adjoint constraints function is given by $C_q^* = \xi_q^* g_q^* = ({\xi_{q^1}^1}^* g_q^{1*}, ..., {\xi_{q^{m+1}}^{m+1}}^* g_q^{m+1*})$. We define $C_q^i \coloneqq g_q^i \xi_{q^i}^i$.

[1] Recall that the equation $v = \mathrm{K}\xi_q^* p$ implies that the momentum $m \coloneqq \mathrm{K}^{-1} v = \xi_q^* p$ is only supported on the shape q

Furthermore we resume:

Corollary 3.16

For the geodesic control $h_{qp} = (h^1_{qp}, ..., h^{m+1}_{qp})$, each component h^i_{qp} can be written as $h^i_{qp} = {\mathrm{Z}^i_{q^i}}^{-1} {\zeta^i_{q^i}}^* ({\xi^i_{q^i}}^* p^i - {\mathrm{C}^i_q}^* \lambda)$.

Proof: The operators Z_q^{-1}, ζ_q^*, ξ_q^* and C_q^* can all be applied componentwise. For $p = (p^1, ..., p^{m+1}) \in \mathrm{T}^*_q\mathcal{O}$ it holds

$$\big(\xi_q^* p \big| v\big)_{V^*,V} = \big(p \big| \xi_q(v)\big)_{\mathrm{T}^*_q\mathcal{O},\mathrm{T}_q\mathcal{O}} = \sum_{i=1}^{m+1} \big(p^i \big| \xi^i_{q^i}(v^i)\big)_{\mathrm{T}^{i*}_q\mathcal{O},\mathrm{T}^i{}_q\mathcal{O}} = \sum_{i=1}^{m+1} \big({\xi^i_{q^i}}^* p^i \big| v^i\big)_{V^*,V}, \quad (118)$$

and thus it follows

$$\xi_q^* p = ({\xi^1_{q^1}}^* p^1, ..., {\xi^{m+1}_{q^{m+1}}}^* p^{m+1}). \quad (119)$$

Similarly, for $\delta = (\delta^1, ..., \delta^{m+1}) \in V^*$ it holds

$$\big(\zeta_q^* \delta \big| h\big)_{\mathrm{H}^*,\mathrm{H}} = \big(\delta \big| \zeta_q(h)\big)_{V^*,V} = \sum_{i=1}^{m+1} \big(\delta^i \big| \zeta^i_{q^i}(h^i)\big)_{V^{i*},V^i} = \sum_{i=1}^{m+1} \big({\zeta^i_{q^i}}^* \delta^i \big| h^i\big)_{\mathrm{H}^{i*},\mathrm{H}^i}, \quad (120)$$

which implies

$$\zeta_q^* \delta = ({\zeta^1_{q^1}}^* \delta^1, ..., {\zeta^{m+1}_{q^{m+1}}}^* \delta^{m+1}). \quad (121)$$

Moreover, $C_q^* = \xi_q^* g_q^*$ can be written as

$$C_q^* \lambda = \xi_q^* g_q^* \lambda = \big({\xi^1_{q^1}}^* {g_q^1}^* \lambda, ..., {\xi^{m+1}_{q^{m+1}}}^* {g_q^{m+1}}^* \lambda\big). \quad (122)$$

The cost $c_q(h)$ of the multi-shape module is defined as the sum of the costs of each module. Therefore we have

$$c_q(h) = \big(\mathrm{Z}_q h \big| h\big)_{\mathrm{H}^*,\mathrm{H}} = \sum_{i=1}^{m+1} \big(\mathrm{Z}^i_{q^i} h^i \big| h^i\big)_{\mathrm{H}^{i*},\mathrm{H}^i} = \big((\mathrm{Z}^1_{q^1} h^1, ..., \mathrm{Z}^{m+1}_{q^{m+1}} h^{m+1}) \big| h\big)_{\mathrm{H}^*,\mathrm{H}}. \quad (123)$$

For the cost operator Z_q it follows $\mathrm{Z}_q = (\mathrm{Z}^1_{q^1}, ..., \mathrm{Z}^{m+1}_{q^{m+1}})$. Therefore it follows for the composition of the operators that

$$\begin{aligned} h_{qp} &= \mathrm{Z}_q^{-1} \zeta_q^* (\xi_q^* p - \mathrm{C}_q^* \lambda) \\ &= ({\mathrm{Z}^1_{q^1}}^{-1} {\zeta^1_{q^1}}^* ({\xi^1_{q^1}}^* p^1 - {\xi^1_{q^1}}^* {g^1_{q^1}}^* \lambda), ..., \\ &\quad {\mathrm{Z}^{m+1}_{q^{m+1}}}^{-1} {\zeta^{m+1}_{q^{m+1}}}^* ({\xi^{m+1}_{q^{m+1}}}^* p^{m+1} - {\xi^{m+1}_{q^{m+1}}}^* {g_q^{m+1}}^* \lambda)) \end{aligned} \quad (124)$$

■

The following lemma finally provides the tools to express the geodesic controls in finite-dimension, in the way that was motivated in figure 7.

Lemma 3.17

Let $\mathbf{M}^{multi}$ be the multi-shape combination of modules $\mathcal{M}^i, i = 1, ..., m$ and back-

ground module $\mathcal{M}^{m+1}$ where $\mathcal{O}^i$ is N_i-dimensional for $i = 1, ..., m$; H^i finite-dimensional for $i = 1, ..., m$; $\mathrm{H}^{m+1} \coloneqq V_{\sigma_{m+1}}$ a RKHS. Let $C_q = g_q \xi_q$ be linear kinetic constraints. For the geodesic control h_{qp}^{m+1} there exists a $N_1 + ... + N_m$-dimensional representation $\bar{h}_{qp}^{m+1} \in \overline{\mathrm{H}}_q^{m+1}$ and a function $f_q \colon \overline{\mathrm{H}}_q^{m+1} \to \mathrm{H}_q^{m+1}$, with

$$f_q(\bar{h}_{qp}^{m+1}) = h_{qp}^{m+1}. \tag{125}$$

The space $\overline{\mathrm{H}}_q^{m+1}$ can be identified with the cotangent space $\mathrm{T}^*_{q^{m+1}}\mathcal{O}^{m+1}$. The representation $\bar{h}_{qp}^{m+1}$ and the function f_q are given by

$$\bar{h}_{qp}^{m+1} = p^{m+1} - g_q^{m+1^*}\lambda \quad \text{and} \quad f_q \colon h \mapsto \mathrm{Z}_{q^{m+1}}^{m+1\ -1} \zeta_{q^{m+1}}^{m+1\ *} \xi_{q^{m+1}}^{m+1\ *}. \tag{126}$$

Proof: From Corollary 3.16 we have $h_{qp}^{m+1} = \mathrm{Z}_{q^{m+1}}^{m+1\ -1} \zeta_{q^{m+1}}^{m+1\ *} (\xi_{q^{m+1}}^{m+1\ *} p^{m+1} - \mathrm{C}_q^{m+1^*}\lambda)$, and with $\mathrm{C}_q^{m+1} = g_q^{m+1}\xi_q^{m+1}$ it follows

$$h_{qp}^{m+1} = \mathrm{Z}_{q^{m+1}}^{m+1\ -1} \zeta_{q^{m+1}}^{m+1\ *} \xi_{q^{m+1}}^{m+1\ *} (p^{m+1} - g_q^{m+1^*}\lambda). \tag{127}$$

So $\bar{h}_{qp}^{m+1} \coloneqq p^{m+1} - g_q^{m+1^*}\lambda$ and $f_q \colon h \mapsto \mathrm{Z}_{q^{m+1}}^{m+1\ -1} \zeta_{q^{m+1}}^{m+1\ *} \xi_{q^{m+1}}^{m+1\ *}$ satisfy $f_q(\bar{h}_{qp}^{m+1}) = h_{qp}^{m+1}$. Because $\mathcal{O}^{m+1} = \prod_{i=1}^m \mathcal{O}^i$ is finite-dimensional, $\mathrm{T}^*_{q^{m+1}}\mathcal{O}^{m+1}$ is finite-dimensional. More precisely,

$$\begin{aligned} \dim(\mathrm{T}^*_{q^{m+1}}\mathcal{O}^{m+1}) = \dim(\mathrm{T}_q(\prod_{i=1}^m \mathcal{O}^i)) = \dim(\prod_{i=1}^m \mathrm{T}^*_{q^i}\mathcal{O}^i) \\ = \sum_{i=1}^m \dim(\mathrm{T}^*_{q^i}\mathcal{O}^i) = \sum_{i=1}^m N_i. \end{aligned} \tag{128}$$

So $\bar{h}_{qp}^{m+1} \in \mathrm{T}^*_{q^{m+1}}\mathcal{O}^{m+1}$ is a $N_1 + ... + N_m$-dimensional representation of h_{qp}^{m+1}. ■

Remark 3.18

In general, there exists a representation $f_q(\bar{h}_{qp}) = h_{qp}$ with $\bar{h}_{qp} \in \mathrm{T}^*_q\mathcal{O}$. For the case of finite-dimensional shapes $q \in \mathcal{O}$, the cotangent space $\mathrm{T}_q\mathcal{O}$ is finite-dimensional. In the case of infinite-dimensional shape spaces one will have to define a finite-dimensional representation $\tilde{q} \in \tilde{\mathcal{O}}$ and a function $\tilde{f}_q \colon \tilde{\mathcal{O}} \to \mathcal{O}; \tilde{q} \mapsto q$ for the implementation. Then the finite representation of h_{qp} lies in $\mathrm{T}^*_{\tilde{q}}\tilde{\mathcal{O}}$ and a function mapping the finite representation $\tilde{h}_{qp} \in \mathrm{T}^*_{\tilde{q}}\tilde{\mathcal{O}}$ to h_{qp} can be defined.

Finally, we reformulate the geodesic equations for problem 3.6 in terms of the finite-dimensional background representation.

Corollary 3.19. Geodesic Variables for Finite-Dimensional Shape Spaces

Let $\mathcal{M}^i = (\mathcal{O}^i, \mathrm{H}^i, \zeta^i, \xi^i, c^i)$ be deformation modules with finite-dimensional shape spaces $\mathcal{O}^i = (\mathbb{R}^d)^{N_i}$. Let $N \coloneqq \sum_{i=1}^m N_i$.
Let $\mathcal{M}^{m+1} = (\mathcal{O}^{m+1}, \overline{\mathrm{H}}^{m+1}, \bar{\zeta}^{m+1}, \bar{\xi}^{m+1}, \bar{c}^{m+1})$ be the finite-dimensional background representation with

- shape space $\mathcal{O}^{m+1} \coloneqq \prod_{i=1}^m \mathcal{O}^i = (\mathbb{R}^d)^N$,
- space of controls $\mathrm{H}^{m+1} = (\mathbb{R}^d)^N$,
- field generator $\bar{\zeta}_q(h) = \sum_{i=1}^m \sum_{j=1}^{N_i} \mathrm{K}_{\sigma_{m+1}}(q_j^i, \cdot) h_j^i$,
- infinitesimal action $\bar{\xi}_q(v) \coloneqq v(q)$, and
- cost $\bar{c}_q(h) = \sum_{i,j} \sum_{k,l} {h_j^i}^\top \tilde{\mathrm{K}}(q_j^i, q_l^k) h_l^k$, and
  cost operator $\overline{\mathrm{Z}}_q = \tilde{\mathrm{K}}_{q^{m+1}, q^{m+1}}$.

Let $\mathbf{M}^{multi}$ be a multi-shape combination of deformation modules $\mathcal{M}^i, i = 1, ..., m+1$. For the associated reduced Hamiltonian $H \colon \mathcal{O} \times \mathrm{T}_q^*\mathcal{O} \mapsto \mathbb{R}$,

$$H(q,p) = \mathcal{H}(q, p, h_{qp}, \lambda_{qp}), \tag{129}$$

the system of equations (100) for the Hamiltonian (99) is equivalent to

$$\begin{aligned} \dot{q} &= \frac{\partial}{\partial p} \mathcal{H}(q, p, h_{qp}, \lambda_{qp}) \\ \dot{p} &= -\frac{\partial}{\partial q} \mathcal{H}(q, p, h_{qp}, \lambda_{qp}) \end{aligned} \tag{130}$$

with geodesic variables

$$\begin{aligned} h_{qp} &= (h_{qp}^1, ..., h_{qp}^m, \bar{h}_{qp}^{m+1}) \\ \text{and} \quad \lambda_{qp} &= (\mathrm{C}_q \zeta_q \mathrm{Z}_q^{-1} \zeta_q^* \mathrm{C}_q^*)^{-1} \mathrm{C}_q \zeta_q \mathrm{Z}_q^{-1} \zeta_q^* \xi_q^* p \end{aligned} \tag{131}$$

where

$$\begin{aligned} h_{qp}^i &= {\mathrm{Z}^i}_{q^i}^{-1} {\zeta^i}_{q^i}^* {\xi^i}_{q^i}^* (p^i - {g^i}_{q^i}^* \lambda_{qp}) \quad \text{for} \quad i = 1, ..., m \\ \bar{h}_{qp}^{m+1} &= p^{m+1} - {g^{m+1}}_{q^{m+1}}^* \lambda_{qp} \end{aligned} \tag{132}$$

As a demonstration of geodesic variables computation we provide the derivation of the explicit terms for the example 3.2, considering translations of landmarks in a background, in the appendix.

The computations will amount to the expressions

$$h_{qp} = \begin{pmatrix} \tilde{\mathrm{K}}^1_{z^1,q^1} & 0 & 0 \\ 0 & \tilde{\mathrm{K}}^2_{z^2,q^2} & 0 \\ 0 & 0 & \mathrm{Id} \end{pmatrix} \left(p - \begin{pmatrix} \lambda \\ -\lambda \end{pmatrix} \right). \tag{133}$$

and

$$\begin{aligned} &\left(\begin{pmatrix} \tilde{\mathrm{K}}^1_{q^1,z^1} \tilde{\mathrm{K}}^1_{z^1,q^1} & 0 \\ 0 & \tilde{\mathrm{K}}^2_{q^2,z^2} \tilde{\mathrm{K}}^2_{z^2,q^2} \end{pmatrix} + \tilde{\mathrm{K}}^3_{q,q} \right) \lambda_{qp} \\ &\qquad = \begin{pmatrix} \tilde{\mathrm{K}}^1_{q^1,z^1} \tilde{\mathrm{K}}^1_{z^1,q^1} & 0 & \tilde{\mathrm{K}}^3_{q^{3,1},q^3} \\ 0 & \tilde{\mathrm{K}}^2_{q^2,z^2} \tilde{\mathrm{K}}^2_{z^2,q^2} & \tilde{\mathrm{K}}^3_{q^{3,2},q^3} \end{pmatrix} p, \end{aligned} \tag{134}$$

Here $\tilde{\mathrm{K}}^i_{x,y} \coloneqq \tilde{\mathrm{K}}^i(x,y)$ is the $d(n_1) \times d(n_2)$ kernel matrix corresponding to the ith module, with values $\left(\tilde{\mathrm{K}}(x,y)\right)_{i,j} = \mathrm{k}(x^i, y^j)$ for $x = (x^1, ..., x^{n_1}) \in (\mathbb{R}^d)^{n_1}$, $y = (y^1, ..., y^{n_2}) \in (\mathbb{R}^d)^{n_2}$ (see also Notation chapter). In the explicit expressions it can be seen that the components of the geodesic controls are linked only implicitly through the variable λ_{qp} in (134).

The expression $(\mathrm{C}_q \zeta_q \mathrm{Z}_q^{-1} \zeta_q^* \mathrm{C}_q^*) \lambda_{qp}$ amounts to a kernel convolution of all components of λ_{qp} with the kernel associated to the background, summed with convolutions of the components of λ_{qp} associated with a module $\mathcal{M}^i$ and the corresponding kernel for each $i = 1, ..., m$. If the scale of the background kernel is chosen small in relation to the distance of points belonging to different shapes, then the cooresponding values in the convolution matrix $\tilde{\mathrm{K}}^3_{q^3,q^3}$ will be very small. This amounts to little influence between the deformations of different shapes. If the scale of the kernel is chosen a higher value, the link between deformations of different shapes becomes more important. This can be observed in practice in numerical experiments and will be pointed out in the next chapter, where we examine practical results of our implementation of the new framework.

Chapter 4: Numerical Results

In order to verify that the approach works numerically, and to get an intuition of its qualitative behaviour, we present the shape registration of two synthetic data sets. The implementation was done in Python using the PyTorch library for automatic differentiation in the optimization.

The basis for the implementation was a class-oriented implementation of the deformation modules framework, provided by Leander Lacroix. It included classes for deformation modules and shape types that we use for our work. In order to extend the model to multiple shapes, a new class for multi-shape combinations has been constructed, where the key point is the automatic generation of the background module and computation of the geodesic variables. Several other adaptions have been made. As a starting point, we used shapes as points in two dimensions, and translation and scaling deformation modules as well as the compound deformation module for the internal combination of modules.

We will compare our newly presented framework to the multi-shape LDDMM framework of Arguillère et al. as well as to LDDMM and compound deformation modules. The computation for the standard LDDMM framework was done using a sum of local translations deformation module, which amounts to the same theoretical solution for the minimization problem, as explained in 2.3.

The optimization was done using the BFGS optimization algorithm from the SciPy package.

4.1 Translation of Shapes in a Background

For a demonstration of the behaviour of the boundary constraints, we consider the example of two discretized circles translated closely in a shared background. The source and target shape are given in figure 8. For this example we chose the L^2-norm between corresponding points as a data attachement term.

Although with all models the target can be reached from the source, the resulting deformation grids and the states during the shooting have a very different appearance.

Figure 9 shows the resulting deformations from the multi-shape deformation modules approach. The scale of the Gaussian kernel was set to $\sigma = 20$ for the region inside the two shapes and $\sigma = 0.5$ for the background. The translation of the shapes is modeled using using one translation vector as control variable, that is supported at the mean of the shapes. Figures (b) and (c) show the translation for the two circles. The grid itself is only bent slightly while the whole grid is translated. For the background module in figure (d) we see a higher amount of deformation in the grid itself.

The points that lie on the circles are translated while points that are further away from the circle boundaries experience a lower translation. Because a high variation in the deformation is allowed, the circles can be translated without being much influenced by the deformation of points that belong to the other circle. Considering the points on the boundary, we see that the deformations are consistent for the deformations inside the

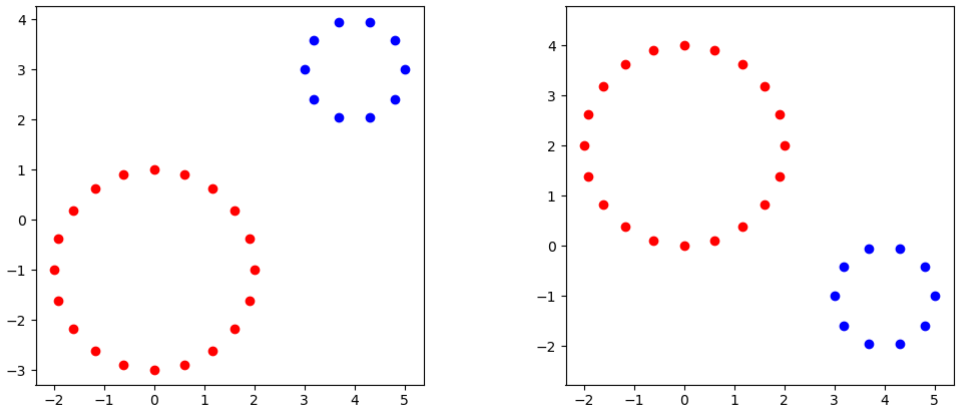

(a) source shapes

(b) target shapes

Figure 8: Source and target shape for translations of circles in a background. Two shapes that represent the discretization of curves are shown. The two shapes are depicted in different colours, indicating which shapes correspond in the two images. For each point in the source the point correspondence in the target is given, such that they can be transformed by one vertical translation.

circle and for the background. The points are transported by the same velocity fields.

The results for the multi-shape LDDMM approach are shown in figure 10. The kernel scales are set to $\sigma = 5$ inside the shapes and $\sigma = 0.5$ for the background. We see similar results as for the multi-shape deformation modules approach. The deformations of the circles are consistent with the deformation of the background thanks to the coundary constraints. The deformation inside the circles is less smooth than for the multi-shape deformation modules approach in figure 9. This could be reduced by using a bigger kernel scale.

Figure 10 shows the results for the LDDMM approach using a Gaussian kernel of scale $\sigma = 5$ and with a scale of $\sigma = 0.5$. With a scale of $\sigma = 5$ the deformation of the two circles influence each other in such a way that they are prevented from coming too close.

Figures 12, 13, 14 and 15 show the iterations of the geodesic shooting over ten time steps. For the multi-shape deformation module approach, the circles preserve their volume over time. In the multi-shape LDDMM approach the circles reduce their radius during the shooting, having a minimal radius at $t = 0.5$. The same behaviour can be observed for standard LDDMM with a kernel scale $\sigma = 0.5$. The radius of the right circle reduces approximately to one third of the radius at time $t = 0$ and $t = 1$. A weaker reduction is happening for the left, bigger circle. This behaviour is typical for LDDMM and can be reduced using multi-shape boundary constraints compared to LDDMM [Arg14]. For the LDDMM setting with a scale of $\sigma = 5$, the bigger scale prevents the circle from getting close to each other. It can be observed that the shapes keep approximately the same distance from each other, resulting in distortion to an ellipse-like shape during the shooting.

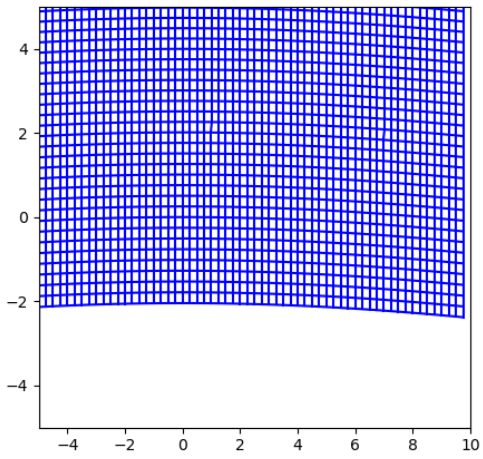

(a) Deformation grid corresponding to the left shape. The whole grid is translated upwards due to a high kernel scale of $\sigma = 20$.

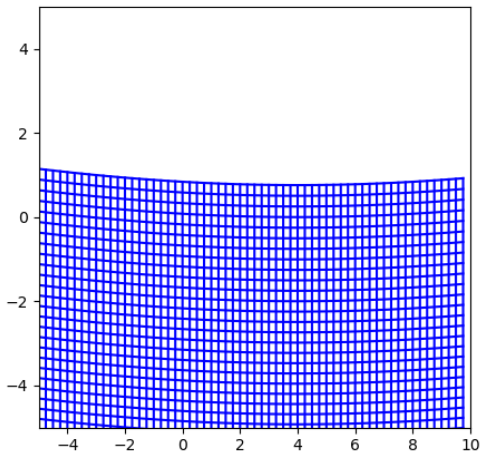

(b) Deformation grid corresponding to the left shape. The whole grid is translated downwards due to a high kernel scale of $\sigma = 20$.

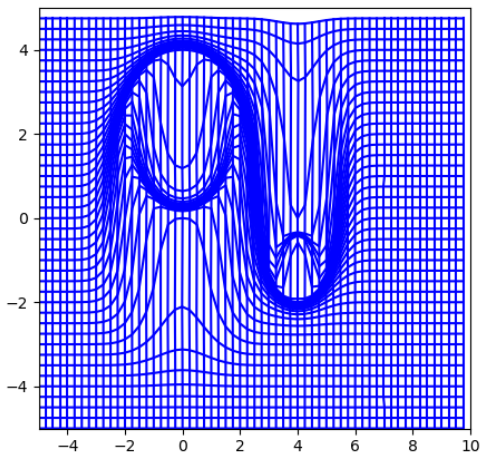

(c) Deformation grid corresponding to the background. The kernel scale is set to $\sigma = 0.5$. The small kernel scale allows an irregular deformation.

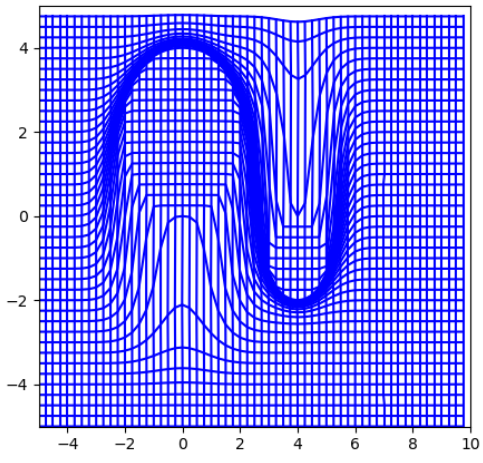

(d) Multi-shape combination of the deformation grids for shapes and background. The combined grid is continuous at the circle boundaries due to the identity boundary constraints.

Figure 9: Deformation grids of the shapes and background and combined grid for the proposed multi-shape deformation modules framework. The deformations inside the two shapes approximate a global translation due to a high kernel scale of $\sigma = 20$. The support for the translation vector is the center of the circle. In the background the kernel scale is chosen to be relatively small ($\sigma = 0.5$), to allow a high deformation variability in smaller regions. The combined grid is continuous at the boundaries of the circles due to the identity constraints.

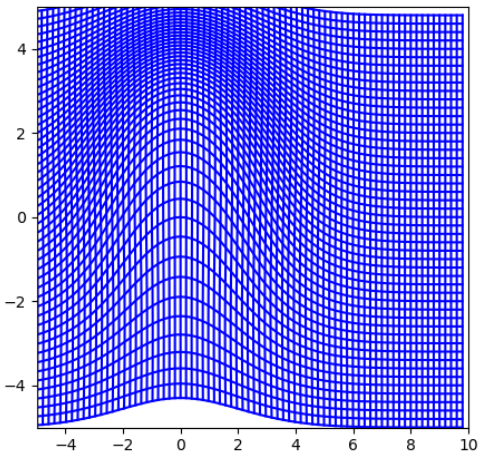

(a) Deformation grid corresponding to the bigger circle. The grid is relatively regular.

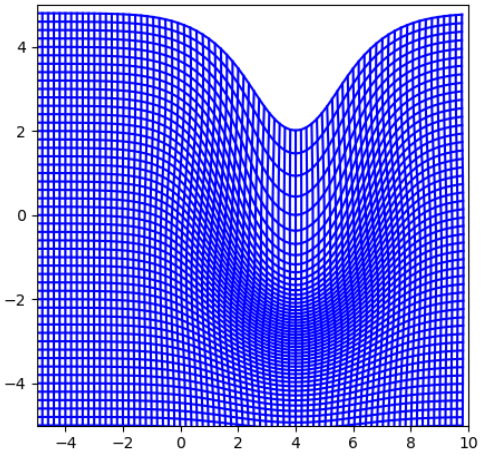

(b) Deformation grid corresponding to the smaller circle. The shape is experiencing a bigger translation relative to its size, which results in a higher deformation compared to the deformation of the bigger circle.

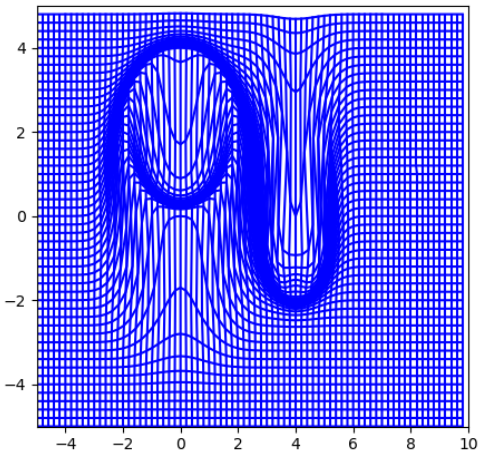

(c) Deformation grid corresponding to the background. The deformation is irregular due to a small kernel scale of $\sigma = 0.5$.

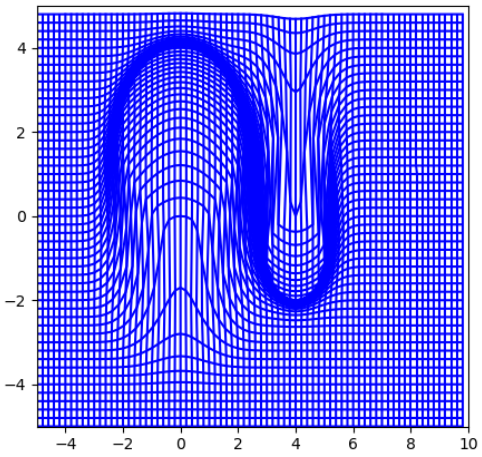

(d) Multi-shape combination of the deformation grid. The grid is continuous at the circles boundaries due to the use of identity constraints.

Figure 10: Deformation grids of the shapes, background and combined grid for the multi-shape LDDMM framework. The kernel scale for the deformation inside the shapes is set to $\sigma = 5$, the scale of the background is $\sigma = 0.5$. The combination of the grids is continuous at the shape boundaries, as in the multi-shape deformation modules setting. Opposed to figure 9, the region inside the circles are more irregular due to the choice of the kernel scale.

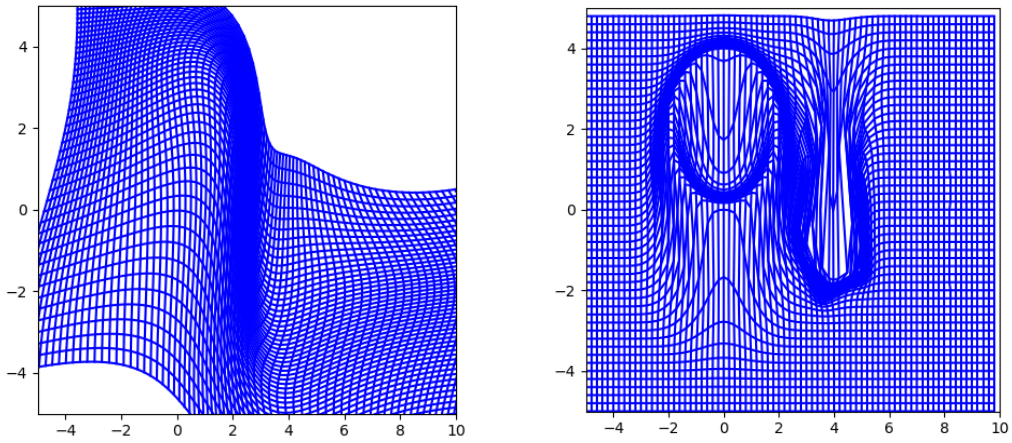

(a) Deformation grid for LDDMM with $\sigma = 5$. The relatively high kernel scale prevents an irregular grid with high deformations.

(b) Deformation grid for LDDMM with $\sigma = 0.5$. The relatively low kernel scale allows for more irregular deformations.

Figure 11: Deformation grids for the LDDMM framework with two different scalings. The deformation with a higher kernel scaling of $\sigma = 5$ forces the grid to high smoothness and prevents high deformations in a small region. The deformation with a low kernel of $\sigma = 0.5$ allows high differences in the translation relatively of close points. The region inside the shapes is not as much influenced by the boundary deformation.

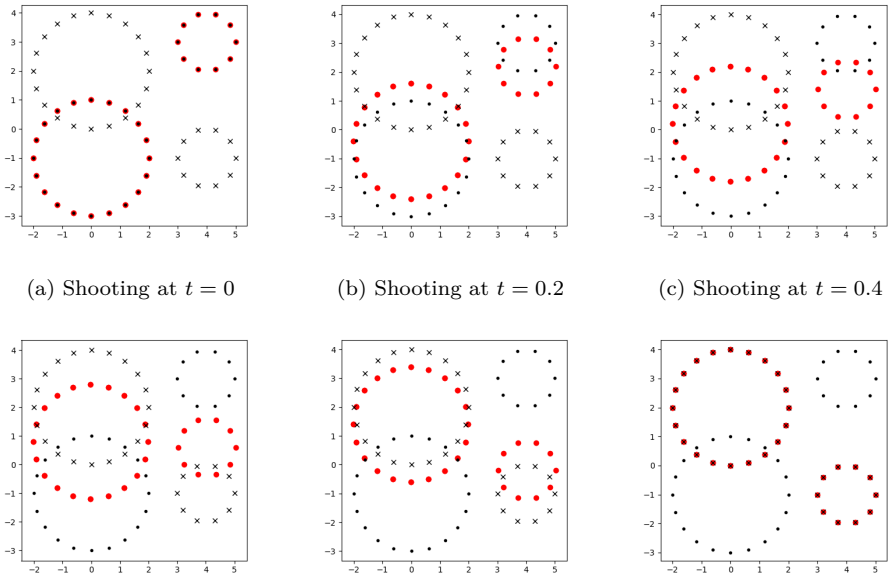

(a) Shooting at $t = 0$

(b) Shooting at $t = 0.2$

(c) Shooting at $t = 0.4$

(d) Shooting at $t = 0.6$

(e) Shooting at $t = 0.8$

(f) Shooting at $t = 1$

Figure 12: Shooting iterations over time for the multi-shape deformation module approach, compare figure 9. The source shapes are marked with black points, the target shapes with black crosses, and the current state q_t during the shooting with red points. During the shooting the circles preserve their appearance and volume.

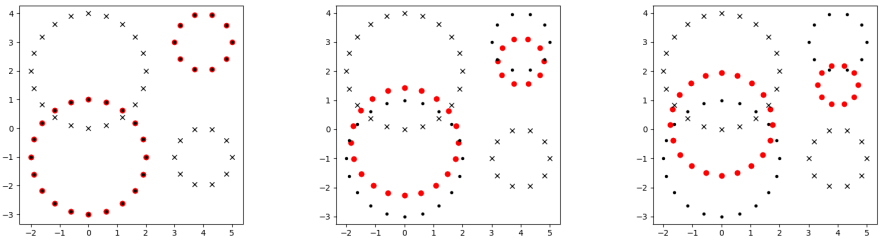

(a) Shooting at $t = 0$ (b) Shooting at $t = 0.2$ (c) Shooting at $t = 0.4$

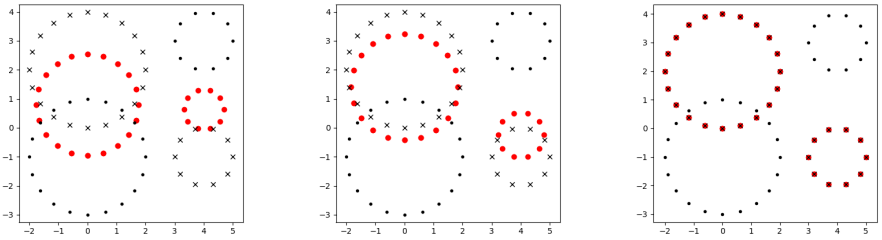

(d) Shooting at $t = 0.6$ (e) Shooting at $t = 0.8$ (f) Shooting at $t = 1$

Figure 13: Shooting iterations over time for the multi-shape LDDMM approach, compare figure 10. During the shooting the circles get slightly smaller than their original radius at time $t = 0$ and $t = 1$. The small scale of the background kernel allows the shapes to come close to each other during the shooting without being influenced by each other.

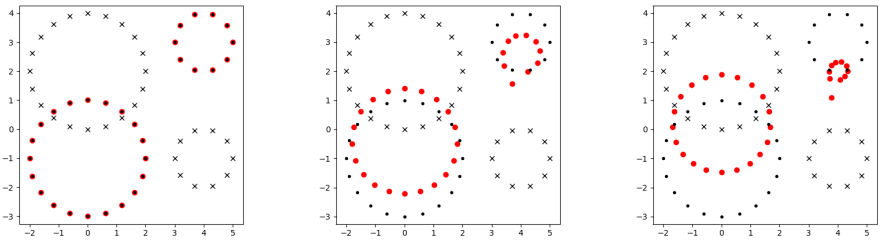

(a) Shooting at $t = 0$ (b) Shooting at $t = 0.2$ (c) Shooting at $t = 0.4$

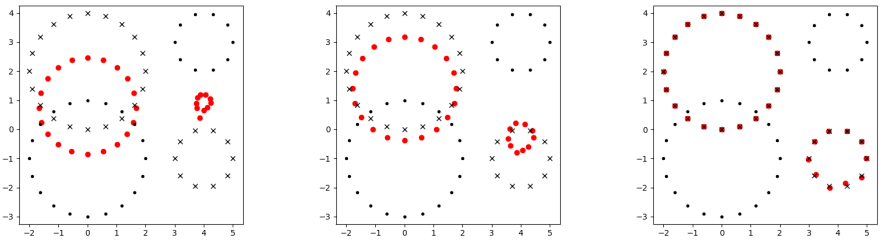

(d) Shooting at $t = 0.6$ (e) Shooting at $t = 0.8$ (f) Shooting at $t = 1$

Figure 14: Shooting iterations over time for LDDMM with $\sigma = 0.5$, compare figure 11b. During the shooting the smaller circle is experiencing a high amount of size reduction. The bigger circle is being reduced to a smaller extent.

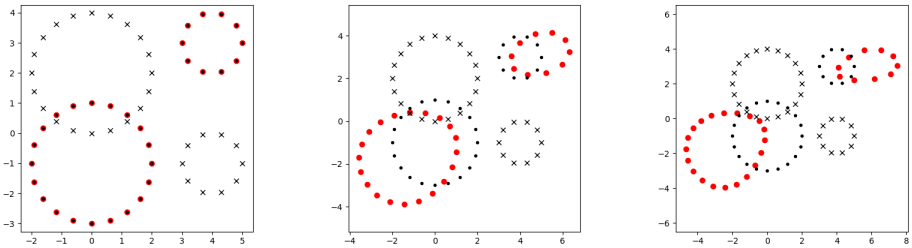

(a) Shooting at $t = 0$ (b) Shooting at $t = 0.2$ (c) Shooting at $t = 0.4$

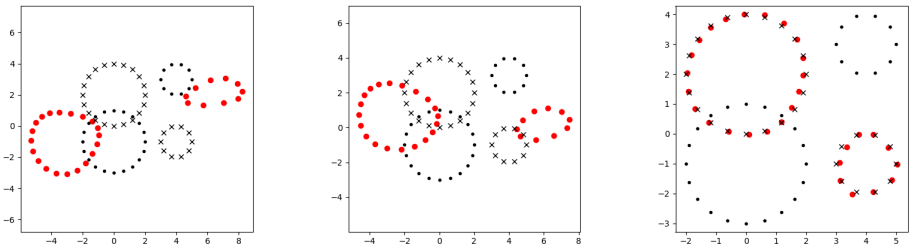

(d) Shooting at $t = 0.6$ (e) Shooting at $t = 0.8$ (f) Shooting at $t = 1$

Figure 15: Shooting iterations over time for LDDMM with $\sigma = 5$, compare figure 11a. The larger kernel scale does not allow the shapes to come close to each other during the shooting. Therefore they are avoiding each other, resulting in an arc-like trajectory. Moreover they are both deformed to ellipse-like irregular shapes during the shooting.

4.2 Local Scalings and Translation

The second example is chosen in order to demonstrate how more complex deformations can be obtained by combining compound modules, acting as an internal combination, and the multi-shape framework, modeling an external combination.

We study the deformation of two peanut-shaped curves, shown in figure 16. Compared to the source shape, the nuts in the target shape are enlarged in one part and reduced in the other part of the shape. This will be modeled with deformation modules for local scalings, as described in section 2.3. We thank Alain Trouvé for providing the code for data generation.

As the similarity measure for the shapes we chose the varifold attachment as introduced in [CT13], which provides a way to compare curves without point correspondence. [2]

The deformation modules for each shape are chosen as a combination of two scalings with a Gaussian kernel scale of $\sigma = 1$ and a local translation with a high scale of $\sigma = 10$ to model the translation of the whole shape. Furthermore, local translations at each point of the curve were added with a high penalty coefficient to facilitate an exact registration.

[2] As pointed out in [CT13], the concept of varifolds provides a way to numerically encode an unoriented manifold. The authors explain how a metric can be built using the theory of reproducing kernels. For further details we refer to [CT13]. At this point we only emphasize the fact that the metric is independent of the parametrization of the manifold and therefore no point correspondence is needed.

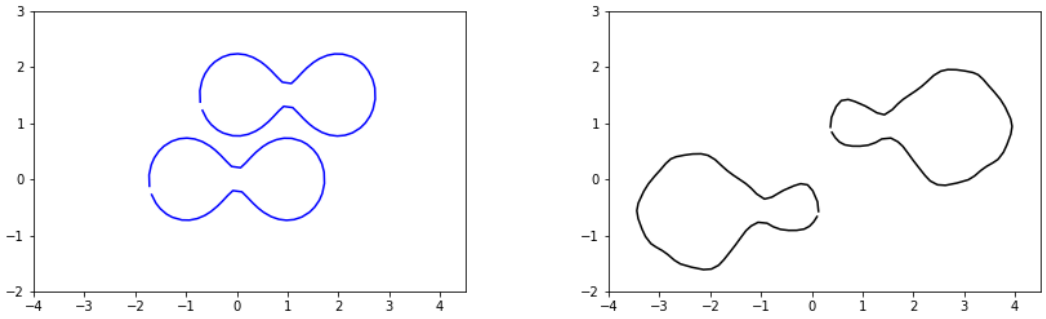

(a) Source shape

(b) Target shape

Figure 16: source and target shape for the peanut-shaped curves, see section 4.2. The target shape results from the source shape by two scalings centered at both halfs of the nut, and a translation of the whole shape in opposite directions. The goal of the registration is to match the above shape in the source to the right shape in the target, and the shape below in the source to the shape on the left in the target.

We use identity constraints at the boundaries for both multi-shape frameworks.

In figure 17, the deformation grid resulting of the multi-shape deformation modules framework are shown. The deformation grids of the shapes, compare figure 17a and 17b, model the scalings of the two seperate shapes, that are combined with the background in figure 17d. For the multi-shape LDDMM framework, the optimization terminated before convergence due to precision loss. The algorithm stopped after two iterations. The resulting deformation grids are shown in figure 18. Comparing with figure 22, it can be seen that the deformed source shape is transformed irregularly into the targets direction. In the LDDMM framework, the algorithm also terminated due to precision loss, after 49 iterations. Compared to the multi-shape LDDMM framework the shapes were transformed closer to the target due to more iterations.

A possible explanation for the numerical errors could be that the computation of the geodesic variables was done in the multi-shape deformation modules setting. This arises due to two kernel multiplications and one inversion, while in LDDMM there is only one kernel multiplication involved [3]. When the points of the shape are close to each other relative to the kernel scale this could have lead to precision loss. For the deformation modules we used for the multi-shape modular framework this difficulty does not arise because the geometrical descriptors of the modules are relatively far from the geometrical descriptors on the boundary.

Figure 20 and 24 show the results of the shape registration using a compound deformation module. The states during the shooting indicate that instead of local scalings, the local translations of the boundary points were used to reach the target. This happened

[3] This appears when computing the term $\xi_q \zeta_q Z_q^{-1} \zeta_q^* \xi^*$. The terms $\xi_q \zeta_q$ and $\zeta_q^* \xi^*$ arise to the same kernel convolution, where the term Z_q^{-1} is the inverse of this convolution in the case of LDDMM. In the computation of the geodesic variables in the original multi-shape LDDMM framework, the whole term corresponds to one convolution with the reproducing kernel. The same appeared when we calculated the expression for the background geodesic control in A.1.

despite the fact that the cost of the boundary translations was strongly penalized (with a factor of 400 instead, opposed to a factor of 1 for scalings and 10 for the translation centered at the mean point of the shapes). This indicates that the compound module is not suitable for settings as in this experiment with deformations happening very close in a very different nature.

From a qualitative point of view it can be said that the multi-shape deformation module approach yields a plausible deformation grid for the considered prior. Using the LDDMM shooting method, a grid that can model a scaling can not be obtained. If the kernel is chosen too big, the deformation of each point influences a bigger region around the point, which prevents deformations of two close shapes from being of very different nature. If the kernel is chosen too small, then the curves representing the boundaries can be deformed very loosely. The space of reachable deformed shapes is bigger. However, a small kernel cannot model the influence of the curve deformation inside the region, which results in less reuglar deformations. Points that lie inside the curves but relatively far from the boundary do not, or only to a small extend, experience the deformation. This can be seen in the grids of the background deformations and in figure 11b, where LDDMM with a small kernel scale was used.

Using a compound deformation module for two close shapes amounts to the same problem as choosing a high scale for the kernel in LDDMM. The two shapes are influencing each other and are prevented from being separated, as seen in figure 20.

This shows that our new framework is capable of building deformations that none of the tested state-of-the-art models can achieve.

Table 1 shows the computation time per iteration during the optimization process for each of the four models. Here it needs to be pointed out that these results do not allow for a quantitative comparison of the modular approach with the LDDMM shooting method. The LDDMM model we use here is the sum of local translations as a special case of deformation module. The computation of the geodesic variables was done in the general modular setting, which involves more complex computations. This leads to a higher computation time than for a standard LDDMM setting.

Moreover there are different types of shooting methods that can be used for LDDMM. The optimization can be done over a momentum $m_t \in V^*$ as a vectorfield, or for a costate $p_t \in \mathrm{T}^*_{q_t}\mathcal{O}$ that has reduced dimensionality (see chapter 2.1.7).

It is also interesting to see that introducing multi-shape boundary constraints in LDDMM leads to time increasing of two orders of magnitude for the examples we considered. Considering the deformation modules, the time per iteration is approximately double when introducing the constraints.

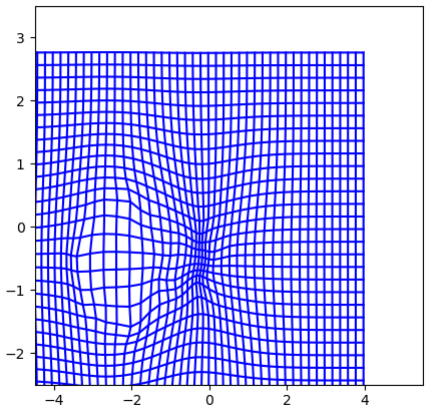

(a) Deformation grid corresponding to the left shape. The deformation models an enlargement of the left part of the shape and reduction of the right part of the peanut-shape. At the same time the whole shape is translated downwards left.

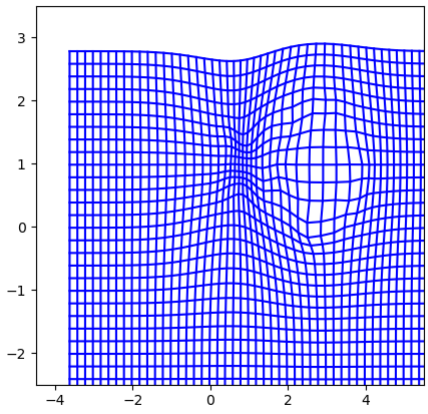

(b) Deformation grid corresponding to the right shape. The enlargement and reduction of the parts are happening in the opposite way from the first shape, while having used the same prior.

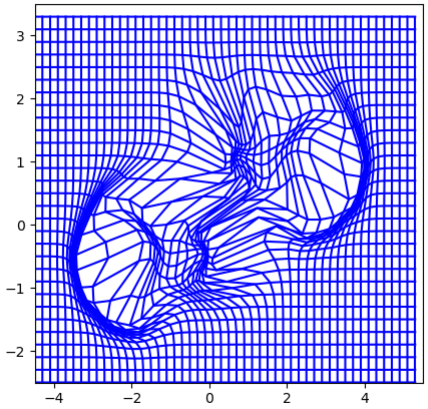

(c) Deformation grid corresponding to the background. Due to a relatively low kernel scale of $\sigma = 0.3$ an irregular grid is achieved where high deformations of close regions are possible.

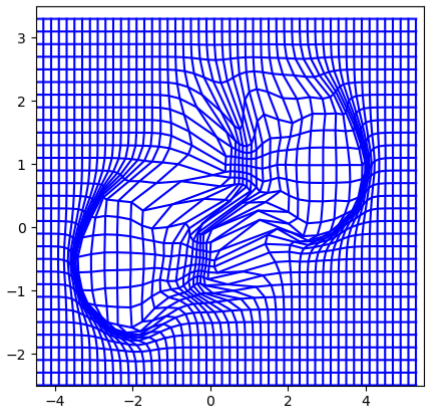

(d) Multi-shape combination of the grids. At the boundary of the shapes, the deformations are forced to be identical for the background and the corresponding shape. The local scalings inside the shape and the translations in opposite directions are happening simultanously.

Figure 17: Deformation grids for both shapes (above), the background (below left) and multi-shape combination grid resulting from the shape registration using the multi-shape deformation modules framework. The deformation grids of the shapes indicate that using deformation modules, a deformation modeling a local scaling can be obtained. The background grid is of low regularity, such that the shapes can be translated in different directions although being close to each other. In the multi-shape combined grid, the local scaling deformation prior the shapes and the independent translation are possible at the same time.

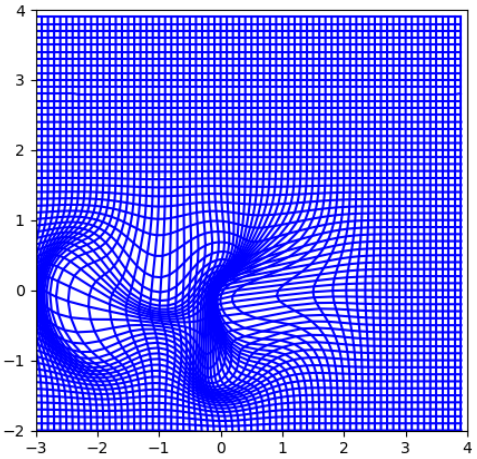

(a) Deformation grid corresponding to the left shape with a kernel scale of $\sigma = 0.5$.

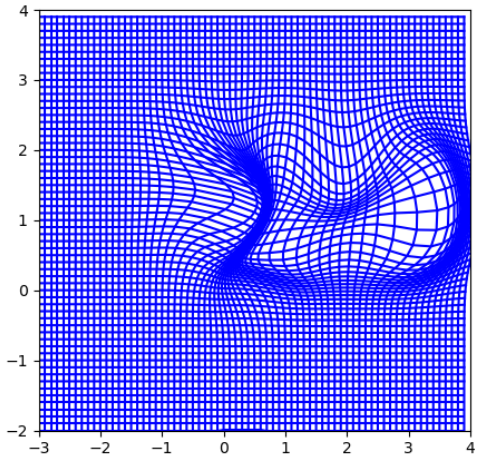

(b) Deformation grid of right shape with a kernel scale of $\sigma = 0.5$.

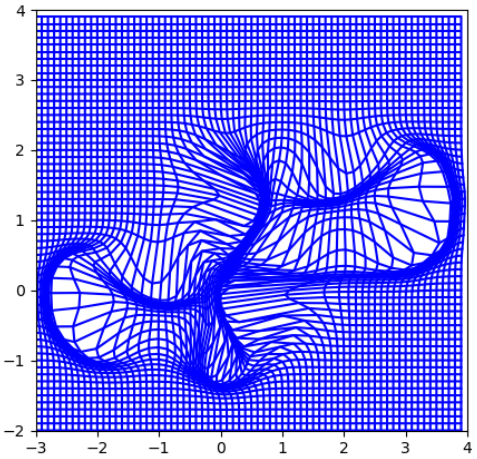

(c) Deformation grid corresponding to the background. The kernel scale was set to $\sigma = 0.2$.

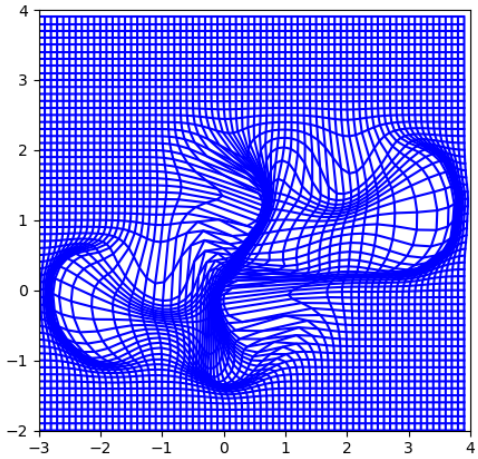

(d) Multi-shape combination of the deformation grids.

Figure 18: Deformation grids for shapes (above), background (below left) and multi-shape combination (below right) resulting from the shape registration using multi-shape LDDMM. Due to numerical precision loss the optimization process terminated before convergence.

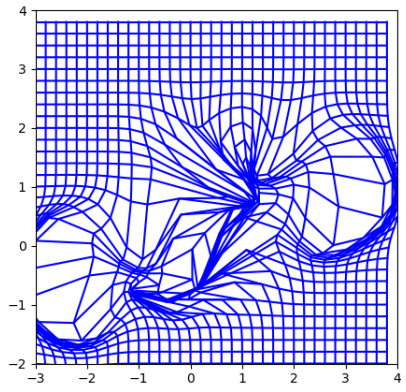

Figure 19: Deformation grid for the shape registration using the LDDMM framework with a Gaussian kernel of scale $\sigma = 0.5$.

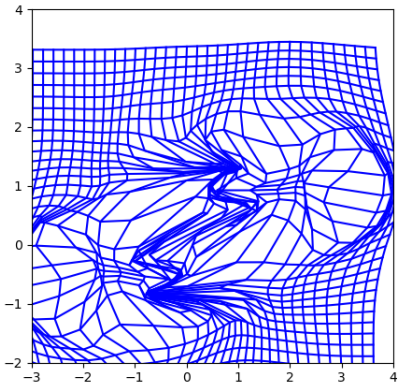

Figure 20: Deformation grid for the compound deformation module framework.

Model	Time per Iteration
Multi-shape deformation modules	16.9s
Multi-shape LDDMM	244s
LDDMM	1.38s
compound deformation module	8.11s

Table 1: Computation time per iteration for the four models tested on the peanuts-dataset. The use of multi-shape boundary constraints increases computation time. The increasing factor is higher for the LDDMM setting than for the deformation modules setting.

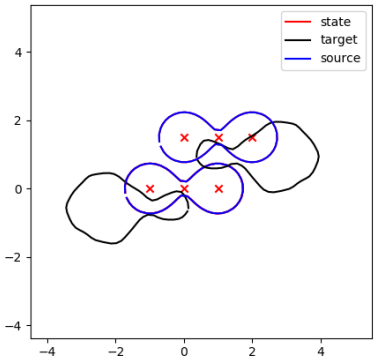

(a) Shooting at $t = 0$

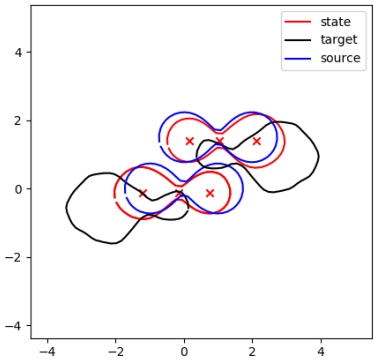

(b) Shooting at $t = 0.2$

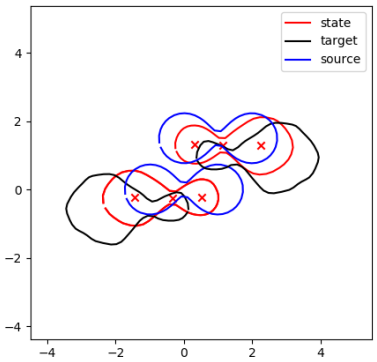

(c) Shooting at $t = 0.4$

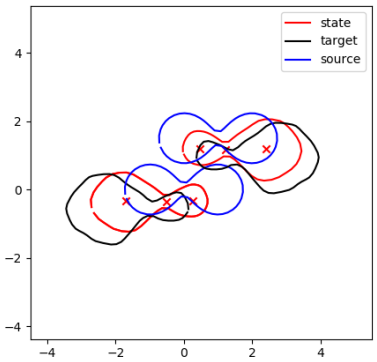

(d) Shooting at $t = 0.6$

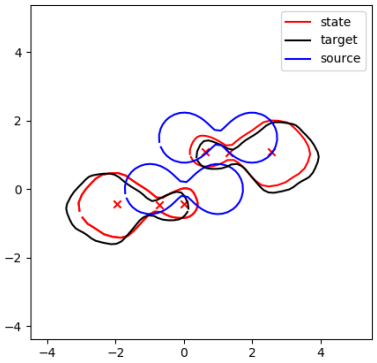

(e) Shooting at $t = 0.8$

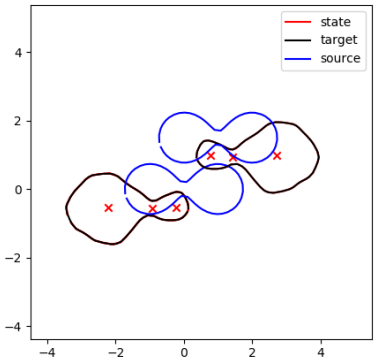

(f) Shooting at $t = 1$

Figure 21: Shooting iterations over time for the multi-shape deformation module approach. The scaling centers and translation point are marked in the shapes. During the shooting the simultanous local scalings and translation of the whole shape can be observed.

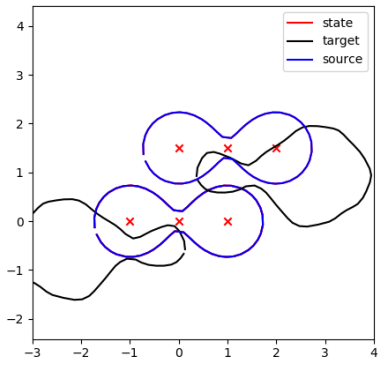

(a) Shooting at $t = 0$

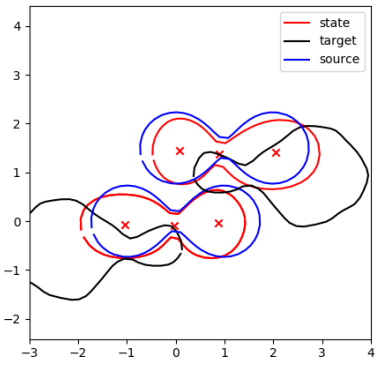

(b) Shooting at $t = 0.2$

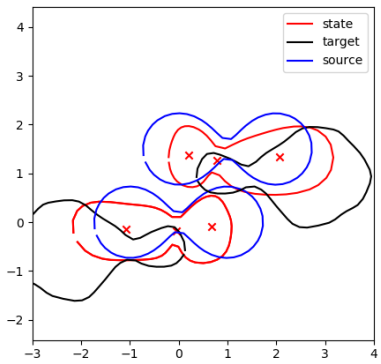

(c) Shooting at $t = 0.4$

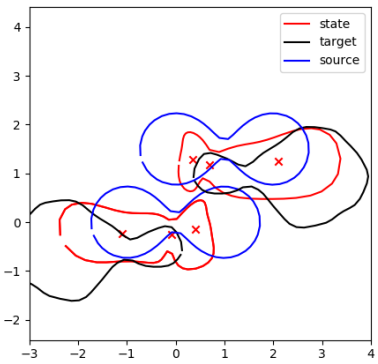

(d) Shooting at $t = 0.6$

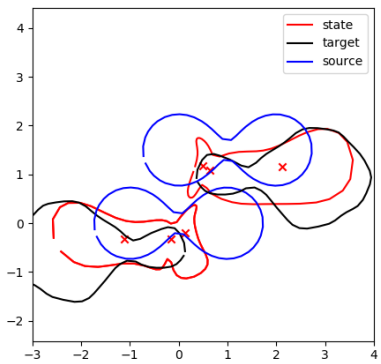

(e) Shooting at $t = 0.8$

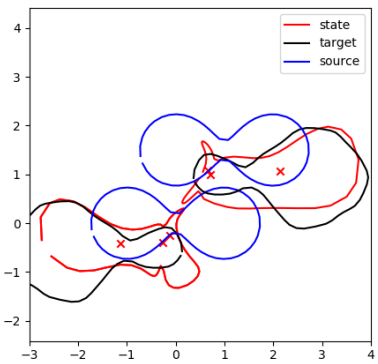

(f) Shooting at $t = 1$

Figure 22: Shooting iterations over time for the multi-shape LDDMM approach. The shapes did not reach the target because the optimization terminated after two iterations due to numerical precision loss. The red crosses mark the location of the geometrical descriptors used for the deformation modules. They do not influence the deformation for the multi-shape LDDMM setting but are marked for comparison.

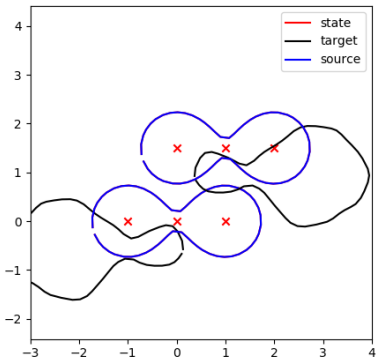

(a) Shooting at $t = 0$

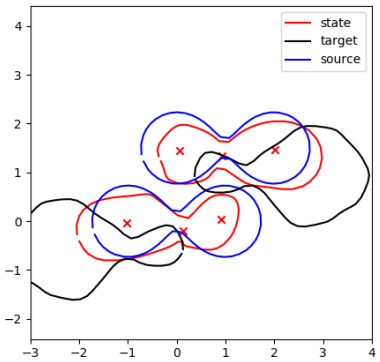

(b) Shooting at $t = 0.2$

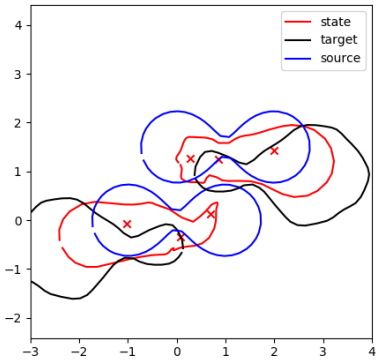

(c) Shooting at $t = 0.4$

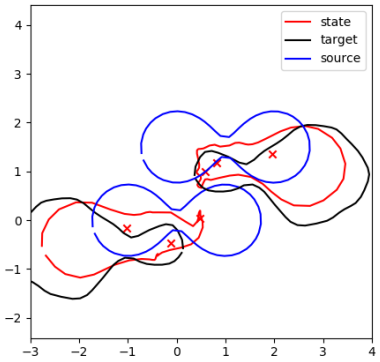

(d) Shooting at $t = 0.6$

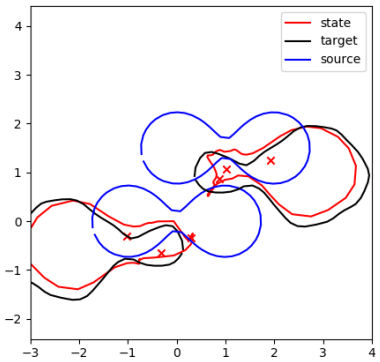

(e) Shooting at $t = 0.8$

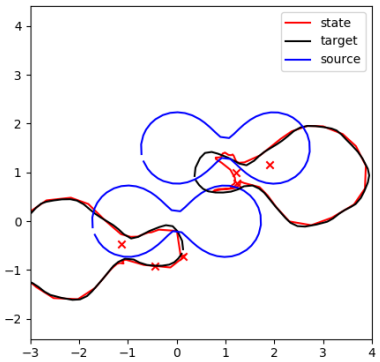

(f) Shooting at $t = 1$

Figure 23: Shooting iterations over time for LDDMM with kernel scale $\sigma = 0.5$. The optimization terminated after 49 iterations due to precision loss. The shapes are deforming irregularly during the shooting. The red crosses mark the location of the geometrical descriptors used for the deformation modules. They do not influence the deformation for the LDDMM setting but are marked for comparison. They are translated in the direction of the other shape.

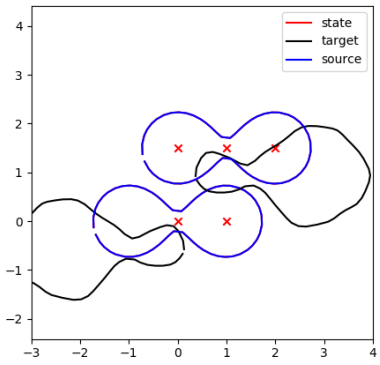

(a) Shooting at $t = 0$

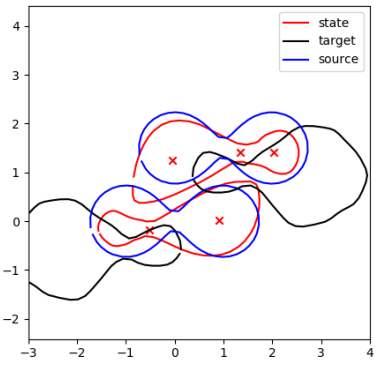

(b) Shooting at $t = 0.2$

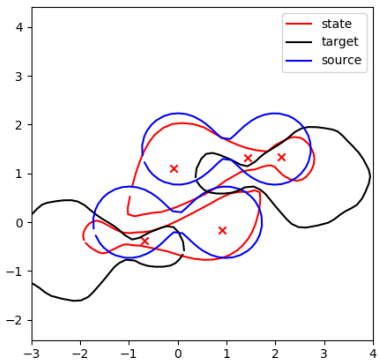

(c) Shooting at $t = 0.4$

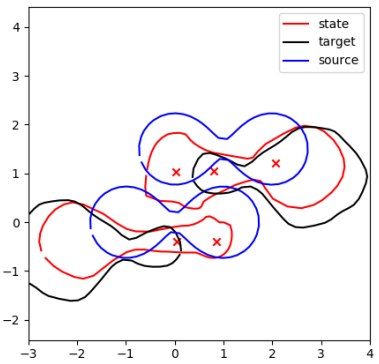

(d) Shooting at $t = 0.6$

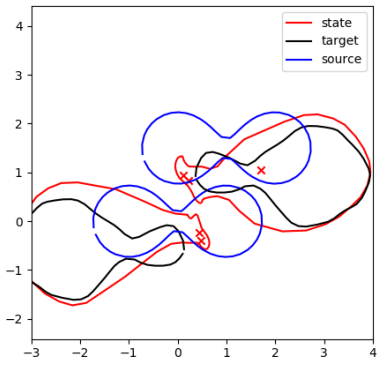

(e) Shooting at $t = 0.8$

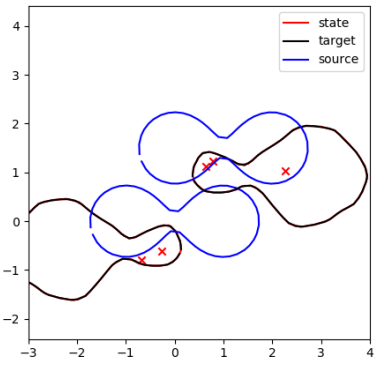

(f) Shooting at $t = 1$

Figure 24: Shooting iterations over time for a compound deformation module. The shapes are deforming irregularly during the shooting and the scaling and translation centers are drawn to the part of the shape that is closer to the other shape. The scalings cannot occur simultanously in the two seperate shapes that lie close together, because the deformations are influencing each other. Therefore most of the deformation results from the local translations of the boundary points, that have been added with a high penalty.

Chapter 5: Conclusion

The purpose of this thesis was to provide a framework for incorporating deformation priors in segmented images and multi-shapes.

We extended the deformation module framework introduced in [Gri16] to a setting where deformation priors in different regions of the ambient space do not influence each other while the overall deformation remains consistent at the region boundaries. This was achieved by incorporating boundary constraints in the optimization problem.

As a first contribution, we stated a new optimization problem that takes into account the two types of prior knowledge: Deformation priors were incorporated by using deformation modules. Consistency at the region boundaries was modeled by constraining the problem to certain region boundary constraints as proposed in [Arg14].

From the theoretical viewpoint, we proved the existence of large deformations as well as existence of geodesics for our new setting. We also computed the geodesic equations for the Hamiltonian system, which are used in practice to compute geodesics.

In terms of numerical results we compared our presented framework to state-of-the-art methods such as multi-shape LDDMM, LDDMM and deformation modules. The results are mainly focused on synthetic examples for pointing out the new possibilities specific to the framework.

While preliminary, the experimental results show that the framework successfully combines the advantages of deformation modules and the constrained multi-shape registration framework.

The high amount of computation for the geodesic variables leads to a computation time of a few minutes for the presented examples. When registering images instead of points and curves an even higher computation time can be expected. For this reason, the model is not yet suitable for real-time computations.

Future Work

As numerical results have only been provided for synthetic data of points and curves it would be interesting to use the method for real medical images. There are promising perspectives within the application on CT and MR abdominal or brain images for which a segmentation is given. Until now the framework has been implemented and tested in two dimensions, which could also be extended to three or more dimensions. For the application on real data the choice of deformation modules for each object is crucial and would have to be studied further. Furthermore different types of boundary constraints can be incorporated, for example in order to allow a sliding motion of objects.

Chapter A: Appendix

A.1 Explicit Formulation of Geodesic Variables for Landmarks with Identity Constraints

The purpose of this section is to give an example of explicit formulations for h_{qp} and λ_{qp} as they are computed in practice for the implementation. We will derive the explicit formulation of h_{qp} and λ_{qp} for the example 3.2, where we considered the case of translations of two shapes in a background. All variables are given for a specific time point. In order to make the notation less dense we omit the time index t in the following.

Let us recall the given setting of the example. We have

- Translation modules $M^i, i = 1, 2$
  - $\mathcal{O}^i = (\mathbb{R}^2)^{N_i}$
  - $H^i = \mathbb{R}^2$
  - $\zeta^i_{q^i}(h^i) = \mathrm{K}_{\sigma_i}(z(q^i), \cdot)h^i \in C^l(\mathbb{R}^2, \mathbb{R}^2)$ with $z(q^i) = \frac{1}{N_i}\sum_{j=1}^{N_i} q_{i,j}$
  - $\xi^i_{q^i}(v^i) = v^i(q^i) \in (\mathbb{R}^2)^{N_i}$
  - $c^i_{q^i}(h^i) = |h^i|^2_{\mathbb{R}^2} \in \mathbb{R}$
- Background module M^3
  - $\mathcal{O}^3 = \mathcal{O}^1 \times \mathcal{O}^2 = \mathbb{R}^{2^{N_1+N_2}}$
  - $H^3 = V_{\sigma_3} \subset C^l(\mathbb{R}^2, \mathbb{R}^2)$
  - $\zeta^3_{q^3}(h^3) = h^3 \in V^3 = V_{\sigma_3}$
  - $\xi^3_{q^3}(v^3) = (v^3(q_1^{3,1}), ..., v^3(q_{N_1}^{3,1}), v^3(q_1^{3,2}), ..., v^3(q_{N_2}^{3,2})) \in (\mathbb{R}^2)^{N_1+N_2}$
  - $c^3_{q^3}(h^3) = |h^3|^2_{H^3} \in \mathbb{R}$
- Identity Constraints

$$\begin{aligned} \mathrm{C}_q(v) = \mathrm{C}_q(v^1, v^2, v^3) &= (v^1(q^1) - v^3(q^{3,1}), v^2(q^2) - v^3(q^{3,2})) \\ &= (v^1(q_1^1) - v^3(q_1^{3,1}), ..., v^1(q_{N_1}^1) - v^3(q_{N_1}^{3,1}), \\ &\quad v^2(q_1^2) - v^3(q_1^{3,2}), ..., v^2(q_{N_2}^2) - v^3(q_{N_2}^{3,2})) \\ &\in (\mathbb{R}^2)^{N_1+N_2} = Y \end{aligned} \tag{135}$$

In the example the background space H^3 is defined as an infinite-dimensional RKHS. We will use its finite-dimensional representation as derived in chapter 3.6.

Finite-Dimensional Representation of the Background Space
As motivated in section 3.6, we will consider a finite-dimensional representation $h_q^3 \in \overline{\mathrm{H}}_q^3 \coloneqq \mathbb{R}^{2(N_1+N_2)}$. Define the function

$$f_q \colon \overline{\mathrm{H}}_q^3 \to \mathrm{H}^3, f_q(h_q^3) \coloneqq \sum_{i=1}^{2} \sum_{j=1}^{N_i} \tilde{\mathrm{K}}(\cdot, q_j^{3,i}) h_j^{3i} \tag{136}$$

for $h_q^3 = (h_1^{3,1}, ..., h_{N_2}^{3,2})$. In this case, f_q is defined as $f_q \coloneqq {\mathrm{Z}^3}_{q^3}^{-1} {\zeta^3}_{q^3}^* {\xi^3_{q^3}}^*$ as in lemma 3.17.

Remark A.1

The following notation is used for a reproducing kernel Hilbert space V.

- K the reproducing kernel
- $\tilde{\mathrm{K}}(x, y)$ the $d \times d$ kernel matrix
- $\mathrm{k}(x, y)$ the Gaussian distribution
- $\tilde{\mathrm{K}}_{a,b} \coloneqq \tilde{\mathrm{K}}(a, b) \in \mathbb{R}^{d(n_1 \times n_2)}$ with $a = (a^1, ..., a^{n_1}) \in \mathbb{R}^{d(n_1)}, b = (b^1, ..., b^{n_2}) \in \mathbb{R}^{d(n_2)}$ the $dn_1 \times dn_2$ kernel matrix with values $\left(\tilde{\mathrm{K}}(a, b)\right)_{i,j} = \mathrm{k}(a^i, b^j)$

In the following sections the terms for the operators $\zeta_q^* \xi_q^*$, Z_q^{-1} and $\zeta_q^* \mathrm{C}_q^*$ will be derived. Subsequently they are composed to obtain the required terms for λ_{qp} and the finite-dimensional representation of h_{qp}.

Explicit Formulation of the Operator $\zeta_q^* \xi_q^*$
To compute the operator $(\xi_q \zeta_q)^* \colon \mathrm{T}_q^* \mathcal{O} \to \mathrm{H}^*$, consider an element $\alpha = (\alpha_1^1, ..., \alpha_{N_2}^{3,2}) \in \mathrm{T}_q^* \mathcal{O} = (\mathbb{R}^2)^{N_1} \times (\mathbb{R}^2)^{N_2} \times (\mathbb{R}^2)^{N_1+N_2}$. The dual pairing of $(\xi_q \zeta_q)^* \alpha$ with an element h of H can be written as

$$\begin{aligned}
\left((\xi_q \zeta_q)^* \alpha | h\right)_{\mathrm{H}^*,\mathrm{H}} &= \left(\alpha | \xi_q \circ \zeta_q(h)\right)_{\mathrm{T}_q^* \mathcal{O}, \mathrm{T}_q \mathcal{O}} \\
&= \left(\alpha | \xi_q(\mathrm{K}_{\sigma_1}(z(q^1), \cdot) h^1, \mathrm{K}_{\sigma_2}(z(q^2), \cdot) h^2, h^3)\right)_{\mathrm{T}_q^* \mathcal{O}, \mathrm{T}_q \mathcal{O}} \\
&= \big(\alpha | \mathrm{K}_{\sigma_1}(z(q^1), q_1^1) h^1, ..., \mathrm{K}_{\sigma_1}(z(q^1), q_{N_1}^1) h^1, \\
&\qquad \mathrm{K}_{\sigma_2}(z(q^2), q_1^2) h^2, ..., \mathrm{K}_{\sigma_2}(z(q^2), q_{N_2}^2) h^2, \\
&\qquad h^3(q_1^{3,1}), ..., h^3(q_{N_2}^{3,2})\big)_{\mathrm{T}_q^* \mathcal{O}, \mathrm{T}_q \mathcal{O}} \\
&= \sum_{j=1}^{N_1} \left(\alpha_j^1 | \mathrm{K}_{\sigma_1}(z(q^1), q_j^1) h^1\right)_{\mathrm{T}^*_{q_j^1} \mathcal{O}^1, \mathrm{T}_{q_j^1} \mathcal{O}^1} \\
&+ \sum_{j=1}^{N_2} \left(\alpha_j^2 | \mathrm{K}_{\sigma_2}(z(q^2), q_j^2) h^2\right)_{\mathrm{T}^*_{q_j^2} \mathcal{O}^2, \mathrm{T}_{q_j^2} \mathcal{O}^2} + \sum_{i=1}^{2} \sum_{j=1}^{N_i} \left(\alpha_j^3 | \delta_{q_j^3} h^3\right)_{\mathrm{T}^*_{q_j^{3,i}} \mathcal{O}^3, \mathrm{T}_{q_j^{3,i}} \mathcal{O}^3}
\end{aligned} \tag{137}$$

$$
\begin{aligned}
&= \sum_{j=1}^{N_1} \left(\mathrm{K}_{\sigma_1}(z(q^1), q^1)\alpha_j^1 | h^1\right)_{\mathrm{H}^{1*},\mathrm{H}^1} + \sum_{j=1}^{N_2} \left(\mathrm{K}_{\sigma_2}(z(q^2), q^2)\alpha_j^2 | h^2\right)_{\mathrm{H}^{2*},\mathrm{H}^2} \\
&\quad + \sum_{i=1}^{2}\sum_{j=1}^{N_i} \left(\delta_{q_j^{3,i}}^{\alpha_j^{3,i}} | h^3\right)_{\mathrm{H}^{3*},\mathrm{H}^3}
\end{aligned} \tag{138}
$$

Here we still have an infinite-dimensional term that will be replaced when considering the mapping f_q and the cost operator $\bar{\mathrm{Z}}_q$ for the finite-dimensional background module.

Explicit Formulation of the Inverse Cost Operator Z_q^{-1}
By definition the cost for $h \in \mathrm{H}$ is

$$
\begin{aligned}
c_q(h) = \sum_{i=1}^{3} c_{q^i}^i(h^i) &= \|h^1\|_{\mathrm{H}^1}^2 + \|h^2\|_{\mathrm{H}^2}^2 + \|h^3\|_{\mathrm{H}^3}^2 \\
&= \langle h^1, h^1\rangle_{\mathbb{R}^2} + \langle h^2, h^2\rangle_{\mathbb{R}^2} + \langle h^3, h^3\rangle_{V_{\sigma_3}} \\
&= \left(h^1 | h^1\right)_{H^{1*},H^1} + \left(h^2 | h^2\right)_{H^{2*},H^2} + \left(\mathrm{K}_{\sigma_3}^{-1} h^3 | h^3\right)_{V_{\sigma_3}^*,V_{\sigma_3}}.
\end{aligned} \tag{139}
$$

For the cost operator Z_q with

$$
\begin{aligned}
\left(\mathrm{Z}_q h | h\right)_{\mathrm{H}^*,\mathrm{H}} &= \sum_{i=1}^{3} \left(\mathrm{Z}_{q^i}^i h^i | h^i\right)_{\mathrm{H}^{i*},\mathrm{H}^i} \\
&= \left(\mathrm{Z}_{q^1}^1 h^1 | h^1\right)_{\mathbb{R}^2,\mathbb{R}^2} + \left(\mathrm{Z}_{q^2}^2 h^2 | h^2\right)_{\mathbb{R}^2,\mathbb{R}^2} + \left(\mathrm{Z}_{q^3}^3 h^3 | h^3\right)_{V_{\sigma_3}^*,V_{\sigma_3}}
\end{aligned} \tag{140}
$$

we obtain

$$
\mathrm{Z}_{q^1}^1 = \mathrm{Id}, \quad \mathrm{Z}_{q^2}^2 = \mathrm{Id} \quad \text{and} \quad \mathrm{Z}_{q^3}^3 = \mathrm{K}_{\sigma_3}^{-1}. \tag{141}
$$

In the following, an equivalent formulation of the geodesic equation (115) will be derived for the finite-dimensional representation $\bar{h}_{qp}^3$.

For this purpose, define the cost function $\bar{c}_q \colon \overline{\mathrm{H}}_q \to \mathbb{R}$ and the cost operator $\overline{\mathrm{Z}}_q \colon \overline{\mathrm{H}}_q^* \to \overline{\mathrm{H}}_q$ such that $c_q(h) = \bar{c}_q(\bar{h}) = \left(\overline{\mathrm{Z}}_q \bar{h} | \bar{h}\right)_{\overline{\mathrm{H}}_q^*,\overline{\mathrm{H}}_q}$ for $h = f_q(\bar{h})$. Then it holds

$$
\left(\overline{\mathrm{Z}}_q \bar{h} | \bar{h}\right)_{\overline{\mathrm{H}}_q^*,\overline{\mathrm{H}}_q} = \left(\mathrm{Z}_q h | h\right)_{\mathrm{H}^*,\mathrm{H}} = \left(\mathrm{Z}_q f_q(\bar{h}) | f_q(\bar{h})\right)_{\mathrm{H}^*,\mathrm{H}} = \left(f_q^* \mathrm{Z}_q f_q h | h\right)_{\overline{\mathrm{H}}_q^*,\overline{\mathrm{H}}_q}, \tag{142}
$$

and thus the cost operators Z_q and $\overline{\mathrm{Z}}_q$ are related in the way that $\overline{\mathrm{Z}}_q = f_q^* \mathrm{Z}_q f_q$. Applying the cost operator to the finite-dimensional representation h_q is equivalent to applying f_q, then applying the cost operator Z_q in H^3 and going back to $\overline{\mathrm{H}}^3$ by f_q^*. Equivalently we have $\mathrm{Z}_q^{-1} = f_q \overline{\mathrm{Z}}_q^{-1} f_q^*$.

Applying the inverse cost to the already obtained term (138) and inserting the definitions of $\overline{\mathrm{Z}}_q^{-1}$ and $f_q^* \delta$ yields

$$
\begin{aligned}
f_q^{-1} {\mathrm{Z}^3}_{q^3}^{-1} (\xi_{q^3}^3 \zeta_{q^3}^3)^* \alpha^3 = {\overline{\mathrm{Z}}^3}_q^{-1} {f_q}^* (\xi_{q^3}^3 \zeta_{q^3}^3)^* \alpha^3 &= {\overline{\mathrm{Z}}^3}_q^{-1} {f_q}^* \Big(\sum_{i,j} \delta_{q_j^{3,i}}^{\alpha_j^{3,i}} \Big) \\
&= \tilde{\mathrm{K}}_{q^3,q^3}^{-1} \tilde{\mathrm{K}}_{q^3,q^3} \alpha^3 = \alpha^3.
\end{aligned} \tag{143}
$$

We see that the kernel convolution cancels out for our choice of f. Finally, we obtain for the finite-dimensional representation,

$$\begin{aligned}(\mathrm{Z}^1_{q^1}{}^{-1}(\xi^1_{q^1}\zeta^1_{q^1})^*\alpha^1, \mathrm{Z}^2_{q^2}{}^{-1}(\xi^2_{q^2}\zeta^2_{q^2})^*\alpha^2, f_q^{-1}\mathrm{Z}^3_{q^3}{}^{-1}(\xi^3_{q^3}\zeta^3_{q^3})^*\alpha^3)\\ = \Big(\tilde{\mathrm{K}}^1_{z^1,q^1}\alpha^1, \tilde{\mathrm{K}}^2_{z^2,q^2}\alpha^2, \alpha^3\Big).\end{aligned} \tag{144}$$

Explicit Formulation of the Operator $\mathrm{C}_q\zeta_q$

For the following computations the vector field generated by ζ_q from h has to be evalulated at the points $q^i_j \in q$. Since the vector fields $\zeta^1_{q^1}(h^1)$ and $\zeta^2_{q^2}(h^2)$ are given by the convolution with the kernel, the evaluation at a point $x \in \mathbb{R}^2$ is straightforward by using the kernel matrix $\tilde{\mathrm{K}}(x, q^i)h^i$. For the infinite-dimensional control $h^3 \in \mathrm{H}^3$, the evaluation $h^3(x)$ can be written as $h^3(x) = (f_q h^3_q)(x)$. This arises to the convolution of $h_q \in \overline{\mathrm{H}}^3$ with the matrix $\tilde{\mathrm{K}}^3(x, q)$, which will be done in the first equality of the following computations.

For an element $h \in \mathrm{H}$ and its finite-dimensional representation $h_q \in \overline{\mathrm{H}}_q$, the applied operator $\mathrm{C}_q\zeta_q$ yields

$$\begin{aligned}\mathrm{C}_q\zeta_q(h) &= \mathrm{C}_q(\zeta^1_{q^1}(h^1), \zeta^2_{q^2}(h^2), f_q h^3_q)\\ &= (\zeta^1_{q^1}(h^1)(q^1) - \zeta^3_{q^3}(h^3)(q^{3,1}), \zeta^2_{q^2}(h^2)(q^2) - \zeta^3_{q^3}(h^3)(q^{3,1}))\\ &= (\tilde{\mathrm{K}}^1(q^1_1, z^1)h^1 - \sum_{i,j}\tilde{\mathrm{K}}^3(q^1_1, q^{3,i}_j)h^{3,i}_j, ..., \tilde{\mathrm{K}}^1(q^1_{N_1}, z^1)h^1 - \sum_{i,j}\tilde{\mathrm{K}}^3(q^{3,i}_{N_1}, q^1_j)h^{3,i}_j,\\ &\quad \tilde{\mathrm{K}}^2(q^2_1, z^2)h^2 - \sum_{i,j}\tilde{\mathrm{K}}^3(q^{3,2}_1, q^{3,i}_j)h^{3,i}_j, ..., \tilde{\mathrm{K}}^2(q^2_{N_2}, z^2)h^2 - \sum_{i,j}\tilde{\mathrm{K}}^3(q^{3,2}_{N_2}, q^{3,i}_j)h^{3,i}_j,)\\ &= (\tilde{\mathrm{K}}^1_{q^1,z^1}h^1 - \tilde{\mathrm{K}}^3_{q^{3,1},q^3}h^3_q, \tilde{\mathrm{K}}^2_{q^2,z^2}h^2 - \tilde{\mathrm{K}}^3_{q^{3,2},q^3}h^3_q)\end{aligned} \tag{145}$$

Explicit Formulation of the Operator $\zeta^*_q\mathrm{C}^*_q$

Let $\lambda = (\lambda^2, \lambda^2) \in \mathrm{Y}^*, h \in \mathrm{H}$ and $h_q \in \overline{\mathrm{H}}_q$ be its finite-dimensional representation. Consider the dual pairing

$$\begin{aligned}(\zeta^*_q\mathrm{C}^*_q\lambda|h)_{\mathrm{H}^*,\mathrm{H}} &= (\lambda|\mathrm{C}_q\zeta_q h)_{\mathrm{Y}^*,\mathrm{Y}}\\ &= (\lambda|\mathrm{C}_q(\tilde{\mathrm{K}}^1(\cdot, z^1)h^1, \tilde{\mathrm{K}}^2(\cdot, z^2)h^2, f(h^3_q))_{\mathrm{Y}^*,\mathrm{Y}}\\ &= (\lambda|\mathrm{C}_q(\tilde{\mathrm{K}}^1(\cdot, z^1)h^1, \tilde{\mathrm{K}}^2(\cdot, z^2)h^2, \sum_{i,j}\tilde{\mathrm{K}}^3(\cdot, q^{3,i}_j)h^i_j))_{\mathrm{Y}^*,\mathrm{Y}}\\ &= (\lambda|\tilde{\mathrm{K}}^1_{q^1,z^1}h^1 - \tilde{\mathrm{K}}^2_{q^{3,1},q^3}h^3_q, \tilde{\mathrm{K}}^2_{q^2,z^2}h^2 - \tilde{\mathrm{K}}^3_{q^{3,1},q^3}h^3_q)_{\mathrm{Y}^*,\mathrm{Y}}\\ &= ((\tilde{\mathrm{K}}^1_{z^1,q^1}\lambda^1, \tilde{\mathrm{K}}^2_{z^2,q^2}\lambda^2, -\tilde{\mathrm{K}}^3_{q^3,q^{3,1}}\lambda^1 - \tilde{\mathrm{K}}^3_{q^3,q^{3,2}}\lambda^2)|(h^1, h^2, h^3_q))_{\overline{\mathrm{H}}^*,\overline{\mathrm{H}}}.\end{aligned} \tag{146}$$

which yields the expression $\zeta^*_q\mathrm{C}^*_q\lambda = (\tilde{\mathrm{K}}^1_{z^1,q^1}\lambda^1, \tilde{\mathrm{K}}^2_{z^2,q^2}\lambda^2, -\tilde{\mathrm{K}}^3_{q^3,q^{3,1}}\lambda^1 - \tilde{\mathrm{K}}^3_{q^3,q^{3,2}}\lambda^2)$

The Inversion of $\mathrm{C}_q\zeta_q\mathrm{Z}_q^{-1}\zeta_q^*\mathrm{C}_q^*$
With the already obtained results from (146), (141) and (145), the expression for $\mathrm{C}_q\zeta_q\mathrm{Z}_q^{-1}\zeta_q^*\mathrm{C}_q^*$ is

$$\begin{aligned}\mathrm{C}_q\zeta_q\mathrm{Z}_q^{-1}\zeta_q^*\mathrm{C}_q^*\lambda &= \mathrm{C}_q\zeta_q\mathrm{Z}_q^{-1}(\tilde{\mathrm{K}}^1_{z^1,q^1}\lambda^1, \tilde{\mathrm{K}}^2_{z^2,q^2}\lambda^2, -\tilde{\mathrm{K}}^3_{q^3,q^{3,1}}\lambda^1 - \tilde{\mathrm{K}}^3_{q^3,q^{3,2}}\lambda^2) \\ &= \mathrm{C}_q\zeta_q(\tilde{\mathrm{K}}^1_{z^1,q^1}\lambda^1, \tilde{\mathrm{K}}^2_{z^2,q^2}\lambda^2, -\lambda) \\ &= (\tilde{\mathrm{K}}^1_{q^1,z^1}\tilde{\mathrm{K}}^1_{z^1,q^1}\lambda^1 + \tilde{\mathrm{K}}^3_{q^{3,1},q^3}\lambda,\ \tilde{\mathrm{K}}^2_{q^2,z^2}\tilde{\mathrm{K}}^2_{z^2,q^2}\lambda^2 + \tilde{\mathrm{K}}^3_{q^{3,2},q^3}\lambda).\end{aligned} \tag{147}$$

From 3.11, we know that this matrix is invertible. In practice the inversion is done by solving the linear system

$$(\mathrm{C}_q\zeta_q\mathrm{Z}_q^{-1}\zeta_q^*\mathrm{C}_q^*)\lambda_{q,p} = \mathrm{C}_q\zeta_q\mathrm{Z}_q^{-1}\zeta_q^*\xi_q^*p. \tag{148}$$

Computing λ_{qp} and h_{qp}
Writing the equation (148) explicitly yields the linear system of equations

$$\begin{aligned}&\left(\begin{pmatrix}\tilde{\mathrm{K}}^1_{q^1,z^1}\tilde{\mathrm{K}}^1_{z^1,q^1} & 0 \\ 0 & \tilde{\mathrm{K}}^2_{q^2,z^2}\tilde{\mathrm{K}}^2_{z^2,q^2}\end{pmatrix} + \tilde{\mathrm{K}}^3_{q,q}\right)\lambda_{qp} \\ &\qquad = \begin{pmatrix}\tilde{\mathrm{K}}^1_{q^1,z^1}\tilde{\mathrm{K}}^1_{z^1,q^1} & 0 & \tilde{\mathrm{K}}^3_{q^{3,1},q^3} \\ 0 & \tilde{\mathrm{K}}^2_{q^2,z^2}\tilde{\mathrm{K}}^2_{z^2,q^2} & \tilde{\mathrm{K}}^3_{q^{3,2},q^3}\end{pmatrix}p,\end{aligned} \tag{149}$$

which is to be solved.

For h_{qp} the explicit expression is

$$\begin{aligned}h_{qp} &= \left(\tilde{\mathrm{K}}^1_{z^1,q^1}p^1, \tilde{\mathrm{K}}^2_{z^2,q^2}p^2, p^3\right) - \left(\tilde{\mathrm{K}}^1_{z^1,q^1}\lambda^1, \tilde{\mathrm{K}}^2_{z^2,q^2}\lambda^2, -\lambda\right) \\ &= \begin{pmatrix}\tilde{\mathrm{K}}^1_{z^1,q^1} & 0 & 0 \\ 0 & \tilde{\mathrm{K}}^2_{z^2,q^2} & 0 \\ 0 & 0 & \mathrm{Id}\end{pmatrix}\left(p - \begin{pmatrix}\lambda \\ -\lambda\end{pmatrix}\right).\end{aligned} \tag{150}$$

Now, with equations (150) and (149) we can compute the explicit geodesic variables h_{qp} and λ_{qp}, that are computed at each time step during the shooting.

References

[ACAP09] Arsigny, Vincent ; Commowick, Olivier ; Ayache, Nicholas ; Pennec, Xavier: A fast and log-euclidean polyaffine framework for locally linear registration. In: *Journal of Mathematical Imaging and Vision* 33 (2009), Nr. 2, S. 222–238

[APA03] Arsigny, Vincent ; Pennec, Xavier ; Ayache, Nicholas: Polyrigid and polyaffine transformations: A new class of diffeomorphisms for locally rigid or affine registration. In: *International Conference on Medical Image Computing and Computer-Assisted Intervention* Springer, 2003, S. 829–837

[Arg14] Arguillère, Silvain: *Géométrie sous-riemannienne en dimension infinie et applications à l'analyse mathématique des formes*, Université Paris VI - Pierre et Marie Curie, Diss., 2014

[Aro50] Aronszajn, Nachman: Theory of reproducing kernels. In: *Transactions of the American mathematical society* 68 (1950), Nr. 3, S. 337–404

[ATTY15a] Arguillère, Sylvain ; Trélat, Emmanuel ; Trouvé, Alain ; Younes, Laurent: Multiple shape registration using constrained optimal control. In: *arXiv preprint arXiv:1503.00758* (2015)

[ATTY15b] Arguillere, Sylvain ; Trélat, Emmanuel ; Trouvé, Alain ; Younes, Laurent: Shape deformation analysis from the optimal control viewpoint. In: *Journal de mathématiques pures et appliquées* 104 (2015), Nr. 1, S. 139–178

[BBM14] Bauer, Martin ; Bruveris, Martins ; Michor, Peter W.: Overview of the geometries of shape spaces and diffeomorphism groups. In: *Journal of Mathematical Imaging and Vision* 50 (2014), Nr. 1-2, S. 60–97

[BH15] Bruveris, Martins ; Holm, Darryl D.: Geometry of image registration: The diffeomorphism group and momentum maps. In: *Geometry, Mechanics, and Dynamics*. Springer, 2015, S. 19–56

[BMTY05] Beg, M F. ; Miller, Michael I. ; Trouvé, Alain ; Younes, Laurent: Computing large deformation metric mappings via geodesic flows of diffeomorphisms. In: *International journal of computer vision* 61 (2005), Nr. 2, S. 139–157

[Bro81] Broit, Chaim: Optimal registration of deformed images. (1981)

[CRM+96] Christensen, Gary E. ; Rabbitt, Richard D. ; Miller, Michael I. u. a.: Deformable templates using large deformation kinematics. In: *IEEE transactions on image processing* 5 (1996), Nr. 10, S. 1435–1447

[CT13] Charon, Nicolas ; Trouvé, Alain: The varifold representation of nonoriented shapes for diffeomorphic registration. In: *SIAM Journal on Imaging Sciences* 6 (2013), Nr. 4, S. 2547–2580

[DGM98] Dupuis, Paul ; Grenander, Ulf ; Miller, Michael I.: Variational problems on flows of diffeomorphisms for image matching. In: *Quarterly of applied mathematics* (1998), S. 587–600

[Gri16] Gris, Barbara: *Modular Approach on Shape Spaces, Sub-Riemannian Geometry and Computational Anatomy*, Université Paris-Saclay, Diss., 2016

[GSS06] Grenander, Ulf ; Srivastava, Anuj ; Saini, Sanjay: Characterization of biological growth using iterated diffeomorphisms. In: *3rd IEEE International Symposium on Biomedical Imaging: Nano to Macro, 2006.* IEEE, 2006, S. 1136–1139

[HSS09] Holm, Darryl D. ; Schmah, Tanya ; Stoica, Cristina: *Geometric mechanics and symmetry: from finite to infinite dimensions.* Bd. 12. Oxford University Press, 2009

[MM07] Michor, Peter W. ; Mumford, David: An overview of the Riemannian metrics on spaces of curves using the Hamiltonian approach. In: *Applied and Computational Harmonic Analysis* 23 (2007), Nr. 1, S. 74–113

[Mod04] Modersitzki, Jan: *Numerical methods for image registration.* Oxford University Press on Demand, 2004

[MR13] Marsden, Jerrold E. ; Ratiu, Tudor S.: *Introduction to mechanics and symmetry: a basic exposition of classical mechanical systems.* Bd. 17. Springer Science & Business Media, 2013

[MSBP15] McLeod, Kristin ; Sermesant, Maxime ; Beerbaum, Philipp ; Pennec, Xavier: Spatio-temporal tensor decomposition of a polyaffine motion model for a better analysis of pathological left ventricular dynamics. In: *IEEE transactions on medical imaging* 34 (2015), Nr. 7, S. 1562–1575

[MTY02] Miller, Michael I. ; Trouvé, Alain ; Younes, Laurent: On the metrics and Euler-Lagrange equations of computational anatomy. In: *Annual review of biomedical engineering* 4 (2002), Nr. 1, S. 375–405

[MTY15] Miller, Michael I. ; Trouvé, Alain ; Younes, Laurent: Hamiltonian systems and optimal control in computational anatomy: 100 years since D'Arcy Thompson. In: *Annual review of biomedical engineering* 17 (2015), S. 447–509

[RDSP15] Rohé, Marc-Michel ; Duchateau, Nicolas ; Sermesant, Maxime ; Pennec, Xavier: Combination of polyaffine transformations and supervised

learning for the automatic diagnosis of LV infarct. In: *Statistical Atlases and Computational Models of the Heart* Springer, 2015, S. 190–198

[SPR12] Seiler, Christof ; Pennec, Xavier ; Reyes, Mauricio: Capturing the multiscale anatomical shape variability with polyaffine transformation trees. In: *Medical image analysis* 16 (2012), Nr. 7, S. 1371–1384

[You10] Younes, Laurent: *Shapes and diffeomorphisms*. Bd. 171. Springer Science & Business Media, 2010

[You12] Younes, Laurent: Constrained diffeomorphic shape evolution. In: *Foundations of Computational Mathematics* 12 (2012), Nr. 3, S. 295–325